RECOMBINANT ELASTIN ANALOGUES AS CELL-ADHESIVE MATRICES FOR VASCULAR TISSUE ENGINEERING

A Dissertation
Presented to
The Academic Faculty

By

Swathi Ravi

In Partial Fulfillment
Of the Requirements for the Degree
Doctor of Philosophy in Biomedical Engineering

Georgia Institute of Technology
December 2010

RECOMBINANT ELASTIN ANALOGUES AS CELL-ADHESIVE MATRICES FOR VASCULAR TISSUE ENGINEERING

Approved by:

Dr. Elliot L. Chaikof, Advisor
Dept. of Biomedical Engineering
Georgia Institute of Technology
Department of Surgery
Emory University School of Medicine

Dr. Larry V. McIntire
Dept. of Biomedical Engineering
Georgia Institute of Technology

Dr. Vincent P. Conticello
School of Chemistry
Emory University

Dr. Thomas Barker
Dept. of Biomedical Engineering
Georgia Institute of Technology

Dr. Steven L. Stice
Regenerative Bioscience Center
University of Georgia

Dr. Hanjoong Jo
Department of Cardiology
Emory School of Medicine

Date Approved: July 19th, 2010

ACKNOWLEDGMENTS

There have been many individuals who have enabled me to achieve my goal of completing a PhD in biomedical engineering. I would like to thank my advisor, Dr. Elliot Chaikof, for all his support and mentorship over the years. His enthusiasm for medical research and its practical applications has inspired my continued interest in the field of cardiovascular engineering and biomaterials science. His patience and encouragement have taught me the importance of persistence in scientific research, and I am truly grateful for his guidance. I would also like to thank Dr. Carolyn Haller for her advice on matters large and small. Carolyn's patience and troubleshooting skills helped me to overcome many of my research nightmares and develop into a better scientist. My sincere appreciation goes out to my thesis committee members: Dr. Thomas Barker, Dr. Larry McIntire, Dr. Vincent Conticello, Dr. Hanjoong Jo, and Dr. Steve Stice for their contributions and investment in my work. I would like to acknowledge the other members of my lab who assisted in various aspects of my project: Dr. Rory Sallach, who took me under her wing when I first started and always made time to share her expertise in genetic and protein engineering; Dr. Venkat Krishnamurthy, who helped mold me into a chemist as I learned solid phase peptide synthesis; Dr. Jing Wen, who assisted me with histology work; Dr. Jeff Caves and Vivek Kumar for their assistance in fabrication of collagen-elastin sheets; Adam Martinez for mechanical analysis of elastin-like gels; Julianty Angsana for assistance in haptotaxis and real time RT-PCR work; and Wensheng Li for her ever-cheerful willingness to make me more precious LysB10.

On a personal note, I would like to thank all the members of the Chaikof lab for their friendship and support. I will especially cherish my memories of celebratory group lunches and dinners, Adam's lively stories and love of Quiznos, Vivek's hilarious adventures, and a shared passion for shopping, junk food consumption, and "girl" talk with Julianty.

Of course, this journey would not have been possible without the unconditional love and support of my family. I want to take this opportunity to thank my mom for pushing me to do more and be more, and to face challenges head-on. I would also like to thank my dad for his unwavering optimism and faith in my abilities. Those Tuesday night phone calls always brought a smile to my face. I also want to thank my brother Shashank for keeping me sane these past few years; he is the one person I can truly confide in during all the good and bad times, and he has been a wonderful friend. Finally, I want to thank Shobha, Bhasker Uncle, and Gouri for all their love and support. I always enjoyed my trips to New Jersey and New York, where they provided me with a home away from home and a safe haven from the chaos of my life in Atlanta.

My time in Atlanta has been filled with wonderful experiences with great friends. I have met some amazing colleagues, friends, and professors at Georgia Tech and Emory University. I especially want to thank my SLARP buddies and fellow biomedical engineering graduate students for their friendship, which I hope will continue to grow stronger over the years. Finally, I would like to acknowledge all the wonderful people I have met through my volunteer experiences with Asha For Education.

This work has been supported in part by the Georgia Institute of Technology NIH training Grant.

TABLE OF CONTENTS

LIST OF TABLES

LIST OF FIGURES

SUMMARY

Biomimetic materials that recapitulate the complex mechanical and biochemical cues in load-bearing tissues are of significant interest in regenerative medicine and tissue engineering applications. Several investigators have endeavored to not only emulate the mechanical properties of the vasculature, but to also mimic the biologic responsiveness of the blood vessel in creating vascular substitutes. Previous studies in our lab generated the elastin-like protein polymer **LysB10**, which was designed with the capability of physical and chemical crosslinks, and was shown to display a range of elastomeric properties that more closely matched those of the native artery. While extensive validation of the mechanical properties of elastin-mimetic polymers has demonstrated their functionality in a number of tissue engineering applications, limited cell growth on the surfaces of the polymers has motivated further optimization for biological interaction. Recent biologically-inspired surface strategies have focused on functionalizing material surfaces with extracellular matrix molecules and bioactive motifs in order to encourage integrin-mediated cellular responses that trigger precise intracellular signaling processes, while limiting nonspecific biomaterial interactions. Consequently, this dissertation addresses three approaches to modulating cellular behavior on elastin-mimetic analogs with the goal of promoting vascular wall healing and tissue regeneration: (1) genetic engineering of elastin-like protein polymers (ELPs) with cell-binding domains, (2) biofunctionalization of elastin-like protein polymers via chemoselective ligation of bioactive ligands, and (3) incorporation of matrix protein fibronectin for engineering of cell-seeded multilamellar collagen-reinforced elastin-like constructs.

We sought to design a second generation elastin-mimetic triblock copolymer with the ability to guide endothelial cell behavior while maintaining the elastomeric properties of the protein polymer. Adhesion-promoting sequences, ligand density, presentation, and clustering,

and ELP morphology were manipulated in order to tailor material properties. Our biomolecular engineering approach introduced cell-adhesive peptide motifs within a bio-inspired recombinant elastin-like protein polymer and was able to elicit an integrin-mediated cellular response.

While genetic engineering has allowed researchers to recombinantly express elastin polypeptides with cell-binding domains and other bioactive ligands to direct cellular behavior, chemical immobilization of short peptides to a recombinant protein polymer surface presents the opportunity to easily incorporate ligands that cannot be processed via the biosynthetic machinery. We were able to develop a bioconjugation strategy for chemoselective ligation of peptides to the recombinant elastin hydrogel surface, and illustrated increased cellular interaction on modified substrates.

Finally, we evaluated the bioactivity and biostability of elastin-mimetic hydrogels with the addition of matrix protein fibronectin. We found that optimized presentation of the fibronectin molecule provided a system in which to present multiple bioactive domains for cellular interaction. Moreover, we utilized this engineered platform to promote cellularization of collagen-reinforced elastin-mimetic multilamellar constructs for vascular tissue engineering applications.

The synthesis of recombinant elastin-like protein polymers that integrate biologic functions of the extracellular matrix provides a novel design strategy for generating clinically durable vascular substitutes. Ultimately, the synthesis of model protein networks provides new insights into the relationship between molecular architecture, biomimetic ligand presentation, and associated cellular responses at the cell-material interface. Understanding how each of these design parameters affects cell response will contribute significantly to the rational engineering of bioactive materials. Potential applications for polymer blends with enhanced mechanical and biological properties include surface coatings on vascular grafts and stents, as well as composite materials for tissue engineered scaffolds and vascular substitutes.

CHAPTER 1

INTRODUCTION

1.1 MOTIVATION AND RATIONALE

Development of a small diameter vascular replacement for coronary bypass surgery has been elusive, even as the incidence of cardiovascular disease remains the leading cause of death in the United States [1]. Limited availability of healthy autologous vessels for bypass grafting procedures has led to the fabrication of prosthetic vascular conduits. Synthetic polymeric materials, while providing the appropriate mechanical strength, lack the compliance and biocompatibility that bioresorbable and naturally occurring protein polymers offer. While these materials are relatively successful in withstanding arterial pressures and are functional as large diameter vascular grafts, they are not suited for small diameter (less than six millimeters) vascular applications due to destructive biological reactions at the blood-material and tissue-material interface [2-5].

Biomimetic materials that recapitulate the complex mechanical and biochemical cues in load-bearing tissues are of significant interest in regenerative medicine and tissue engineering applications. One approach in generating suitable materials is to mirror the multiscale structural hierarchy of the extracellular matrix itself. Thus, proper selection and assembly of scaffolds that replicate the anatomic features of the tissue of interest is vital in promoting tissue integration and directing cellular behavior. The generation of protein polymers that mimic native structural proteins and adopt the characteristics of the vascular wall offers a unique strategy to develop a vascular graft with clinical performance results that match or exceed those of a native vessel. Additionally, endothelialization of the luminal surfaces of vascular conduits has been proposed to mimic the biologic responsiveness of native vasculature. Studies involving the *in vitro*

endothelialization of grafts with cultured endothelial cells prior to implantation have shown that a confluent endothelium prevents thrombogenic complications and improves long-term patency [6-13]. Ultimately, the success of these strategies is dependent on controlling cell-material interactions, including cell migration, adhesion, extracellular matrix production, and proliferation on modified surfaces, in order to drive tissue regeneration and integration.

The development of recombinant elastin-mimetic proteins has demonstrated that through selective engineering of block structure, a wide range of mechanical responses can be produced. Previous studies in our lab have explored the design of elastin-like protein polymers (ELPs) with the capability of physical and chemical crosslinks, and have yielded elastomeric properties that more closely match those of the native artery [14]. Moreover, these protein polymers have been used as non-thrombogenic hydrogel coatings on the luminal surface of ePTFE prostheses [15]. Biocompatibility studies of the elastin-mimetic **LysB10** have revealed long-term *in vivo* biostability and minimal inflammatory responses, which makes **LysB10** an ideal candidate in engineering tissues and biocompatible surface coatings.

The extracellular matrix is a complex structural component of tissues composed of adhesive proteins, growth factors, and proteoglycans. Recent biologically-inspired surface strategies have focused on functionalizing material surfaces with extracellular matrix molecules and bioactive motifs in order to encourage integrin-mediated cellular responses that trigger precise intracellular signaling processes, while limiting nonspecific biomaterial interactions. While extensive validation of the mechanical properties of elastin-mimetic polymers has demonstrated their functionality in a number of tissue engineering applications, limited cell growth on the surfaces of the polymers has motivated further optimization for biological interaction. Consequently, the ***long term goal*** encompassing this work is to engineer bioactive surfaces on elastin-like protein polymers that specifically direct cellular behavior in order to improve vascular wall regeneration. We anticipate that recombinant proteins with enhanced

mechanical and biological properties can be utilized as surface coatings on vascular grafts and stents, and as composite materials for vascular tissue engineering.

1.2 CENTRAL HYPOTHESIS AND SPECIFIC AIMS

The ***central hypothesis*** encompassing the work in this manuscript is that vascular wall regeneration can be achieved with the use of recombinant elastin-mimetic protein polymers that are functionalized with bioactive domains mimicking the extracellular matrix, thus providing a rational approach for generating an elastin substitute for tissue engineered vascular grafts. In particular, elastin analogs that are able to form both physical and chemical croslinks were investigated for their ability to direct endothelial cell and mesenchymal stem cell behavior. Consequently, the ***overall objectives*** of this dissertation are to obtain an understanding of (1) the structural features of recombinant protein polymers and their functionalized derivatives which govern optimized presentation of bioactive molecules within the stable polymer network; and (2) the directed behavior of cells on modified elastin-like substrates.

The central hypothesis was tested with the following specific aims. The goal of ***Specific Aim 1*** was to synthesize and characterize the second generation of recombinant elastin-mimetic protein polymers with genetically engineered cell-binding sequences. We ***hypothesized*** that an elastin analog containing alphavbeta3 integrin-binding sequence V2 would enhance endothelial cell adhesion and migration to the otherwise non-adhesive polymer surface. Moreover, genetic engineering techniques enabled us to control spatial distribution and optimize ligand presentation. We tested the ability of the novel recombinant protein polymer V2 to direct endothelial cell behavior using a number of *in vitro* studies, and the results are presented in Chapter 3.

The goal of ***Specific Aim 2*** was to develop a chemoselective approach to conjugate bioactive peptides to the elastin-mimetic protein polymer hydrogel surface in order to modulate cellular behavior. We ***anticipated*** that the reaction between thiol-derivatized **LysB10** and

maleimide-terminated RGD peptide would enable localized delivery of bioactive ligand for surface functionality. We tested this hypothesis by assessing the ability of conjugated **LysB10**-RGD surfaces to promote endothelial and mesenchymal stem cell adhesion, proliferation, migration, and spreading. These results are presented in Chapter 4.

The goal of ***Specific Aim 3*** was to evaluate the bioactivity and biostability of elastin-mimetic hydrogels with the addition of matrix protein fibronectin. We ***hypothesized*** that optimized presentation of the fibronectin molecule would provide a system in which to present multiple bioactive domains for cellular interaction. Moreover, we anticipated that this engineered platform would promote cellularization of collagen-reinforced elastin-mimetic multilamellar constructs for vascular tissue engineering applications. We tested our hypothesis with a number of *in vitro* endpoints to determine endothelial and mesenchymal stem cell behavior.

1.3 SIGNIFICANCE

The synthesis of recombinant elastin-like protein polymers that integrate biologic functions of the extracellular matrix provides a novel design strategy for generating clinically durable vascular substitutes. The motivation for incorporating biomolecular analogs of elastin into current engineering schemes is two-fold: (1) the generation of a non-thrombogenic acellular conduit will stimulate *in situ* arterial wall regeneration by displaying cell-binding sites and matrix assembly motifs for migration and proliferating vascular wall cells that are repopulating the construct, and (2) fabrication of cell-seeded constructs will promote accelerated vascular tissue regeneration. Ultimately, the synthesis of model protein networks provides new insights into the relationship between molecular architecture, biomimetic ligand presentation, and associated cellular responses at the cell-material interface. Understanding how each of these design parameters affects cell response will contribute significantly to the rational engineering of bioactive materials. Potential applications for polymer blends with enhanced mechanical and

biological properties include surface coatings on vascular grafts and stents, as well as composite materials for tissue engineered scaffolds and vascular substitutes.

CHAPTER 2

Background and Literature Review

2.1 Challenges and current approaches to vascular tissue engineering

Coronary and peripheral vascular bypass graft procedures are performed in approximately 600,000 patients each year in the United States, most commonly with the saphenous vein or the internal mammary artery [1]. Although the use of autogenous vascular substitutes has had a major impact on advancing the field of reconstructive arterial surgery, these tissue sources may be inadequate or unavailable. Moreover, their harvest adds time, cost, and the potential for additional morbidity to the surgical procedure [16-18]. Currently, ePTFE, Dacron, and polyurethane are used to fabricate synthetic vascular grafts [19]. However, owing to thrombus formation and compliance mismatch, none of these materials have proved suitable for generating grafts less than 6 millimeters in diameter that would be required to replace the saphenous vein, internal mammary or radial artery as a vascular substitute [2-5].

The functional importance of normal physiologic responses of the vascular wall in controlling thrombosis and inflammation has guided attempts to closely mimic the native arterial wall in the design of a new generation of vascular prostheses. These features include the structural components collagen and elastin, which are responsible for the tensile strength and viscoelasticity of the blood vessel, and create a fatigue-resistant tissue with long-term durability [20]. Furthermore, the endothelial lining in the native vasculature not only serves as a protective, thromboresistant barrier between blood and the surrounding tissue, but also controls vessel tone, platelet activation and leukocyte adhesion. Other elements that define an ideal biomaterial necessary to the design of a vascular graft are biocompatibility, infection resistance, suturability and off-the-shelf availability.

The first tissue-engineered blood vessel substitute was created by Weinberg and Bell in 1986 [21]. They generated cultures of bovine endothelial cells, smooth muscle cells, and fibroblasts in layers of collagen gel supported by a Dacron mesh. Although physiologic pressures were sustained for only 3 to 6 weeks, they did demonstrate the feasibility of a tissue engineered graft with human cells. Since then, strategies to create a suitable material for a vascular graft have focused on three areas of research: coatings and surface chemical modifications of synthetic materials, biodegradable scaffolds, and biopolymers. Each group can be further organized into tissue engineering strategies for *in situ* vascular regeneration, in which the body's natural healing response is modulated by material design and fabrication, or strategies for *ex vivo* formation of a blood vessel substitute, whereby *in vitro* culture of human cells on polymer substrates before implantation defines their mechanical and biological properties.

Polymer Functionalization

The poor patency rates of synthetic polymers have motivated further strategies to functionalize the luminal surface of grafts and direct tissue regeneration. Coatings, chemical and protein modifications, and endothelial cell seeding on otherwise inert materials have been employed to improve endothelialization and inhibit inflammation [22-25]. As a result, carbon deposition, photodischarge, and plasma discharge technologies have been utilized to deposit reactive groups onto polymer surfaces to interact with cell-specific peptides and influence protein adsorption to the surface [26]. For example, Nishibe and colleagues found that in a dog carotid implant model, fibronectin bonding improved graft healing in high-porosity ePTFE grafts [27]. Recent studies have documented that cell adhesion peptide sequences, such as the P15 peptide found in type I collagen, increase endothelial cell adhesion to ePTFE *in vivo* via integrin-specific binding [28]. Endothelial cell attachment can be significantly improved on surfaces

coupled with another potent adhesion peptide, RGD, when compared with fibronectin-coated grafts [29, 30]. To this end, Zilla and colleagues were able to improve cell retention on shear stressed grafts by precoating them with RGD-crosslinked fibrin [6]. In addition, delivery of growth factors from polymer surfaces has also facilitated the rate of *in situ* endothelialization [28, 31]. For example, ePTFE grafts impregnated with fibrin glue containing fibroblast growth factor (FGF)-1 and heparin have promoted transmural endothelialization and smooth muscle cell proliferation in a dog model [32-34].

Several investigators have endeavored to endothelialize the luminal surfaces of synthetic vascular grafts to mimic the biologic responsiveness of the native vasculature [6-13]. The success of cell transplantation is limited because of difficulties in cell sourcing and cell attachment and retention during pulsatile flow conditions [35]. Strategies that promote *in situ* regeneration of a functional endothelial lining have also met with difficulties owing to chronic inflammatory and prothrombotic responses to the synthetic polymeric materials [36]. Endothelial cells that display a procoagulant phenotype can, in principle, promote rather than retard thrombosis [37]. Furthermore, activated ECs may increase growth factor production and secretion that encourages smooth muscle cell (SMC) proliferation. Indeed, subintimal SMC proliferation occurs predominantly in areas that have an overlying endothelium [33]. This response can be seen with ePTFE grafts coated with anti-CD34 antibodies and implanted in pigs [38]. While the antibodies are able to capture endothelial progenitor cells and increase endothelial cell coverage, intimal hyperplasia at the distal anastomosis is significantly increased at four weeks. The high rates of aneurysm and thrombus formation on vascular substitutes have led researchers to focus on modulating adverse inflammatory responses. One such example is the creation of nitric oxide (NO)-producing polyurethanes, in which the NO donor diazeniumdiolate is covalently bound to a polyurethane backbone [39]. Nitric oxide is produced by endothelial cells and functions to regulate vascular tone, prevent platelet aggregation, and

inhibit smooth muscle hyperplasia. Consequently, *in vitro* studies investigating the release of nitric oxide from modified polyurethane films have determined that the material does reduce platelet adhesion and vascular smooth muscle cell growth, while stimulating endothelial cell growth [40].

Degradable Scaffolds

The use of biodegradable polymers as scaffolds on which layers of cells are grown is an alternate tissue engineering approach for the development of a functional vascular graft. The scaffold degrades and is replaced and remodeled by the extracellular matrix (ECM) secreted by the cells. Polyglycolic acid (PGA) is commonly used in tissue engineering applications as it degrades through hydrolysis of its ester bonds, and glycolic acid, in turn, is metabolized and eliminated as water and carbon dioxide. PGA loses its strength *in vivo* within 4 weeks and is completely absorbed by 6 months. Biodegradation rates can be controlled by copolymerization with other polymers, such as poly-L-lactic acid (PLLA), polyhydroxyalkanoate (PHA), polycaprolactone-copolylactic acid, and polyethylene glycol [41-48].

Several investigators have explored the potential of PGA composite scaffolds in fabricating vascular conduits *in situ and ex vivo.* For example, partially resorbable Dacron grafts have facilitated infiltration and proliferation of vascular cells, and promotion of capillary growth [49]. The regenerative potential of these conduits has led to further PGA and Dacron fiber blends with the purpose of optimizing compositional ratios for *in vivo* healing responses and graft strength maintenance [50, 51]. As *in situ* regeneration via polymer degradation limits exact control over the remodeling process, other groups have demonstrated the ability to construct functional grafts *ex vivo*. Mooney and colleagues have seeded cells onto a PLLA/polylactide-coglycolide (PLGA) copolymer-coated PGA mesh [46, 52]. Similarly, Vacanti and colleagues used PLGA to generate capillary networks for artificial microvasculature applications [53].

Furthermore, Niklason and colleagues have developed a pulsatile bioreactor to remodel PGA scaffolds seeded with bovine smooth muscle and endothelial cells [54]. After a 10-week culture period, the resulting tissue engineered vessel displayed a burst pressure of up to 2300 mm Hg. After 5 weeks, the PGA scaffold had degraded to 15% of its initial mass. Consequently, mechanical stability was dependent on smooth muscle cell production of collagen and culture medium supplements that promoted collagen crosslinking. Although the lumen of the graft did not present a confluent endothelium lining, vessels did display contractile responses to serotonin, prostaglandin, and endothelin-1, and implants remained patent for 1 month in a swine model. Attempts to translate this approach to human cells have led to poor mechanical properties due to the limited proliferative capacity of human SMCs, especially when harvested from elderly patients. In addition, the notable absence of elastic fibers could limit fatigue resistance and predispose the vessels to subsequent aneurysmal degeneration.

Polyhydroxyalkanoates (PHA), linear polyesters that are produced by bacterial fermentation of sugar or lipids, have also been employed in graft design, as they can be modified to display a wide range of degradation rates and mechanical properties. Shum-Tim et al. engineered an aortic graft consisting of a polymer scaffold of PGA and polyhydroxyoctanoate (PHO) seeded with ovine carotid artery cells [55]. The inner layer of the construct was made of nonwoven mesh of PGA fibers, while the outer layers were composed of nonporous PHO. The PGA scaffold promoted cellular growth and extracellular matrix production, while the slower degradation rate of PHO provided mechanical support as this remodeling occurred. Significantly, the graft did not require extensive *in vitro* conditioning. The construct was implanted directly in the abdominal aorta of lambs with 100% patency noted at five months. Histological analysis revealed that the remodeled graft contained uniform collagen and elastin fibers that had aligned in the direction of blood flow. The mechanical stress-strain curve of the engineered construct approached that of the native vessel, although some permanent

deformation was observed six months after implantation, indicating either insufficient or non-crosslinked elastin. Fu and colleagues investigated the effects of ascorbic acid and basic fibroblast growth factor, which stimulated cells on a PGA-poly(4-hydroxybutyrate) construct to proliferate and generate large quantities of collagen, thereby accelerating the improvement in mechanical integrity [56].

Yet another versatile polymer, polycaprolactone (PCL), slowly degrades by hydrolysis of ester linkages, with elimination of the resultant fragments by macrophages and giant cells. Shin'oka et al. reported the use of PCL-based scaffolds to engineer venous blood vessels [57, 58]. The PCL-PLA copolymer was reinforced with woven PGA and seeded with autologous smooth muscle and endothelial cells harvested from a peripheral vein. After 10 days, the construct was implanted as a pulmonary bypass graft into a four-year old child [59]. Subsequent studies with autologous bone marrow cells on the constructs have reported > 95% patency at a mean follow-up of 16 months [60]. Further evaluation of endothelial cell function and mechanical properties of vascular grafts constructed with autologous bone marrow cells was conducted with a canine inferior vena cava model [61]. Interestingly, the biochemical properties and wall thickness of cell-seeded scaffolds were similar to those of the vena cava 6 months after implantation.

Biodegradable polymer systems provide the opportunity for spatial and temporal release of various growth factors to promote vascular wall regeneration. For example, vascular endothelial growth factor release from PLGA scaffolds has been shown to promote angiogenesis *in situ* [62]. Likewise, FGF-2 release from poly(ester urethane) urea (PEUU) scaffolds amalgamates the favorable mechanical properties of polyurethanes with the bioactivity of an angiogenic protein [63]. While degradation via hydrolysis serves as a powerful tool in vascular tissue engineering to control the release of bioactive molecules from the polymer

matrix, incorporation of proteolytic sites into the material can further optimize presentation of these molecules to the surrounding environment via cell-mediated degradation.

Although tissue-engineered vascular grafts based on biodegradable scaffolds have yielded promising results, some drawbacks exist. Challenges of cell sourcing are compounded by long culture periods that range between 2 and 6 months, and the proliferative capacity of cells isolated from elderly patients is limited. The mechanical strength of the materials may be comparable to that of native vessels, but compliance mismatch limits long-term patency.

Biopolymers

An alternative strategy to synthetic and degradable scaffold-based vascular grafts is the manipulation of proteins that constitute the architecture of native ECM. The generation of protein polymers that mimic native structural proteins and adopt the characteristics of the arterial wall offers a unique approach to develop a vascular graft. Ultimately, the success of this approach is dependent on appropriate cell migration, adhesion, and proliferation, as well as extracellular matrix production, on the biomimetic surfaces.

One such protein is Type I collagen, a major ECM component in the blood vessel [64]. Collagen fibers function to limit high strain deformation, thereby preventing critical rupture of the vascular wall [65, 66]. Collagen gels and fibers reconstituted from purified collagen are ideal in artificial blood vessel development due to their low inflammatory and antigenic responses [67]. Furthermore, integrin binding sequences in collagen allow for cell adhesion during fibrillogenesis. As mentioned previously, Weinberg and Bell first reported the use of collagen gels as substrates for cells in vascular tissue engineering. Since then, Habermehl and colleagues have developed a process to obtain large quantitites of collagen from rat tail tendons to scale up production [68].

Variables such as fiber orientation, crosslinking conditions, and cell seeding techniques have been explored to improve the mechanical integrity of collagen-based constructs. A wide range of crosslinking agents can enhance covalent links between the collagen fibers, the most efficient of which is glutaraldehyde [69]. The cytotoxicity of this chemical, however, has led to the development of alternative crosslinking mechanisms, such as the cytocompatible chemical genipin, the enzymatic reactions of lysyl oxidase and transglutaminase, as well as photocrosslinking [70-72]. Various groups have investigated fiber orientation and smooth muscle cell alignment as a means to increase mechanical properties in the circumferential direction of a tubular construct [73-75]. Preconditioning treatments involve applying mechanical strain or shear stress to the construct and compaction of SMC-containing collagen gels around a mandrel in order to increase mechanical strength [76-78].

The shortcomings of a stiff collagen-based scaffold have motivated researchers to explore the potential of more elastic fibrin gels in vascular tissue engineering [79]. Fibrin is formed when fibrinogen polymerizes into a fibrillar mesh with the addition of thrombin. An advantage of this biopolymer is the ability to produce it with the patient's own blood, thereby preventing an inflammatory response upon implantation [80]. Fibrin also binds to critical proteins that direct cell fate, such as fibronectin and vascular endothelial growth factor [81]. *In vivo* degradation can be controlled with the proteinase inhibitor aprotonin and crosslinking agents, although there are concerns that the concentrated presence of these natural proteins may interfere with local coagulation cascades [82].

Interestingly, smooth muscle cells embedded in fibrin gels produce more collagen and ECM than cells that are entrapped in collagen gels [83]. One such example is the fibrin-based vascular graft developed by Swartz and colleagues, who incorporated ovine SMCs and endothelial cells into the gel [84]. The grafts were implanted in the jugular veins of lambs, and remained patent for 15 weeks. Upon histologic examination, the constructs were found to

contain both collagen and elastin, with the mechanical integrity comparable to that of native coronary arteries. Furthermore, Tranquillo and colleagues demonstrated that the enmeshed SMCs directed compaction and alignment of both the fibrin fibers and the cell-synthesized collagen fibers in a circumferential orientation around a nonadhesive mandrel [85].

The elasticity afforded by fibrin-based grafts is a critical factor in vascular tissue engineering design. Researchers have also explored the potential of incorporating scaffolds with more extensible proteins such as elastin, a key structural element in native vasculature. Crosslinked elastic fibers form concentric rings around the medial layer of arteries, providing elasticity to the vascular graft by stretching under a stress and recoiling back to the original dimensions as the load is released [86-89]. In addition, elastin regulates vascular smooth muscle cell activity by inhibiting SMC proliferation. Unlike collagen, the stable crosslinked fiber network of native elastin makes isolation and purification techniques difficult. Therefore, different strategies have emerged to incorporate elastin into tubular constructs. Whereas some investigators have attempted to promote elastogenesis in vascular grafts indirectly with smooth muscle cell culture techniques [90-92], others have developed protocols to process insoluble and soluble elastin [93]. One such example includes a freeze-drying protocol for collagen and elastin to produce a porous scaffold [94].

More recently, the development of recombinant genetic and protein engineering has enabled the synthesis of bio-inspired protein polymers that not only mimic structural proteins but also direct cellular fate by emulating the extracellular matrix *in vivo* [95-98]. Specifically, polymers with pentapeptide repeat motifs similar to VPGVG exhibit elastic behavior with features that are consistent with native elastin, including a mobile backbone and the presence of beta turns [99-102]. The biosynthetic machinery of micro-organisms can be exploited to produce significant quantities of these recombinant protein polymers that have been designed from primary amino acid sequences and self-assemble into a distinct three-dimensional folded

structure [100, 103]. These elastin-mimetic biopolymers, in turn, can be cast as hydrogels or electrospun into nanofibrous scaffolds [104-108].

Nanocomposites

Recent developments in the field of nanotechnology have facilitated vascular tissue-engineering efforts in mimicking the nanostructure of native vasculature, thereby directing mechanical and biologic performance of the bulk material. One such application is electrospinning of synthetic polymers and naturally occurring materials into nanofibers [41, 101, 109-111]. The advantages of this strategy include the ability to form scaffolds with high porosity as well as high surface area-to-volume ratio, thus simulating the dimensions and structure of native collagen and elastin fibrils [112, 113]. In particular, He and colleagues have demonstrated the utility of electrospinning with the generation of a nanofibrous scaffold composed of collagen-blended degradable poly(L-lactic acid)-co-poly(ε-caprolactone) [114]. Results indicated that the blended nanofibers supported endothelial cell attachment and spreading, and preserved the endothelial cell phenotype.

Enhancement of base material properties with the addition of fillers has resulted in various nanocomposites. In general, these materials have demonstrated a reduction in thrombogenicity while improving mechanical properties. For example, Kannan and colleagues have generated a polymer based on poly(carbonate-urea)urethane (PCU) and polyhedral oligomeric silsesquioxane nanoparticles, and have reported the nanocomposite's heparin-like behavior at the blood-material interface [115, 116]. Furthermore, the polymer displayed a greater degree of compliance match to natural arteries compared to ePTFE and Dacron. Other groups have utilized the strength and flexibility of carbon nanotubes as fillers to enhance base polymer properties [117, 118]. These efforts have indicated that although the composite

polymers decrease thrombogenicity on their surfaces, toxicity of carbon nanotubes remains a concern [119, 120].

Biologic Tissue Sources

Decellularized allogeneic or xenogenic tubular tissues that contain an intact and structurally organized ECM have been investigated as vascular conduits, which include human umbilical vein and bovine and porcine carotid arteries. Although a readily available supply of artificial arteries is attractive, drawbacks include the inability to tailor matrix content and architecture, progressive biodegradation, and the risk of viral transmission from animal tissue. Decellularization removes most cellular antigenic components in allogeneic and xenogeneic tissue. A combination of physical agitation, chemical surfactant removal, and enzymatic digestion disrupts cells and removes protein, lipids, and nucleotide remnants [121-124]. Following decellularization, chemical crosslinking is used to enhance mechanical strength and reduce immunogenicity [125, 126]. The addition of an external support such as a Dacron mesh is also common to provide mechanical strength and prevent late dilation. Efforts to improve the durability and the healing response of decellularized scaffolds have included coating with heparin and FGF, as well as seeding with endothelial cells, bone marrow-derived cells, and adipose-derived stem cells [127-135].

Alternative tubular tissue sources have been utilized as vascular substitutes as well. For example, decellularized small intestinal submucosa (SIS) is composed of collagen, fibronectin, proteoglycans, growth factors, glycosaminoglycans, and glycoproteins [136]. Consequently, implantation of the SIS construct as a vascular graft leads to neovascularization, host cell migration and adhesion, and matrix remodeling [137-140]. The development of a tissue-engineered vascular conduit from yet another avascular tissue source has been documented by Campbell and colleagues [141]. The intraperitoneal graft model employs the peritoneal cavity

as an *in situ* bioreactor for the creation of a tubular construct seeded with layers of host cells. The investigators observed that foreign objects implanted into the peritoneal cavity became encapsulated by a fibrous capsule containing myofibroblasts and a surrounding layer of mesothelial cells [142]. They then inserted Silastic tubing into the peritoneal cavities of dogs, rabbits, and rates. After 2 to 3 weeks, the tubing was removed, and the cell-encapsulated construct was grafted into the carotid artery (rabbit), abdominal aorta (rat), and femoral artery (dog) of the animal in which it was grown [143, 144]. Remodeling of the autologous grafts included differentiation of myofibroblasts to smooth muscle-like cells, increased wall thickness, elastin and collagen production, and circumferential alignment of cells and matrix proteins [145]. The constructs displayed endothelium-dependent relaxation when stimulated with acetylcholine and were patent in rabbits for at least 16 months and in dogs for 6.5 months.

Recently, sheet-based tissue engineering and bioreactor conditions have enabled the expansion of *in vitro* culture of cells into a cohesive cell sheet comprised of various cell types and endogenously expressed extracellular matrix. Thermoresponsive polymers, such as poly N-isopropylacrylamide and methylcellulose, have served as coatings on culture flasks in order to facilitate the removal of cultured cells and underlying ECM as a uniform sheet. These sheets have been further processed into blood vessels by layering and wrapping them around a mandrel for incubation [146-148]. While this maturation period can be as extensive as ten weeks, the resulting graft does not require exogenous biomaterials for mechanical support. L'Heureux at al have demonstrated the utility of assembling arterial bypass grafts exclusively from a patient's own cells by implanting the substitutes into primate models [149]. *In vivo* results indicated that the grafts were antithrombogenic and mechanically stable for 8 months, with histology and microscopy displaying complete tissue integration, regeneration of a vascular media, as well as elastogenesis and a collagen fiber network.

Concluding Remarks and Future Perspectives

The development of a synthetic arterial substitute represents a major milestone of twentieth century medicine yielding technology that has saved the lives of millions of patients. Nonetheless, a durable small-caliber (d<6mm) conduit remains elusive, and patency rates for infrainguinal revascularization through the use of a prosthetic graft have changed little over the past 30 years. The challenges of creating the ideal tissue engineered vascular substitute are numerous, but significant progress has been made to understand the importance of both the mechanical and biologic requirements of biomaterials for this application. Investigators continue to strive for the generation of multifunctional materials with optimized release and presentation of bioactive molecules in order to guide *in situ* vascular regeneration. For example, the challenges of sufficiently balancing polymer degradation rates with ECM production and cellular infiltration has resulted in polymers designed with cell-binding sequences, enzymatic cleavage sites, and tethering of chemoattractant molecules [150, 151]. This “bottom-up” approach to materials design enables researchers to finely modulate the nanostructure of a material in order to influence its bulk properties. The success of these efforts will depend on the generation of composite scaffolds that mimic the complexity of native vascular matrix in order to improve elasticity and compliance of the native blood vessel while inhibiting adverse responses at the blood-material interface. *In vitro*, *in vivo*, and computational models are also providing new insights into the complex interplay of cellular, biochemical, and biomechanical processes that lead to graft failure. However, a better understanding of vascular progenitor cell biology is required to harness the potential of progenitor cells in endothelialization of arterial grafts. Through continued collaboration among vascular surgeons, biologists, material scientists, and biomedical engineers, existing barriers in the creation of an arterial substitute will undoubtedly be broken.

2.2 Extracellular Matrix (ECM): Composition and Role

The extracellular matrix is a meshwork of fibrous proteins surrounded by glycosaminoglycans, growth factors, and cytokines sequestered by the matrix [152] . These components provide mechanical support to resident cells and serve as biochemical cues for intracellular communication. Moreover, most cells are able to actively secrete and remodel the extracellular matrix during tissue formation and repair. ECM proteins are multifunctional molecules, and include collagen, elastin, fibronectin, fibrinogen, vitronectin, and laminin [153].

While ECM proteins play fundamental roles in providing mechanical stability to cells, they also serve to promote cell adhesion and intracellular signaling critical to tissue function. The interaction between ECM molecules and cell surface receptors regulates cell behavior by activating intracellular pathways, and results in precise alterations in cell spreading, migration, and differentiation [154]. In particular, cells recognize ECM ligands primarily via integrins. Integrins are transmembrane , heterodimeric proteins consisting of two associated subunits (alpha and beta) [154]. While integrins bind to the ECM through their extracellular domains, they are linked to the cytoskeleton via intracellular domains. Most integrins recognize key motifs as binding sites, such as the ubiquitous arginine-glycine-aspartic acid (RGD) sequence present in a variety of ECM proteins. Integrin binding is a dynamic process that requires mechanical coupling to the ligand. This activation involves conformation changes in the receptor into high affinity orientations, which then translates intracellularly into aggregation and clustering of focal adhesion molecules. Ultimately, focal adhesion formation leads to stable links between the ECM and cellular cytoskeleton, as well as activation of discrete signaling pathways. The coupling of integrins and ECM ligands modulates and directs a number of cell functions, including adhesion, spreading, proliferation, migration, transcription factor activity, and differentiation [154]. Engagement of distinct integrins will often direct particular cell responses in various tissues. For example, interaction with alphavbeta3 integrins leads to endothelial cell proliferation and migration.

2.3 Fibronectin

Fibronectin is a 440 kDa matrix associated glycoprotein that is found as a fibrillar network in the ECM and in the blood plasma at a concentration of approximately 300 ug/mL [155]. Fibrillar fibronectin matrix is also secreted and organized by cells themselves, and is responsible for regulating a number of cell functions via intracellular signaling pathways, including cell cycle progression, migration, differentiation, and assembly of other ECM components [156-158]. The protein exists as a dimer that is covalently linked by two disulfide bonds near the C-terminus of each monomer. In addition, each monomeric unit is composed of repeating domains named type I, II, and III, which in turn are grouped together into functional domains with specific bioactivity. Fibronectin serves as a multifunctional ligand that binds directly to cells, as well as heparin, collagen, and fibrin molecules, thereby modulating the ECM microenvironment [159].

Pretreatment of vascular grafts with fibronectin has been investigated by several groups in order to improve *in vitro* and *in vivo* endothelialization of graft surfaces [160]. Fibronectin has been shown to improve endothelial cell binding and spreading, and to enhance shear stress-induced adhesion strength with the onset of blood flow. For example, Nishibe and colleagues covalently bonded fibronectin to the luminal surface of ePTFE grafts and demonstrated accelerated transmural tissue ingrowth and neointima formation in both canine and porcine models [27, 161]. Although there were concerns that fibronectin treatment would increase graft thrombogenicity due to platelet activation and adhesion, no significant decrease in patency was observed. On the contrary, thrombus area was significantly lower on fibronectin-coated grafts compared to untreated ePTFE grafts.

2.4 Fibronectin-derived integrin-selective ligands

Fibronectin contains many cell recognition sites that, when isolated, are able to mimic the biological activity of the entire ECM molecule to varying degrees. The most well-known sequence is the peptide RGD, which is recognized primarily by the alpha5beta1 and alphavbeta3 integrin receptors, but has also been found to bind to approximately 12 other receptors [162]. For this reason, RGD is most often employed in coating synthetic surfaces for enhanced biological interaction. The sequence is able to maintain both affinity and specificity when flanked by residues taken from the native protein. For example, it has been shown that linear GRGDSP retains the highest bioactivity, followed by RGDS, and then RGD [163]. Recombinant fragments of fibronectin incorporating the 10^{th} type III repeat (RGD) and the 9^{th} type II repeat (PHSRN or synergy site) have demonstrated over a 40-fold increase alpha5beta1 integrin selectivity and adhesion strength [164]. Furthermore, conformation of the sequence itself influences the manner in which it is presented to the cell receptor, and has been shown to regulate integrin selectivity. In particular, the cyclopeptide RGD enhances binding to the alphavbeta3 integrin over the linear sequence [165]. In addition, immobilized cyclic RGD peptides have been able to support higher shear stress cell detachment resistance compared to linear peptides [166, 167]. Cyclic RGD coating of stents deployed in porcine coronary arteries resulted in increased endothelial cell coverage as well as reduced neointimal and stenosis areas [167].

The lack of integrin specificity associated with RGD is tempered by another fibronectin-derived ligand, REDV. REDV was isolated from the alternatively spliced V region of fibronectin distant from the central cell-binding domain (residues 1-25 of the IIICS), and was found to primarily associate with alpha4beta1 integrin, which is expressed in a limited number of cell lines, including leukocytes, endothelial cells, and some muscle and fibroblast cell lines, but not in platelets [168, 169]. For example, investigators found that REDV peptides coated on microfluidic devices and subjected to shear stress preferentially bound to endothelial cells over smooth muscle cells [170].

Most cell types remodel synthetic substrates by depositing their own ECM in order to ensure effective biochemical and mechanotransduction signaling. An important facet of ECM architecture and fibronectin functionality is the self-assembly of fibronectin monomers into a fibrillar structure. This process is facilitated by fibronectin-fibronectin binding domains in the protein itself. In particular, a 13-amino acid sequence, AHEEICTTNEGVM, isolated from the fibronectin collagen binding domain, nucleates the assembly of robust fibrillar fibronectin matrix, which in turn serves as a template for collagen I fiber assembly and enhanced cellular responses, such as high cell adhesion and proliferation rates [171]. Based on the relationship between matrix assembly and FN13 density, a nucleation theory was proposed for the functionality of FN13, in which the sequence bridges extended forms of the fibronectin dimer, thereby assisting matrix assembly [172]. Ultimately, the significance of a FN13-functionalized material lies in its ability to directly promote cell-mediated synthesis of fibrillar ECM in order to control cellular function.

2.5 Laminin-derived motifs

Laminins are a family of heterotrimeric glycoproteins that assemble into a crosslinked network, interwoven with type IV collagen fibers [173]. Bioactive domains within laminin have been identified as short motifs which regulate cell functions, including the ever-present RGD sequence. Furthermore, YIGSR peptide-functionalized materials promote adhesion and spreading of numerous cell lines, including endothelial cells, fibroblasts, smooth muscle cells, and nerve cells [174-176]. Interestingly, YIGSR does not interact with integrins on the cell surface, but binds to a 67-kDa laminin receptor (67LR) [177]. Previous *in vitro* studies demonstrated that YIGSR incorporated into a polyurethane urea backbone (PUUYIGSR-PEG) inhibited platelet adhesion while increasing endothelial cell adhesion, spreading, and migration [178, 179]. However, in comparison to the RGD motif, YIGSR displays slower spreading rates

and less focal adhesion formation. Other studies have located the IKVAV sequence, which has been able to promote neurite outgrowth, cell adhesion, and tumor growth [180].

2.6 Collagen-mimetic and elastin-derived cell-adhesive ligands

Adhesion sequences have been identified that regulate collagen-integrin interactions, including the peptide DGEA and the alpha2beta1-specific hexapeptide sequence GFOGER from collagen I. Once again, tertiary structure plays a key role in the affinity and adhesive strength of these motifs, with a stable triple-helical structure presenting the ligand to the integrin binding site. While immobilized DGEA peptide from collagen was reported to mediate alpha2beta1 integrin-based neurite outgrowth [181, 182], extensive work with GFOGER peptide coatings have targeted the alpha2beta1 receptor on osteoblasts for improved bone formation, matrix calcification, and functional osseointegration [183, 184].

The sequence VAPG, isolated from elastin, is a non-integrin binding ligand that interacts with the laminin receptor 67LR, and has proven to be a potent chemoattractant to fibroblasts, endothelial cells, smooth muscle cells, and certain tumor cells [185]. However, surfaces coated with VAPG have demonstrated enhanced smooth muscle cell adhesion compared to endothelial cells and fibroblasts [170].

2.7 CCN1 and its biomimetic derivatives: Role in vascular regeneration

We have chosen to utilize a non-RGD ligand isolated from CCN1, a matrix-associated protein known to play a critical role in vascular tissue regeneration and wound healing [186-190]. CCN1, or cysteine-rich 61, is a secreted heparin-binding protein of 40 kDa that displays pro-angiogenic activities, including endothelial cell adhesion, migration, proliferation, and tubule formation [191]. As a regulator of vascular development, CCN1 controls a set of genes responsible for angiogenesis and matrix remodeling. CCN1-null mice undergo embryonic death due to vascular defects in the placental labyrinth and loss of vascular integrity in the embryo.

Furthermore, larger vessels of CCN1-deficient mice display a disorganized basal lamina, a reduced number of smooth muscle cells, and apoptotic vascular cells [192]. Overexpression of CCN1 promotes vascularization and tumor growth, and is associated with human breast cancer [186, 193]. The protein also promotes migration and adhesion of circulating endothelial progenitor cells, while inducing them to secrete various growth factors and chemokines to remodel the vascular wall [194].

CCN1 is non-covalently associated with the extracellular matrix and communicates with cells via interactions between distinct sequences and cell surface integrins [195, 196]. The protein is organized into four structural domains with sequence similarities to: insulin-like growth factor-binding protein (domain I), von Willebrand factor type C repeat (domain II), thrombospondin type I repeat (domain III), and carboxyl-terminal domains of extracellular matrix proteins such as mucins (domain IV). Mechanistically, distinct integrins are involved in mediating the role of CCN1, depending on cell type and function. For example, CCN1 binds directly to alphavbeta3 to mediate a range of biological responses, such as promoting cell adhesion and survival, stimulating chemotaxis, and inducing DNA synthesis and tubule formation [197]. CCN1 protects activated endothelial cells from apoptosis by ligation to integrin $\alpha_v\beta_3$ and supports smooth muscle cell adhesion and migration through $\alpha_6\beta_1$ with heparan sulfate proteoglycans (HSPGs) as coreceptors [198]. Furthermore, adhesion to CCN1 in platelets and monocytes is mediated through integrins $\alpha_{IIb}\beta_3$ and $\alpha_M\beta_2$, respectively [199]. Paradoxically, CCN1 induces fibroblast apoptosis through adhesion receptors $\alpha_6\beta_1$ and HSPG syndecan-4 [200].

Previous analysis of a C-terminal truncated CCN1 mutant indicated the presence of an integrin alpha6beta1 binding site within the first three domains. A 17-residue sequence, designated T1 (GQKCIVQTTSWSQCSKS), was first isolated from domain III of CCN1, and was found to be a novel integrin alpha6beta1 binding site in fibroblasts [201]. It is also recognized as

a regulator in angiogenesis due to observations that T1 blocks CCN1-induced endothelial tubule formation. Thus, T1 provides the basis for the development of peptide mimetics to examine the role of alpha6beta1 in CCN1-induced angiogenesis. Additional binding sites were discovered in the 16-residue sequences, H1 (KGKKCSKTKKSPEPVR) and H2 (FTYAGCSSVKKYRPKY), isolated from domain IV of CCN1, with the ability to support alpha6beta1- and HSPG-dependent cell adhesion [202].

Previous studies also indicated the presence of an alphavbeta3 binding site within the first three domains of CCN1. Furthermore, deletion analysis revealed that a fragment containing domains II and III was sufficient to support alphavbeta3- mediated cell adhesion. This study led to an analysis of a panel of synthetic peptides to determine the exact region of biological activity. Thus, a 20 amino acid sequence in the von Willebrand factor type C repeat (domain II) of CCN1 was identified as a site that binds specifically to the alphavbeta3 integrin [203]. The sequence (NCKHQCTCIDGAVGCIPLCP) supports alphavbeta3- mediated endothelial cell adhesion in a dose-dependent manner, with the aspartate residue playing a key structural role in presenting the peptide to the ligand-binding pocket of the integrin. These conclusions were based on the following observations: (1) while immobilized V2 peptide was shown to support HUVEC adhesion, blocking studies revealed that addition of the integrin alphavbeta3 antagonist LM609 inhibited this adhesion. (2) Soluble V2 was able to prevent direct binding of purified alphavbeta3 to full-length, wild type CCN1 in a dose-dependent manner. (3) Alanine substitution of the single aspartate residue completely abolished the adhesion of HUVECs to the V2 peptide.

Although V2 peptide does not bear any similarities in sequence homology to other ligands of alphavbeta3, it does contain certain amino acids thought to be important in binding the integrin. For example, the aspartate residue has been identified to play a key role in ligand binding to alphavbeta3 [204, 205]. Furthermore, studies on disintegrins and phage display analysis of alphavbeta3 binding sites have suggested that flanking cysteine residues may form

disulfide bonds to present binding sequences as a loop to the integrin active site [206-208]. While the aspartate and cysteine residues in V2 are critical to the peptide's functionality, the presence of disulfide bonds within the V2 peptide has not been explored.

2.8 Structural requirements in designing a vascular graft

The challenges of vascular tissue engineering include mechanical strength, elasticity, compliance match to the adjacent native vessel, and non-thrombogenicity. A detailed look at the vessel anatomy is instructive in addressing these challenges. While the tunica intima is composed of a non-thrombogenic endothelial monolayer and the tunica adventitia provides structural support with collagenous extracellular matrix and fibroblasts, the tunica media is composed of lamellar units of smooth muscle cells, elastin fibers, and collagen fibrils [87]. The elastic lamellar units are arranged in concentric rings around the arterial media, and enable the artery to maintain physiologic systolic and diastolic blood pressures. In particular, elastin is the dominant extracellular matrix protein deposited in the medial layer, and comprises 50% of the arterial wall's dry weight. Smooth muscle cells secrete the monomer tropoelastin (72 kDa) as a soluble protein, and post-translational modifications such as enzymatic crosslinking via lysyl oxidase result in an insoluble elastin matrix. The elastin monomer is organized into hydrophobic and crosslinking domains. While the hydrophobic domains are rich in the amino acids valine, glycine, and proline, lysine residues separated by alanines facilitate intermolecular crosslinking [209-211].

Elastin and collagen play critical structural and regulatory roles in the arterial wall by dictating tissue mechanics in response to blood flow. Stiff collagen fibers prevent aneurysm formation by limiting high strain deformations. Elastin, in contrast, allows for distensibility and elastic recovery in low-strain environments, thereby preventing tissue creep due to cyclic loading. Elastin also maximizes the resilience, durability, and health of the blood vessel tissue

by absorbing energy from mechanical loading of the arterial wall and releasing that energy in the form of diastolic blood pressure rather than dissipating that energy as heat [86, 88, 89, 212]. Furthermore, elastin regulates vascular smooth muscle cell proliferation, phenotype, and organization by participating in biomechanical signaling between vascular smooth muscle cells and the surrounding extracellular matrix [213, 214]. This bioactivity is especially crucial in inhibiting intimal hyperplasia.

2.9. Protein engineering: a biosynthetic strategy for the fabrication of a vascular graft

The native blood vessel's matrix composition and architecture have been closely studied to elucidate structure-function relationships. The ability to tailor the mechanical and biologic performances of polymers for vascular tissue engineering applications is similarly dependent upon the monomeric building blocks. The development of recombinant protein engineering enables the synthesis of bio-inspired protein polymers that not only mimic structural proteins but also direct cellular fate by emulating the extracellular matrix *in vivo*. The biosynthetic machinery of micro-organisms can be exploited to produce significant quantities of recombinant protein polymers that have been designed from primary amino acid sequences and translate to a distinct three-dimensional folded structure [96, 97, 100, 103, 215]. The most significant impact of this strategy is the capacity to introduce precise changes in the amino acid sequence to modulate properties of the entire protein network.

The protein engineering process begins by cloning a selected artificial gene and verifying its sequence. The gene is then placed in a second expression vector that contains a promoter site for recognition by mRNA polymerase and regulation of protein production from the gene of interest. The expression plasmid is transformed into the bacterial host, and the host cells are allowed to grow to high cell density. After sufficient cell density is reached, expression of the desired protein is induced. As a final step, protein purification techniques isolate the desired product from crude bacteria cell lysates.

2.10 Rational design of peptide sequences for elastin-mimetic protein polymers

Native elastin's intrinsic insolubility has limited its use in biomedical applications. Unlike collagen, the stable crosslinked fiber network of native elastin makes isolation and purification techniques difficult. However, structural and sequence analyses of tropoelastin have determined that pentapeptide repeat motifs similar to VPGVG exhibit elastic behavior with features that are consistent with native elastin, including a mobile backbone and the presence of β turns [99, 101]. Genetic and protein engineering techniques have enabled the synthesis of protein polymers containing these repeat domains [102]. Furthermore, elastin-like protein (ELP) polymers display an inverse temperature transition (T_t), defined by their high solubility and random coil conformations in aqueous solutions and ordered structure formation upon raising the temperature of the system [216]. The loss of entropy resulting from the β-spiral conformation is compensated by the release of multiple water molecules from the polymer chain [99]. The elastic properties of the polymer are maintained with the valine, proline, and glycine residues [102, 106]. However, the coacervation temperature can be modulated by varying the fourth (X) position residue in the pentapeptide (VPGXG) sequence [217]. While hydrophobic residues lower the T_t of the protein polymer, polar amino acids such as glutamic acid increase the phase transition temperature. Other parameters that affect the T_t are pH, protein concentration, and the relative proportions of hydrophobic and hydrophilic residues [106]. In addition, substituting an alanine residue in place of the third glycine in the repeat sequence changes the mechanical properties of the polymer from elastomeric to plastic.

The synthesis of amphiphilic triblock ELP copolymers (ABA) consisting of hydrophobic (A) and hydrophilic (B) domains results in the formation of a hydrogel. The copolymer undergoes selective aggregation of the more hydrophobic blocks above their T_t to form a physically crosslinked network, while the hydrophilic domains remain solvated in an aqeous solution [218, 219]. Thus, elastin-mimetic protein copolymers represent a unique class of

thermoreversible hydrogels for tissue engineering applications, as their gelation properties can be finely tuned for physiologically relevant conditions. More specifically, Chilkoti and colleagues have demonstrated the potential of elastin-like block copolymers as injectable biomaterials that can form *in situ* load-bearing hydrogel scaffolds [220]. Additional studies conducted by Keeley and colleagues as well as Chaikof and coworkers have reported that platelet activation and adhesion is minimal on recombinant elastin-like polymer surfaces [15, 221]. This feature makes them attractive candidates for blood-contacting materials such as non-thrombogenic vascular graft coatings or electrospun nanofibrous scaffolds.

The introduction of residues with reactive side groups, such as glutamic acid and lysine, enable the protein polymer to be further functionalized to control structural and biologic parameters, including permeability, swelling ratio, viscoelasticity, mechanical strength, biostability, and biocompatibility. For example, enzymatic crosslinking of native elastin stabilizes the fiber network through the deamination of ε-amino groups on lysine side chains [222, 223]. Similarly, various lysine crosslinking strategies for elastin-mimetic protein polymers have been investigated to increase their elastic modulus and tensile strength, and include enzymatic-based as well as chemical crosslinking approaches [224, 225]. Colleagues in the Chaikof lab reported the synthesis of **LysB10**, a triblock elastin-like protein polymer, capable of physical and chemical crosslinking that stabilize mechanical responses and biostability of the protein polymers [14]. Synthetic gene construction was utilized to insert lysine crosslinking sites at positions flanking the hydrophobic and hydrophilic domains. Rheological analysis of the expressed recombinant protein polymer confirmed the formation of a viscoelastic gel above 13°C. Below the coacervation temperature, non-crosslinked copolymer films dissolved immediately due to disruption of physical crosslinks, while glutaraldehyde-crosslinked films retained approximately 86% of their mass. In addition, preconditioned crosslinked polymer films exhibited a two- to three-fold increase in Young's modulus and a 50% decrease in strain at failure, with a slight increase in ultimate tensile strength, as compared to non-crosslinked films.

While crosslinking enhanced strength and modulus, a small reduction in resilience was noted. Table 2.1 summarizes the mechanical parameters evaluated in **LysB10**.

2.11 Functionalizaton of elastin-like protein polymers

Genetic Engineering

Various groups have incorporated bioactive ligands into elastin-like protein polymers (ELPs) to mimic the functions of the extracellular matrix and guide cellular behavior. To date, the majority of these recombinant proteins have been genetically engineered with relatively short block sequences that limit structural polymorphism (see Table 2.2). The ligands chosen to add to the elastin-like backbone provide structural, mechanical, biochemical, and degradative properties to the elastin-like scaffolds for a wide range of tissue engineering applications. For example, Girotti and coworkers have placed elastase target sequences (VGVAPG) in an elastin analog to control proteolytic degradation of the structural scaffold in response to cellular infiltration and tissue repair during wound healing [226, 227]. Similarly, sequences sensitive to cleavage by urokinase plasminogen activator (uPA) have been genetically engineered into ELPs in order to induce local neuronal remodeling of the ECM-mimetic . Tirrell and colleagues have been able to increase endothelial cell attachment and spreading on protein substrates comprised of elastin sequences by incorporating the well-characterized cell-binding domain RGD. They have also targeted the endothelial cell surface integrin $\alpha_4\beta_1$ with the CS5 sequence isolated from fibronectin (GEEIQIGHIPREDVDYHLYP) in order to achieve endothelial cell adhesion. The relationship between cell adhesion and the spatial distribution of bioactive domains within the context of the CS5 protein polymer has been explored as well. It has been demonstrated that ELPs with lysine crosslinking sites in the interior of the elastin domain are unable to support adhesion, while ELPs with N- and C-terminal crosslinking sites enable high rates of endothelial cell spreading and adhesion. Crosslinked ELP films have been PEGylated in

order to reduce nonspecific cell adhesion on surfaces [228]. These studies underscore the importance of minimizing conformational interference with ligand-receptor affinity and accessibility. Table 2.2 displays previous work with genetically engineered cell-responsive peptide domains within elastin-like polypeptides.

Chemical Modification

While genetic engineering enables precise control in amino acid sequence, further functionalization of the amino acid side chains requires chemical modification. For example, Nagapudi and colleagues modified the lysine residues in their ELPs to methacrylate moieties in order to facilitate site-specific solid-state photocrosslinking [229]. Kaufmann and colleagues were able to achieve solution phase chemical conjugation of linear GRGDSF-OH to the glutamic acid in an ELP-polypeptide in order to promote osteoblast adhesion [230]. Their results indicate a 50% grafting efficiency of RGD molecules to the polypeptide backbone (4 RGDs per ELP molecule). Interestingly, the investigators were not able to detect any cell adhesion on those ELP hydrogels that were chemically conjugated to RGD via a solid-state reaction scheme. Teeuwan and colleagues were able to promote site-specific coupling of proteins to ELPs via Cu-catalyzed azide-alkyne cycloaddion, thereby synthesizing “clickable” ELP derivatives [231].

2.12 Applications of Elastin-like Proteins

Elastin plays a vital role as a structural protein in many tissues [87]. Moreover, the capacity of elastin-based protein polymers to be processed as gels, films, or nanofibers demonstrates their versatility in a number of tissue engineering applications. For example, Urry and colleagues have found that elastin-like thin hydrogels act as effective physical barriers to adhesion formation in a contaminated peritoneal wound model [232]. ELPs have also been utilized as drug delivery vehicles to target tumors *in vivo* [233, 234]. The load-bearing properties of the ELP have been investigated for use as cartilage and intervertebral disc repair, small-

diameter vascular grafts [228, 235-238], stem cell matrices [239], scaffolds for promotion of neuronal repair [240], and cell sheets [241, 242].

Table 2.1. Summary of mechanical parameters of LysB10.

Protein	Treatment	Resilience (%)	Young's Modulus DMTA (MPa)	Young's Modulus Minimat (MPa)	UTS (MPa)	Strain at Failure (%)
LysB10	GTA Xlinked	39±1*	1.10±0.45*	1.60±0.48*	3.62±0.98	223±30*
LysB10	Non-Xlinked	52±2	0.49±0.03	0.53±0.02	2.88±0.71	463±43

$p<0.05$ between crosslinked and non-crosslinked samples
Average values obtained from 3-10 replicates. Resilience and Young's modulus determined from DMTA testing. Young's modulus, ultimate tensile stress (UTS), and % strain determined from Minimat testing.

Table 2.2. Design of cell-interactive domain within the context of elastin-like protein polymers.

Reference	Elastin Sequence	Functional Domain	Biological Activity
[243]	$[(APGVGV)_{12}$-**RGD**$]_4$	RGD sequence is a cell-binding domain that engages multiple integrins on cell surface, including $\alpha_5\beta_1$ and $\alpha_v\beta_3$	Fibroblast adhesion on substrate coated with 500nM ELP solution was ~ 80% of that on fibronectin-coated surface (100nM solution)
[244]	{LDYAVTG**RGD**SPASSK PIA$[(VPGIG)_2$VPGKG(VP GIG$)_2]_4$VP$\}_3$-LE	RGD is a cell-binding domain that engages multiple integrins on cell surface, including $\alpha_5\beta_1$ and $\alpha_v\beta_3$	RGD-ELP was ~ 50% as effective as fibronectin in promoting CHO cell spreading on coated substrates
[238]	(a) [LD**CS5**$(GVPGI)_{40}]_3$LE (b) [LD**CS5**$(GVPGI)_{20}]_5$LE **CS5** = GEEIQIG HIP**REDV**DYHLYP	CS5 is a cell-binding domain isolated from fibronectin that engages with the integrin $\alpha_4\beta_1$	(b) substrates were 4.5 times more effective in supporting HUVEC adhesion compared to (a)
[237]	(a) (LD-YAVTG**RGD**SPASS KPIA$(VPGIG)_2$VPGK G$(VPGIG)_2)_4$VP$)_3$-LE (b) (LD-EEIQIG HIP**REDV**DYHLYPG($(VPGIG)_2$VPGKG(VP GIG$)_2)_4$VP$)_3$-LE	While RGD sequence binds multiple integrins, REDV more specifically binds to integrin $\alpha_4\beta_1$	RGD-ELP coated substrates were 2.5 times more effective in supporting HUVEC adhesion than REDV-ELP coated substrates. Furthermore, HUVECs spread more rapidly on RGD-ELP coated surfaces than on REDV coated surfaces.
[235, 236]	(a) {LD**CS5**-G $[(VPGIG)_2$VPGK G$(VPGIG)_2]_4$VP$\}_3$ LE (b) RKTMG[LD**CS5**G $(VPGIG)_{25}$VP$]_3$-LEKAAKLE	CS5 is a cell-binding domain isolated from fibronectin that engages with the integrin $\alpha_4\beta_1$	(b) substrates supported higher HUVEC adhesion and rapid spreading compared to (a)
[233]	**Bac**-(VGVGVPGVGVPGGGV PGAG VPGVG VPGVGVPGVGVPGGG VP GAGVPGGGVPG$)_{15}$-**p21** Bac = MRRIRPRPPRLPRPRPR PLPFPPRP p21 = GRKRRQTSMTDFYHSK RRLIFSKRKP	Cell penetrating peptide Bac, a 24 amino acid peptide of the bactenecin family, has been shown to deliver cargo inside cells and was used to facilitate entry of ELP across cell membrane. p21 peptide mimetic has been shown to exhibit cyclin-CDK inhibitory activity and also inhibit human cancer cell proliferation	The use of hyperthermia (42°C) increased the antiproliferative effect of Bac-ELP1-p2 in ovarian cancer cells. Nuclear-localized polypeptide enriched in the heated cells. Also induced caspase activation, PARP cleavage, and cell cycle arrest in S-phase and G2/M-phase. These studies indicate that ELP is a promising macromolecular carrier for the delivery of cell cycle inhibitory peptides to solid tumors.

[240]	(a) {LDASTVYAVTG **RGD**SPASSAA SA $[(VPGIG)_2VPGK G(VPGIG)_2]_3VP\}_4$ -LE (b) {LDASAA**GRILA RGEINF**AAASA $[(VPGIG)_2VPGK G(VPGIG)_2]_3VP\}_4$ -LE (c) {LDASVCDPG**YI GSR**CDDCASSA $[(VPGIG)_2VPGK G(VPGIG)_2]_3VP\}_4$ -LE	b. Neural cell adhesion molecule is a cell-cell adhesion protein c. YIGSR is a cell-binding sequence isolated from laminin-1	RGD-ELP enhanced neurite extension of PC-12 cells. The NCAM and YIGSR analogues have yet to be evaluated.

CHAPTER 3

Genetic engineering of elastin-mimetic protein polymer with cell-binding domains

3.1 INTRODUCTION

Extracellular matrices provide structural and signaling cues that organize and regulate cellular behavior and activity, leading to tissue repair and homeostasis [245, 246]. However, the inability of synthetic materials to reconstitute higher order structures of native extracellular matrix limits biointeraction for regenerative medicine. To induce specific cell and tissue responses, biomaterials are being developed to incorporate defined biomolecules, such as adhesion ligands and growth factors. The use of recombinant fragments extracted from ECM proteins offers many advantages over entire ECM molecules, including reduced antigenicity, enhanced integrin specificity, and coating of a higher density of bioactive epitopes. Ultimately, the success of this approach is dependent on appropriate cell migration, adhesion, proliferation, and extracellular matrix production, on the biomimetic surfaces.

The development of genetic and recombinant protein engineering has enabled the synthesis of bio-inspired protein polymers composed of repetitive amino acid sequences and peptide blocks, whose structural complexity impart specific mechanical, chemical, and biologic properties [215, 218]. The biosynthetic machinery of micro-organisms can be exploited to produce significant quantities of recombinant protein polymers that have been designed from primary amino acid sequences and translate to a distinct three-dimensional folded structure [96, 97, 100, 103, 246]. The most significant impact of this strategy is the capacity to introduce precise changes in the amino acid sequence to modulate properties of the entire protein network. This “bottom-up” approach to materials design enables researchers to finely modulate the nanostructure of a material in order to influence its bulk properties.

Recently, we reported a new class of recombinant elastin-mimetic protein polymer for the purpose of designing materials for small-diameter vascular grafts [14]. Synthetic grafts have been known to fail *in vivo* due to compliance mismatch between the grafts and surrounding arterial tissue [2-5]. Therefore, researchers have explored the potential of incorporating scaffolds with more extensible proteins such as elastin, a key structural element in native vasculature [87]. While native elastin's intrinsic insolubility has limited its use in biomedical applications, structural and sequence analyses of tropoelastin have determined that pentapeptide repeat motifs similar to VPGVG exhibit elastomeric behavior with features that are consistent with native elastin, including a mobile backbone and the presence of β turns [247, 248]. Therefore, elastin-like protein polymer **LysB10** was designed with the capability of physical and chemical crosslinks, and was shown to display a range of elastomeric properties that more closely match those of the native artery [14, 222-225]. This amphiphilic triblock copolymer (ABA) consisting of hydrophobic (A) and hydrophilic (B) domains was synthesized such that phase separation of the more hydrophobic blocks occurs in water under physiologically relevant conditions to form virtual crosslinks, while the hydrophilic domains remain non-crosslinked and solvated by the aqeous environment [218, 219]. Thus, elastin-like protein copolymers (ELPs) represent a unique class of thermoreversible hydrogels for soft tissue engineering applications. Furthermore, this multiblock system results in structural polymorphism and the potential for a wide range of functional responses, including mechanical and biological performance.

The generation of protein polymers that mimic native structural proteins and adopt the characteristics of the arterial wall offers a unique approach to develop a vascular graft. Several investigators have endeavored to minimize graft failure due to thrombosis and intimal hyperplasia by mimicking the biologic responsiveness of the native vasculature. In particular, the poor patency rates of synthetic polymers have motivated strategies to functionalize the

luminal surface of grafts in order to promote endothelialization of the material surface [7, 9, 11, 12, 26-29, 31, 32, 34, 249, 250].

The goal of this work was to add desired biological functionality to the recombinant elastin analog **LysB10**. It was postulated that the elastin analog containing an $\alpha_v\beta_3$ integrin-binding sequence would enhance endothelial cell adhesion and migration to an otherwise non-adhesive substrate, thereby facilitating repopulation of vascular cells and endothelialization. To this end, a 20 amino acid cell binding sequence named V2, isolated from the pro-angiogenic protein CCN1, was incorporated into the central domain of **LysB10.** Genetic engineering techniques enabled facile control over multiblock molecular assembly, which in turn led to optimized spatial distribution and presentation of bioactive peptides incorporated into the previously studied protein polymer **LysB10**.In this chapter, we describe the design, production, and characterization of a cell-adhesive artificial protein polymer for use in vascular tissue engineering applications. The results demonstrate that polymer morphology and surface ligand density influence endothelial cell activity and integrin-binding specificity.

3.2 MATERIALS AND METHODS

Reagents, Antibodies, and Cells

Single-stranded V2 oligonucleotides were purchased from Sigma Genosys. BL21(DE3) and Top10F' E.coli cell line was obtained from Invitrogen. Bacterial cell culture reagents were obtained from Fisher Scientific. TALON column purification kit was purchased from Clontech. The 20 amino acid peptide V2 (NCKHQCTCIDGAVGCIPLCP) and scrambled peptide (NCKHQCTCIAGAVGCIPLCP) were custom-synthesized by Invitrogen. Fibronectin and vitronectin solutions were purchased from Sigma Aldrich. Human umbilical vein endothelial cells and cell culture reagents were obtained from Clonetics. Monoclonal mouse anti-human integrin $\alpha_v\beta_3$, mouse anti-human E-selectin, and mouse anti-human ICAM-1 antibodies were purchased from Millipore. Monoclonal anti-vinculin (clone hVIN-1) was purchased from Sigma Aldrich. Immunostaining reagents goat anti-mouse IgG antibody, streptavidin-AlexaFluor 488, phalloidin-AlexaFluor 568, and ProLong Gold antifade reagent with DAPI were all purchased from Invitrogen (Molecular Probes).

Synthetic gene construction of bioactive domains

Work on various ELPs has indicated that biologic responses can be produced through selective engineering of the bioactive domain (see Table 2.2). Moreover, ligand clustering leads to integrin receptor aggregation and increased adhesion strength [251]. In light of these investigations, the V2 domain was designed as a 10-repeat block, approximately 15% of the ELP molecular weight composition. Sequences were based on preferred codon usage to enable expression from E.coli expression systems. The elastin analog **V2** was designed and synthesized so that the integrin-binding sequence was inserted in the central elastomeric domain of triblock **LysB10 (**Table 3.1, Scheme 3.1). Crosslinking residues were sequestered

between the hydrophobic and hydrophilic domains, and at the terminal ends of the protein polymer.

Single stranded oligonucleotides encoding the sense and anti-sense strands of V2 monomer units were chemically synthesized to include flanking BamHI/HinDIII restriction sites, as well as internal BbsI/BsmBI restriction sites flanking the monomer sequences. The DNA was diluted in 10 mM Tris buffer (pH 8) to a final concentration of 0.5 mg/mL to begin the protocol for double-stranded DNA formation. A solution of 10 µg of each corresponding oligonucleotide strand, 5M NaCl, 1M $MgCl_2$, and sterile ddH_2O in a final volume of 200 µL was subjected to an annealing procedure initiated at a reaction temperature of 99°C, with temperature decrements of 0.5°C every 3 min to a final reaction temperature of 30°C for 15 minutes. The resulting double-stranded DNA cassette was analyzed by agarose gel electrophoresis (4% GTG NuSieve agarose, 1X TBE buffer), with the V2 monomer being 127 base pairs long. Double-stranded synthetic DNA was phosphorylated during a 2-hour incubation period with T4 Polynucleotide Kinase (New England Biolabs) in the presence of T4 DNA ligase buffer with 10 mM ATPs (New England Biolabs). Enzymes and other protein contaminants were removed with phenol/chloroform/isoamyl alcohol (25:24:1) and the double-stranded DNA (dsDNA) was recovered through an ethanol precipitation. The dsDNA units were then placed in a plasmid in order to select for the correct insert sequences and further cloning work.

The pZErO-1 acceptor plasmid (1 µg), was prepared via BamHI and HinDIII double digestion for 30 minutes, followed by heat inactivation of the enzymes at 65°C. The monomer units were designed with BamHI and HinDIII overhangs to enable cloning into pZErO-1 at these restriction sites. The DNA cassette and respective acceptor plasmid were ligated together in a 10 µl volume in the presence of T4 DNA ligase at 16°C for 30 min. A 2µL aliquot of the ligation reaction was used to transform 40 µL of electrocompetent TOP10F' E. coli cells. A total of 100

Table 3.1. Molecular assembly of elastin analogs.

Elastin Analog	N-terminal Plastic Domain (A_n)	Elastic Domain (B)	Bioactive Domain (C)	C-terminal Plastic Domain (A_c)	Final Design
LysB10	VPAVGK[(VPAVG)(IPAVG)$_4$][(IPAVG)$_5$]$_{33}$	(IPAVG)KAAK(VPGAG)(VPGAG)$_2$VPGEG(VPGAG)$_2$]$_{28}$(VPAVG)KAAK(VPGAG)	----	[(VPAVG)(IPAVG)$_4$[(IPAVG)$_5$]$_{33}$IPAVGKAAKA	**A_nBA_c**
V2	VPAVGK[(VPAVG)(IPAVG)$_4$][(IPAVG)$_5$]$_{33}$	(IPAVG)KAAK(VPGAG)(VPGAG)$_2$VPGEG(VPGAG)$_2$]$_{14}$—**C**—[(VPGAG)$_2$VPGEG(VPGAG)$_2$]$_{14}$(VPAVG)KAAK(VPGAG)	[VPGVG-GG-NCKHQCTCIDGAVGCIPLCP-GG-PGVG]$_{10}$	[(VPAVG)(IPAVG)$_4$[(IPAVG)$_5$]$_{33}$IPAVGKAAKA	**A_nBA_c**

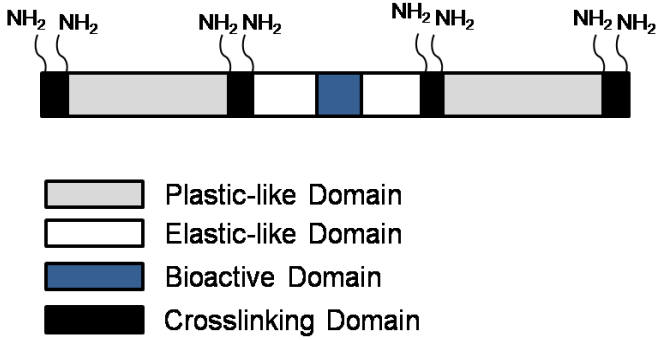

Scheme 3.1. Design of recombinant V2 copolymer

μL of the transformation mixture was spread onto low salt Luria Broth (LSLB) agar supplemented with Zeocin (50 μg/μL). The plates were incubated for 16 hours at 37°C, and five colonies were selected from each plate to inoculate 5 mL cultures of LSLB/Zeocin. Cultures were rotary incubated for 12 hours at 37°C. Plasmid DNA was isolated following a Qiagen Spin Miniprep protocol (Qiagen, Inc.). DNA was screened by a BamHI and HinDIII double digestion. Positive transformants were verified by agarose gel electrophoresis (4% GTG NuSieve agarose, 1X TBE buffer). Automated DNA sequencing utilizing the M13 forward and M13 reverse primers confirmed correct DNA products.

Recombinant plasmids containing correct inserts of each of the selected sequences were re-transformed into competent Top 10F' cells and plated on LSLB agar plates under Zeocin antibiotic resistance. A single colony from each plate was used to inoculate 500 mL LSLB medium and grown overnight at 37°C in a shaker at 225 rpm. Preparative amounts of plasmid DNA were isolated using QIAfilter Plasmid Maxi protocol (Qiagen, Inc). Monomer cassettes were excised from the plasmid via sequential digestion by *Bbs*I (10U/μL) and *Bsm*B I (10U/μL) restriction enzymes. Fragments were isolated via preparative gel electrophoresis (4% GTG NuSieve, 1 X TBE buffer), extracted using Amicon Ultrafree Centrifugal Filter Units (Milipore), and isolated via ethanol precipitation.

Multimerization reactions utilized 3.0 μg of the *Bbs*I/*Bsm*BI digested DNA and ligated monomers end-to-end via T4 DNA ligase. Multimer mixtures were separated by size using agarose gel electrophoresis (1% agarose, 1 X TBE buffer). Concatemers were excised in blocks, <500 bp, 500-1000 bp, 1000-3000 bp, and purified using Zymoclean Gel DNA Recovery protocol (Zymo Research, Inc). Multimers of 500-1000 and 1000-3000 bp in size were ligated into the acceptor plasmid at the *Bbs*I site at 16°C for 16 hours. The acceptor plasmid was prepared from the pZErO-1 plasmid containing the original monomer repeat unit associated with each gene. The acceptor plasmids were digested with *Bbs*I, and dephosphorylated via SAP

(Shrimp Alkaline Phosphatase) to prevent self ligation. Ligation mixtures were used to transform competent Top 10F' cells and 100µL of the transformation mixture was plated on LSLB/Zeocin agar plates. DNA from positive clones were isolated via Qiagen Spin Miniprep and screened through double digestion using *Bam*HI and *HinD*III restriction enzymes. Clones of predetermined sizes were isolated (10-repeat monomer units of V2). Similarly, the elastic (midblock) unit $(VPGAG)_2VPGEG(VPGAG)_2$, which was previously synthesized in the lab, was multimerized to a 14-repeat block for further cloning work. Scheme 3.2 demonstrates the multimerization technique.

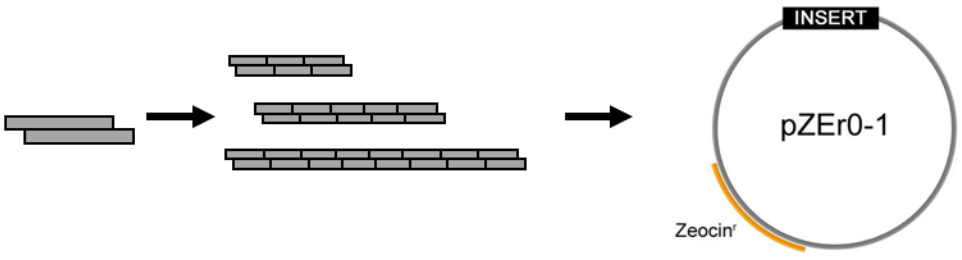

Scheme 3.2. Multimerization of DNA monomers for the synthesis of repeat polypeptides. dsDNA monomers are ligated to form DNA multimers of various lengths. The target length is inserted into the cloning vector for further gene assembly.

Assembly of V2 triblock

Previous work with the plastic blocks was utilized to assemble the **V2** triblock. Coupling of the plastic block from **LysB10** with the short (14-repeat) elastic block was attained with *Bsm*BI/*Xma*I and *Bbs*I/*Xma*I restriction digestions, respectively, and ligation of the large fragments from each plasmid digestion. Briefly, the larger fragment from each of these digestions was isolated via preparative gel electrophoresis (1% agarose, 0.7X TBE) and purified using the Zymoclean gel recovery kit. The plastic and elastic fragments were ligated by T4 DNA ligase, transformed into Top 10F', and plated on LSLB plates under Zeocin resistance. As the *Xma*I site cuts within the Zeocin coding region, only clones containing the correctly assembled diblock, and thus, the correctly reassembled antibiotic resistance coding region, will propagate, as seen in Scheme 3.3. Insert sequence was verified with DNA sequencing. The V2 domain was coupled to the A_nB block with a similar digestion scheme, and verified with agarose gel electrophoresis analysis of a BamHI and HinDIII double digestion and DNA sequencing. To form the triblock, the A_nB_{14}-$V2_{10}$ block was digested with *Bsm*BI /*Xma*I and the plasmid containing the $B_{14}A_c$ block with *Bbs* I/ *Xma*I. Similar protocols for ligation, transformation, and propagation were followed. Via antibiotic selection, only colonies containing the correctly assembled triblock survived. As a final step, the gene was placed into the lysine adaptor.

The lysine adaptor is a 50-bp DNA cassette designed with *Bsm*BI restriction enzyme cut sites midway through the cassette for insertion of an insert. The adaptor encodes for a single N-terminal lysine residue and two C-terminal lysine residues. The careful positioning of lysine residues has been incorporated to enhance the potential of intermolecular crosslinking. Furthermore, it enables cloning into the final expression vector by correctly inserting the gene of interest in frame with the N-terminal polyhistidine tag. The V2 triblock was extracted from the pZErO-1 plasmid with *Bbs*I and *Bsm*BI sequential digestion and subsequent purification, while the lysine adaptor was digested with *Bsm*BI and SAP dephosphorylated in preparation for

triblock insertion. Ligation of the insert and adaptor vector was performed, and the ligation reaction was transformed into Top10F' cells, as described above. Colonies that grew on the LSLB agar plates under Zeocin resistance were screened via agarose gel electrophoresis analysis of a *Bam*HI and *Hin*DIII double digestion. DNA sequencing confirmed correct insertion and sequence of the gene within the adaptor.

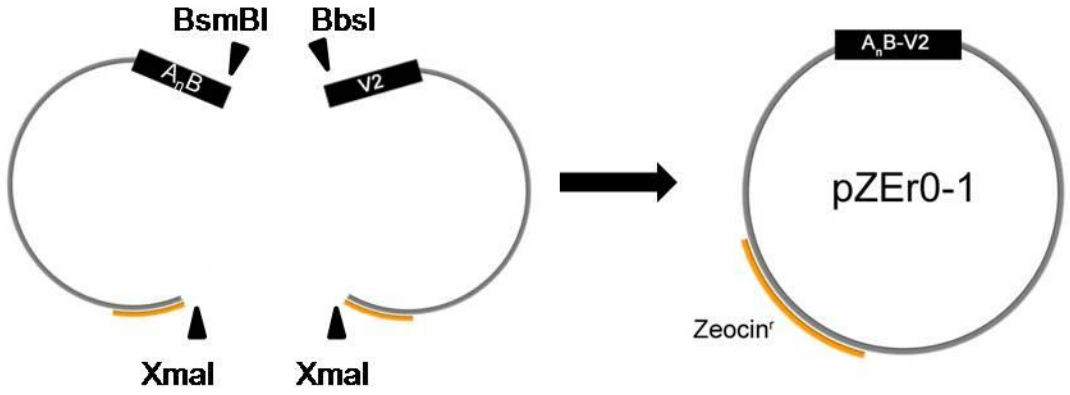

Scheme 3.3. General cloning strategy in the assembly of the V2 gene. Coupling of the V2 domain to the N-terminal elastin diblock begins with restriction enzyme double digestion and purification of the appropriate plasmid fragments. The fragments are then ligated together, with the resulting plasmids transformed into E.coli cells. As the *Xma*I site cuts within the Zeocin coding region, only clones containing the correctly assembled plasmid, and thus, the correctly reassembled antibiotic resistance coding region, will propagate. Once the V2 block was coupled to the N-terminal elastin diblock, the cloning strategy was again repeated with the C-terminal elastin block.

Expression vector

The pQE80-L expression plasmid (1 µg, Qiagen, Inc) was prepared via *Bam*HI and *Hin*DIII double digestion, followed by gel isolation and purification. The V2 gene was released from the pZErO-1 vector at analogous sites. Adaptor and plasmid were ligated together in the presence of T4 DNA ligase at 16°C for 16 hours. A 2 µL aliquot of the ligation reaction mixture was used to transform 40 µL of electrocompetent Top10F' cells. A 100 µL aliquot of the transformation mixture was spread onto LB agar supplemented with ampicillin (100 µg/µL). The plates were incubated for 16 hours at 37°C. Colonies were selected from each plate to inoculate 5 mL cultures of LB/ampicillin media. Cultures were rotary incubated for 16 hours at 37°C. Plasmid DNA was isolated and screened by a *Bam*HI and *Hin*DIII double digestion. Positive transformants were verified by agarose gel and submitted to automated DNA sequencing utilizing the T7 promoter and T7 terminator primers. The pQE-80L plasmid contains an N-terminal histidine tag which allows for downstream purification and detection methodologies.

Protein expression and purification

The high-level expression of proteins in E.coli using the pQE vectors is based on T5 promoter transcription-translation system. Briefly, expression of recombinant proteins encoded by the pQE vectors is induced by addition of isopropyl-β-D-thiogalactoside (IPTG), which binds to the lac repressor protein and inactivates it. Once this occurs, the host cell's RNA polymerase can recognize the T5 promoter, and transcribe the downstream sequence. Once the triblock genes were placed in the pQE80L vector, they were transformed into the E.coli expression strain BL21(DE3). 35 mL of Luria Broth (LB) media with 100 µg/µL ampicillin was inoculated with the E.coli cells containing the V2 plasmids and grown for 16 hours at 37°C. Large scale expression was performed in an orbital shaker (225rpm) at 37°C in Luria Broth medium supplemented with ampicillin (100 µg/µL) by further inoculating 500 mL LB media with 25 mL of

the overnight cultures and ampicillin antibiotic. Cells were grown until the optical density reached 0.8 (approximately 2 hours). IPTG (1 mM) was added to the culture to induce protein expression for 4 hours.

The purification protocol of the protein products was modified from earlier work with **LysB10**. Cells were harvested via centrifugation (4°C/1660rcf/20 min), the cell pellet resuspended in equilibration buffer (50 mM sodium phosphate, 300 mM sodium chloride, pH 7.0), and stored at -80°C. Frozen cells were lysed via three freeze (-80°C)/thaw cycles. Once cells were resuspended, six cycles of sonication, consisting of 20 second bursts followed by 20 second rests in an ice bath, were utilized to completely break the cells. Unbroken cells were pelleted out during a centrifugation spin, resuspended in buffer, and resonicated. The cold cell lysate was centrifuged at 20,000g for 40 minutes at 4°C. The supernatant was transferred to a cold, sterile tube and poly(ethyleneimine) (PEI) was added to a final concentration of 0.5% to precipitate out nucleic acids and contaminating cellular material. The contaminants were removed by another centrifugation cycle at 20,000g for 40 minutes at 4°C, and the supernatant was transferred to a sterile tube. The elastin-mimetic protein was salted out of solution by adding NaCl to a 2M final concentration for 45 minutes at 25°C. The precipitate was recovered with 9500g/15minute/25°C centrifugation (hot spin). The supernatant was then discarded and the protein pellet was resuspended in cold, sterile PBS for 20 minutes. The solution was then centrifuged at 20,000g for 40 minutes at 4°C (cold spin) to remove unwanted contaminates. The supernatant was once again placed in a sterile tube and NaCl was added to precipitate out the protein. The hot and cold spin cycles were repeated twice more before the histidine-tagged proteins were further purified and isolated via cobalt-based affinity chromatography. The protein solutions were dialyzed to remove salt and PEI and reconstituted in TALON equilibration buffer.

TALON Resins (Clontech) are durable, cobalt-based immobilized metal affinity chromatography resins designed to purify recombinant polyhistidine-tagged proteins with

enhanced selectivity. The resin was placed in a sterilized glass column to settle, and a batch/gravity-flow protocol was followed, according to the manufacturer's guidelines. All work was conducted in a cold room (4°C), with solution temperatures well below the inverse transition temperature. The protein sample was applied to the column and incubated with the resin for 30 minutes, with gentle mixing on a platform shaker. The solution was then allowed to drain by gravity from the resin and column, with the flow-through re-loaded to the column to ensure complete protein binding to the resin. The resin was then washed with 20 resin volumes of equilibration/wash buffer (50 mM sodium-phosphate, 300 mM sodium chloride, 5 mM imidazole, pH 7.0) in order to remove nonspecific protein binding interactions. The second wash buffer contained 6M urea in order to remove endotoxin from the resin. A final wash of 10 resin volumes of equilibration/wash buffer rinsed the column of urea buffer before recombinant protein was eluted from the resin with the addition of 5 volumes of elution buffer (50 mM sodium-phosphate, 300 mM sodium chloride, 250 mM imidazole, pH 7.0). The eluted protein solution was concentrated, dialyzed, and frozen before being lyophilized.

Identification of elastin-mimetic proteins

Sodium dodecyl sulfate-polyacrylamide gel electrophoresis (SDS-PAGE) analysis revealed protein bands at 250 kDa. A total of 40 µg of elastin-mimetic proteins was run along with molecular weight markers (Precision Plus Protein Kaleidoscope, Bio-Rad) on a 7.5% gel and stained with Coomassie stain (Bio-Rad). Amino acid composition analysis was performed by the W.M. Keck Biotechnology Resource Laboratory at Yale University. Lyophilized protein was resuspended in HPLC grade water and filter-sterilized with a 0.22 um filter. Solutions of 1 mg/mL were submitted for analysis, with samples hydrolyzed in 6N HCl and the resulting amino acids examined with a Beckman Model 7300 ion exchange instrument. Improved quantitation of cysteine was obtained via performic acid oxidation. It is important to note that following normal acid hydrolysis, proline values are artificially elevated (Table 3.2).

Differential Scanning Micro-Calorimetry (Micro-DSC)

Experiments were performed using a Setaram Micro DSC III calorimeter (Setaram Inc, France). Lyophilized protein samples of 1 mg/mL were first dissolved at 4°C in sterile distilled, deionized water. The solutions were then filter-sterilized through a 0.22 µm syringe filter. The thermal transition data was investigated over a temperature range of 4°C to 70°C at a scan rate of 1°C/min. Reversibility was confirmed upon cooling of the sample back to 4°C following the initial scan. Data was analyzed using SETSOFT 200 software (Setaram Inc, France).

Substrate preparation

Lyophilized protein was allowed to dissolve in phosphate buffered saline at 4°C for 16 hours before being sterile-filtered through a 0.22 um syringe filter. Protein solutions were prepared in PBS to final concentrations of 10, 5, 2.5, 1, 0.5, and 0.1 mg/mL. 50uL of each solution was evenly spread in four wells of a non tissue-culture treated polystyrene 96-well plate. The protein was then allowed to passively adsorb for 6 hours at 37°C before rinsing the wells three times with PBS. Fibronectin was adsorbed in a similar manner from a 50 µg/mL solution in PBS. Blocking of non-specific interactions was achieved by placing 0.5% heat-inactivated bovine serum albumin (BSA) in wells for 1 hour before once again rinsing three times with PBS. Wells treated with BSA only were used as negative controls.

V2 hydrogels were fabricated by casting the protein solutions into non tissue culture treated polystyrene wells at 4°C, and subsequently placing the 96-well plate in a 37°C incubator for 2 hours. The resulting soft gel adhered firmly to the bottom of the wells, and was crosslinked with a 6 mg/mL genipin solution for 24 hours. Excess genipin was removed with PBS rinsing over a 12 hour period.

Cell Studies

Protein Adsorption

Protein polymers that were adsorbed onto polystyrene plates were quantified via the bicinchoninic acid (BCA) method (kit purchased by Pierce). To create a calibration curve, known concentrations of protein solutions were added to the 96-well plate, as documented by the Tirrell group [237].

Adhesion

Human umbilical vein endothelial cells (HUVECs) were purchased from Clonetics and maintained in endothelial growth medium-2 (EGM-2, 2% serum, Clonetics). They were kept in a humidified, 5% CO_2 environment at 37°C, and passaged every 2 days via standard culture techniques. HUVECs between passages 3 and 10 were used for all experiments. To begin, cells were harvested with Cell Dissociation Solution (EDTA, glycerol, sodium citrate, PBS, from Sigma) in order to maintain integrin functionality on the cell surface. After centrifugation at 220g for 5 minutes, cell suspensions were prepared at a density of 200,000 cells/mL in basal medium containing 0.5% bovine serum albumin (BSA). For peptide inhibition studies, detached HUVECs were treated with LM609 (50 ug/mL) and soluble V2 peptides (1 mM) for 30 minutes at room temperature before plating. 100uL of the cell suspension was plated into each well treated with elastin-mimetic protein polymer, and after incubation at 37°C for 4 hours, wells were washed three times with phosphate-buffered saline (PBS). Cell adhesion activity was evaluated with the CyQuant Cell Proliferation Assay Kit (Molecular Probes), which utilizes a fluorescent dye with strong fluorescence enhancement when bound to cellular nucleic acids (excitation/emission maxima ~480/520 nm). Briefly, after thawing frozen cells to enhance lysis, the CyQuant cell lysis buffer was added to each sample, along with CyQuant fluorescence reagent. Samples

were then measured in a microplate spectrofluorometer. Results were normalized to adhesion levels on fibronectin-coated wells, which acted as the positive control.

Haptotactic migration

Haptotactic cell migration assays were performed using modified Boyden chambers (Transwell filters, 80um pore size). The lower surfaces of the filter membranes were coated with 10 mg/mL and 5 mg/mL **LysB10** and **V2** solutions. Positive control filters were coated with 50 ug/mL solutions of vitronectin. 80,000 cells were placed in the upper chamber of each well insert in 0.2% BSA-containing media. Cells were allowed to migrate across inserts for 6 hours at 37°C. Cells were fixed in 10% formaldehyde and stained in hematoxylin, after which the upper membrane surface was swabbed with a wet cotton swab and rinsed in distilled, deionized water. The average number of migrated cells in six randomly chosen 40x magnification fields of view per insert was taken to quantify the extent of migration. In addition, the experiment was run in triplicate.

Fluorescence microscopy

Fluorescent staining of cytoskeletal components were performed on HUVECs cultured on elastin-mimetic protein polymer-coated polystyrene 8-well chamber slides (Nalge Nunc, International). 200uL cell suspensions (approximately 15,000 cells/well) were seeded onto the slides and cultured for a period of 4 hours in serum-free medium. To achieve HUVEC activation, 100 ng/mL of TNFα was added to cells cultured on fibronectin-coated slides for 4 hours prior to immunostaining. Cells were fixed in 4% paraformaldehyde (10 minutes), permeabilized with PBS containing 0.5% Triton X-100 (10 minutes), rinsed once with 100 mM glycine (10 minutes), and incubated with block buffer (PBS+/+, 0.2% Triton X-100, 6% goat serum) for 1 hour at room temperature. For F-actin staining, cells were incubated with Alexa Fluor 568-conjugated phalloidin for 30 minutes. Vinculin staining was performed with 10ug/mL mouse anti-human

vinculin IgG1 (1 hour incubation), 2.5 ug/mL biotinylated goat anti-mouse IgG secondary (45 minute incubation), and 2.5 ug/mL streptavidin-AlexaFluor 488 tertiary (30 minutes). Nuclei were counterstained with Prolong Gold mounting medium with DAPI, and the resultant staining was imaged using confocal microscopy (Emory University). 10ug/mL solutions of E-selectin and ICAM-1 monoclonal antibodies were substituted into the above protocol in order to evaluate HUVEC activation/quiescence states.

Statistical Analysis

Comparison between groups was analyzed via ANOVA and a paired, two-tailed student's t-test, with $p<0.05$ considered to be significant. Results are presented as mean ± standard deviation. Data represent characteristic results from a particular experimental run (each group run in quadruplicate), although at least three independent runs were conducted.

3.3 RESULTS

Synthesis of V2 protein copolymer

Previous work with the elastomer **LysB10** has demonstrated that a chemically crosslinkable ELP significantly increases the material's tensile strength and creep resistance. The improved mechanical properties make this polymer an ideal candidate for subsequent studies in the rational design of second generation proteins. Work on various ELPs has indicated that biologic responses can be produced through selective engineering of the bioactive domain. In light of these investigations, V2 repeats were designed as approximately 15% of the ELP molecular weight composition. Sequences were based on preferred codon usage to enable expression from E.coli expression systems. As Figure 3.1A demonstrates, final assembly of the V2 triblock yields a gene size of 8.4 kilobases (kb), while the size of vector pQE80L is 4.8 kb.

Small-scale expression cultures of the two analogs was first pursued to verify recombinant protein expression from E coli, and a time-course analysis of this expression was performed via SDS-PAGE to optimize the induction conditions (Figure 3.1B). The theoretical molecular weight of **V2** is 233.1 kDa. Sodium dodecyl sulfate-polyacrylamide gel electrophoresis (SDS-PAGE) analysis revealed that before IPTG induction (time=0 hours), the recombinant protein was not expressed. However, Coomassie staining displayed an increasing intensity of protein bands at around 250 kDa with 1mM IPTG induction from one to four hours. As previously reported, molecular weights observed by SDS-PAGE for elastin-mimetic proteins are approximately 20% greater than calculated molecular weights due to their relative hydrophobicity. With the confirmation of **V2** protein production over a 4 hour time course, large scale expression and purification were performed for each recombinant protein. Dialysis and lyophilization resulted in protein **V2** as a fibrous solid in yields of 35 mg/L of culture.

Bacterial endotoxin contamination of the resulting protein was evaluated with the Limulus Amebocyte Lysate (LAL) assay, a quantitative test for gram-negative endotoxin. Repeated testing (n=5) of various purified batches of **LysB10** and **V2** indicate that endotoxin content was below the level of 0.1 EU/mg, where 1 EU = 100 pg of endotoxin. This is acceptable for further cell studies, as clinically used alginate (Pronova sodium alginate) contains 100 EU/g.

The inverse temperature transition is a key feature of elastin-mimetic protein polymers, as discussed earlier. Specifically, the endothermic peak seen in Figure 3.2 is consistent with phase separation of the hydrophobic endlocks into beta turn aggregates. Differential scanning microcalorimetry of dilute aqueous solutions of **V2** (1 mg/mL) confirmed the presence of a single endothermic transition at 21°C. In comparison, **LysB10**, a more hydrophobic protein polymer, forms a viscoelastic gel at temperatures above 13°C [14].

Surface adsorption of LysB10 and V2

The hydrophobic nature of the elastin-like polypeptides allows for passive adsorption of the proteins onto non tissue culture-treated polystyrene. In particular, the ability to precisely characterize the relationship between input ELP concentration and adsorbed ELP surface density enables us to modulate ligand presentation for optimal cellular behavior. To this end, protein polymer solutions ranging from 0.1 – 10 mg/mL were physically adsorbed onto substrates, after which a quantitation assay was performed. It was demonstrated that the two protein polymers, **LysB10** and **V2**, followed a similar adsorptive profile, presumably through self-assembly into thin hydrogel surface layers. Furthermore, it was found that adsorbed surface density increased linearly with the concentration of the protein solutions (Figure 3.3A). This data indicates that control over peptide density can be achieved by varying coating concentration accordingly.

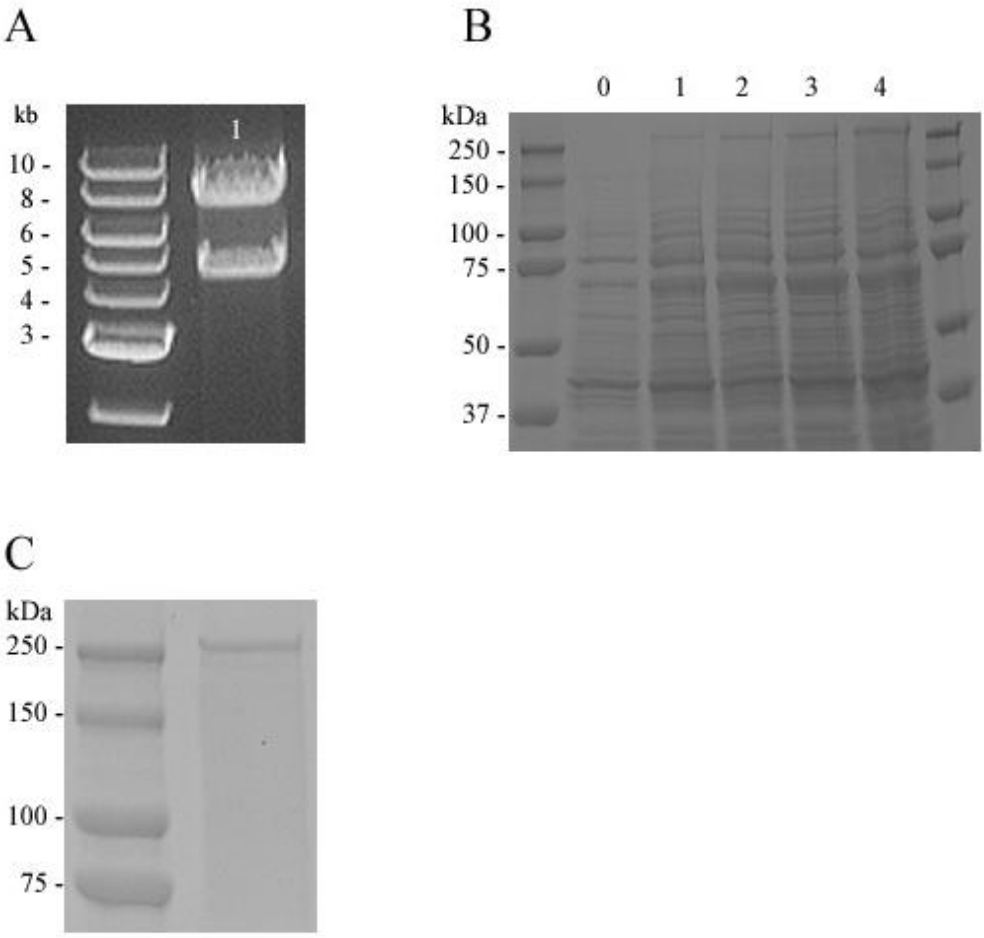

Figure 3.1. (A) Analytical restriction digests of elastin plasmids. 1% TAE (Tris-acetate-EDTA) agarose gel depicting the gene and vector sizes of the final construct after BamHI/HinDIII digests. A 1 kilobase (kb) DNA standard ladder was used on the left of the gel to determine the appropriate DNA size. **(B)** Protein expression analysis of V2 analogue over a 4-hour timecourse, starting with time=0 (no IPTG) through 4 hours after IPTG induction. Briefly, cells were grown to an optical density of 0.8 in Luria Broth supplemented with ampicillin. Before IPTG induction, an aliquot of culture was sampled for SDS-PAGE analysis (time=0 hrs). IPTG was then added to the culture for a final concentration of 1 mM to induce recombinant protein expression. The culture was maintained at 37°C for 4 hours, with samples taken hourly for expression analysis. Cells were harvested by centrifugation, resuspended in 1X PBS, and exposed to three freeze/thaw cycles to ensure cell lysis. The lysates were then run on a gel to determine expression levels over a time course of 4 hours. Protein staining was performed with Coomassie stain. **(C)** SDS-PAGE analysis of **V2** analogue after purification. Coomassie staining was utilized to visualize the protein bands. Molecular weight markers indicate size. The SDS-PAGE gels display the purity of the protein product after reconstituting 1 mg of lyophilized protein into 1 mL of distilled, deionized molecular grade water. The gel displays one clean band, with limited contamination products.

Table 3.2. Amino acid composition analysis

Amino Acids	Observed mol% (expected mol%)
Alanine	17.4 (17)
Histidine	0.9 (0.6)
Threonine	0.2 (0.4)
Glutamic Acid	0.7 (1)
Glycine	25.7 (26)
Valine	18.3 (19.2)
Isoleucine	15.3 (13)
Proline	21.8 (18.8)
Lysine	0.4 (0.6)
Methionine	-
Asparagine	0.5 (0.4)
Glutamine	0.4 (0.4)
Aspartic Acid	0.5 (0.4)
Leucine	0.3 (0.4)
Cysteine	1.2 (1.9)

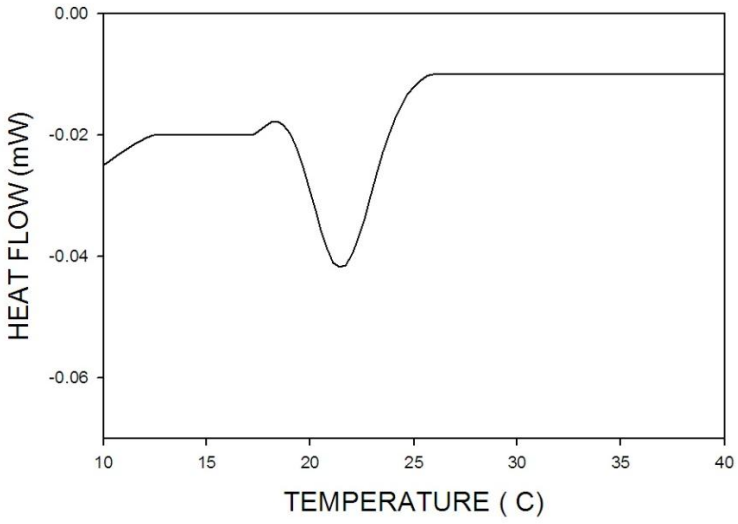

Figure 3.2. Differential scanning microcalorimetry of **V2**, indicating an inverse temperature transition at 21°C.

Adhesion, Specificity, and Migration of HUVECs on ELP-coated Surfaces

A comparative analysis of human umbilical vein endothelial cell (HUVEC) adhesion on elastin-like protein polymer (ELP)-coated surfaces was the first step in identifying those formulations that promoted enhanced bioactivity. To this end, a range of protein polymer densities was assessed for their ability to support robust cell adhesion. Serum-free culture was utilized to minimize competitive adsorption effects occurring with other serum proteins. **LysB10** (with no cell-binding site) concentrations were compared to **V2** (containing cell-binding sites). All values reported were corrected against the negative control, which was defined as blank wells blocked with 0.5% BSA. The data was further normalized against the fibronectin positive control and were presented as fraction of adherent cells relative to that on fibronectin-coated substrates under a given set of conditions. As Figure 3.3B demonstrates, **LysB10** was unable to support robust cell attachment, while surface concentrations of **V2** (above 40 pmol/cm^2) were able to increase adhesive efficiency.

In order to evaluate whether HUVEC adhesion to **V2** is mediated through integrin specificity, competitive inhibitors of $\alpha_v\beta_3$ function were employed. As Figure 3.4 demonstrates, substrates were no longer able to sustain adhesion of HUVECs treated with the anti- $\alpha_v\beta_3$ monoclonal antibody LM609. HUVEC treatment with soluble V2 peptide blocked adhesion as well, but this muted response was recovered when cells were treated with scrambled soluble peptide. Taken together, these results indicate that the V2 sequence localized within the elastin-like protein polymer is critical in supporting $\alpha_v\beta_3$-mediated HUVEC adhesion.

The $\alpha_v\beta_3$ integrin is known to have a critical role in cell migration and survival [252]. Given these findings, an *in vitro* haptotaxis assay was performed to determine whether HUVECs would readily migrate toward immobilized **V2**. In particular, the lower surfaces of Boyden chamber filter membranes were coated with 10 mg/mL and 5 mg/mL **LysB10** and **V2** solutions.

Positive control filters were coated with 50 ug/mL solutions of vitronectin. HUVECs were seeded onto the upper membrane of the Boyden chamber, and the extent of HUVEC migration across the membrane (towards the immobilized chemoattractant) was evaluated after 6 hours. The results showed that **V2** significantly induced HUVEC migration compared to **LysB10**. This result was concentration-dependent as well, with a higher **V2** density stimulating an increased migratory effect (Figure 3.5).

Immunofluorescence Analysis

Since HUVECs assemble robust focal adhesions containing clustered integrins and intracellular structural and signaling proteins, focal adhesion assembly as well as cytoskeletal organization on the engineered interfaces was examined. In particular, two markers were chosen to further evaluate cell function: F-actin stress fibers and vinculin, a focal adhesion associated protein that functions as a linker between actin filaments and integrins (Figure 3.6). Well-developed actin stress fiber network and vinculin clustering was apparent with **V2**-coated and fibronectin-coated substrates. However, on the **LysB10**-coated surface, actin and vinculin were nonspecifically distributed throughout the few adherent cells, which assumed rounded morphologies. These results further confirm that cell adhesion is mediated through integrin-ligand binding, and the **V2**-coated surface is sufficiently robust to induce cytoskeletal organization and focal adhesion formation characteristic of well-spread cells.

Further functionality of the HUVECs was assessed with immunofluorescence staining of the cellular adhesion molecules ICAM-1 and E-selectin, which are upregulated in activated HUVECs and mediate rolling of blood leukocytes in microvessels at sites of inflammation. The functional state of an endothelial cell monolayer determines its ability to act as a thromboresistant barrier for blood-contacting material applications. Therefore, the success of an endothelialized surface is dependent on either activation or quiescence of the endothelial cells.

Cells that were cultured on fibronectin-coated polystyrene and maintained in culture overnight in serum-free media assumed a quiescent state, with little ICAM-1 and E-selectin expression on the cell surface. Activation of HUVECs was achieved by adding 100ng/mL TNFα to the media for 4 hours. The positive and negative controls were compared to those cells adherent for 4 hours in serum-free media on **V2**-coated surfaces. Limited ICAM-1 and E-selectin staining was observed. Thus, endothelial cells are not only able to adhere, spread, and migrate on substrates coated with **V2** protein polymer, but can maintain a quiescent state phenotype (Figure 3.7).

V2 Hydrogels

While the surface coating method (passive adsorption onto a two-dimensional surface) utilized in analyzing the ELPs provided some insight into their functionality, alternative formulations of the ELPs were also explored. In particular, the triblock construction of plastic and elastic domains in **V2** and **LysB10** facilitates the formation of three dimensional hydrogels at physiologic temperatures. Furthermore, the physical crosslinks resulting from the aggregation of hydrophobic, plastic blocks within the ELPs can be stabilized by chemical crosslinking of the lysine residues. While previous work by Sallach and colleagues have demonstrated the superior mechanical properties of **LysB10** films and hydrogels for soft tissue engineering applications, it was hypothesized that the hydrophilic elastic domains that are solvated by an aqueous environment should provide a favorable setting for the presentation of localized bioactive sequences for improved biological responses. Thus, 10 mg/mL and 5 mg/mL solutions of recombinant ELPs were formulated into soft gels at 37°C and stabilized by genipin crosslinking of the lysine residues. HUVEC adhesion was approximately twice as effective on genipin-crosslinked **V2** as on **LysB10** hydrogels. (Figure 3.8). Integrin-specific adhesion was observed on **V2** hydrogels while a background level of nonspecific adhesion was seen on **LysB10** gels.

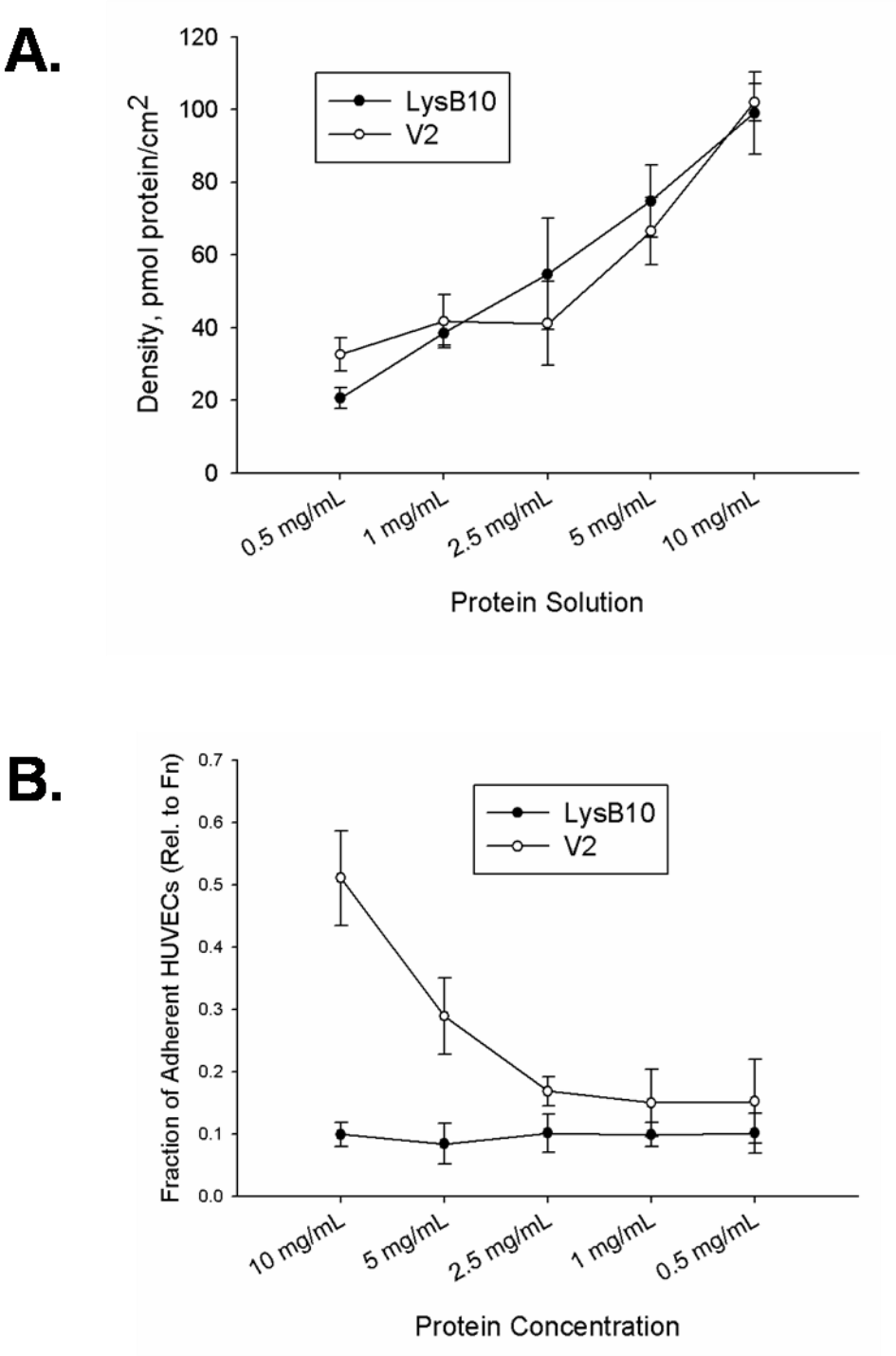

Figure 3.3. (A) V2 and **LysB10** protein solutions ranging from 0.5 mg/mL to 10 mg/mL were adsorbed at 37°C. Quantitation was performed with bicinchoninic acid protein assay. **(B)** HUVEC adhesion to varying amounts of adsorbed proteins. 50 ug/mL fibronectin was allowed to adsorb to surfaces to serve as a positive control, and all data was normalized to this control. Data represent one of three similar experiments, with each condition run in quadruplicate.

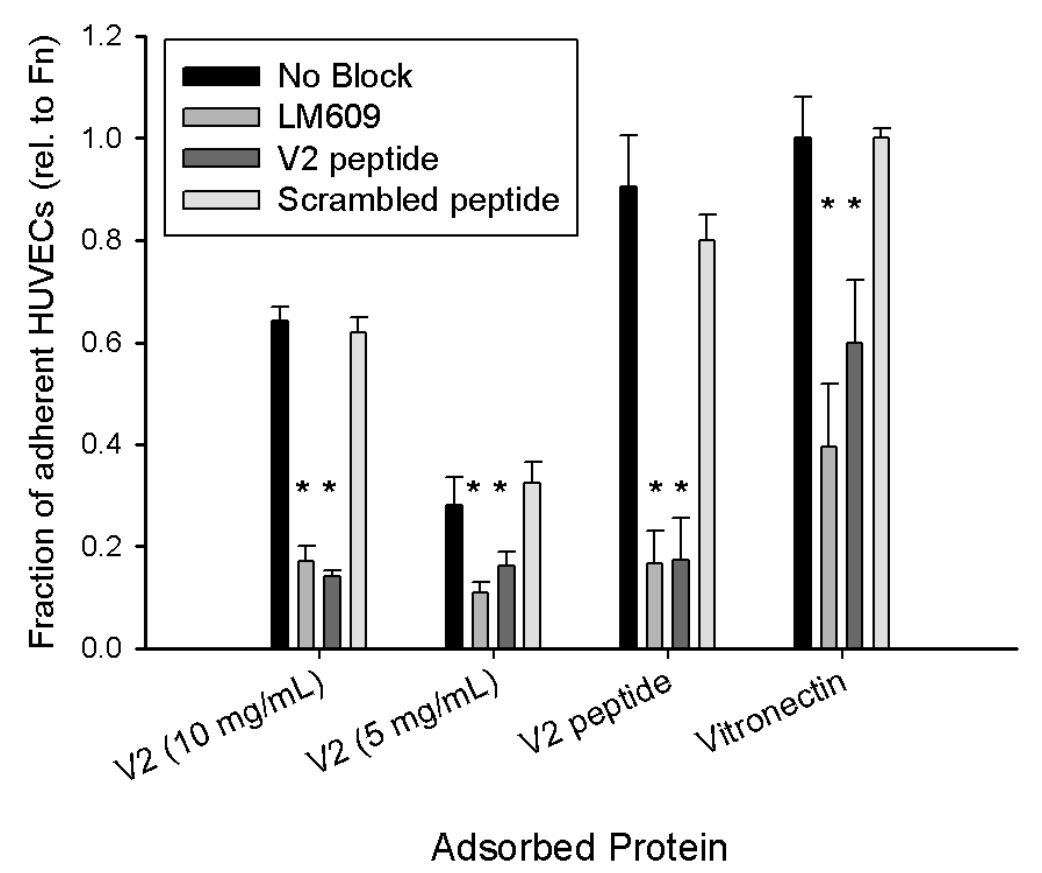

Figure 3.4. HUVEC adhesion and specificity to adsorbed protein polymer **V2**. The protein polymer supports $\alpha_v\beta_3$-dependent HUVEC adhesion. Cells were treated with LM609 (50 ug/mL) antibody, soluble V2 peptide (1mM), and scrambled V2 peptide (1mM) for 30 minutes prior to plating. All data was normalized to the fibronectin control. Data represent one of three similar experiments, with each condition run in quadruplicate. All values reported were corrected against blank wells blocked with 0.5% BSA. Competitive inhibitors LM609 and V2 peptide significantly reduced cell adhesion to substrates (***** versus 'no block' treatment group, $p<0.05$).

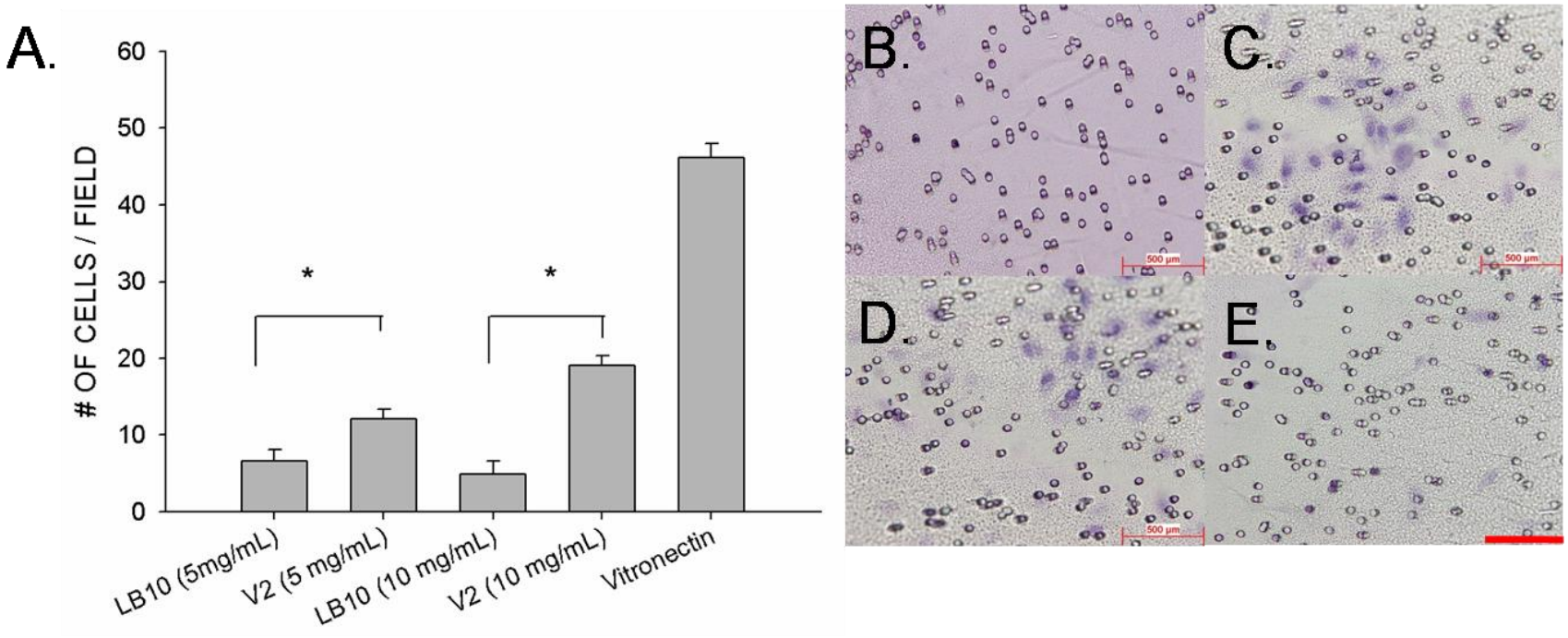

Figure 3.5. Haptotactic migration assay. 80,000 cells were allowed to migrate across inserts for 5 hours at 37°C. The average number of migrated cells in six randomly chosen fields of view per insert was taken to quantify the extent of migration. Red bars signify 500 um. **(A)** Quantitation of cells counted. Representative images of cells migrated to the lower insert surfaces of **(B)** 10mg/mL **LysB10** (C) Vitronectin (D) 10 mg/mL **V2** and (E) 5 mg/mL **V2**. *p<0.05

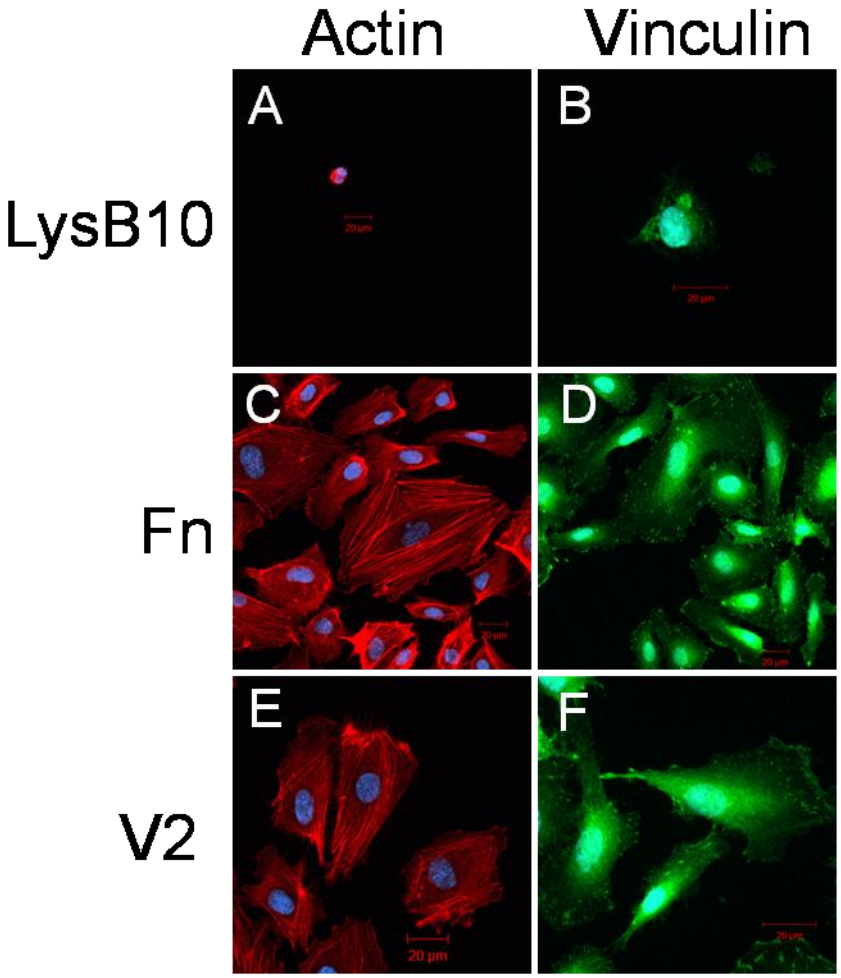

Figure 3.6. Representative confocal images of HUVECs cultured on adsorbed proteins for a period of 6 hours in serum-free media. Red bars represent 20um. 10 mg/mL LysB10 (A & B) and V2 solutions (E & F), along with 50 ug/mL fibronectin solution (C & D), were allowed to adsorb to glass slides and blocked in 0.5% BSA prior to cell seeding. Fluorescently labeled actin is shown in red (A, C, & E), while vinculin is displayed in green (B, D, & F).

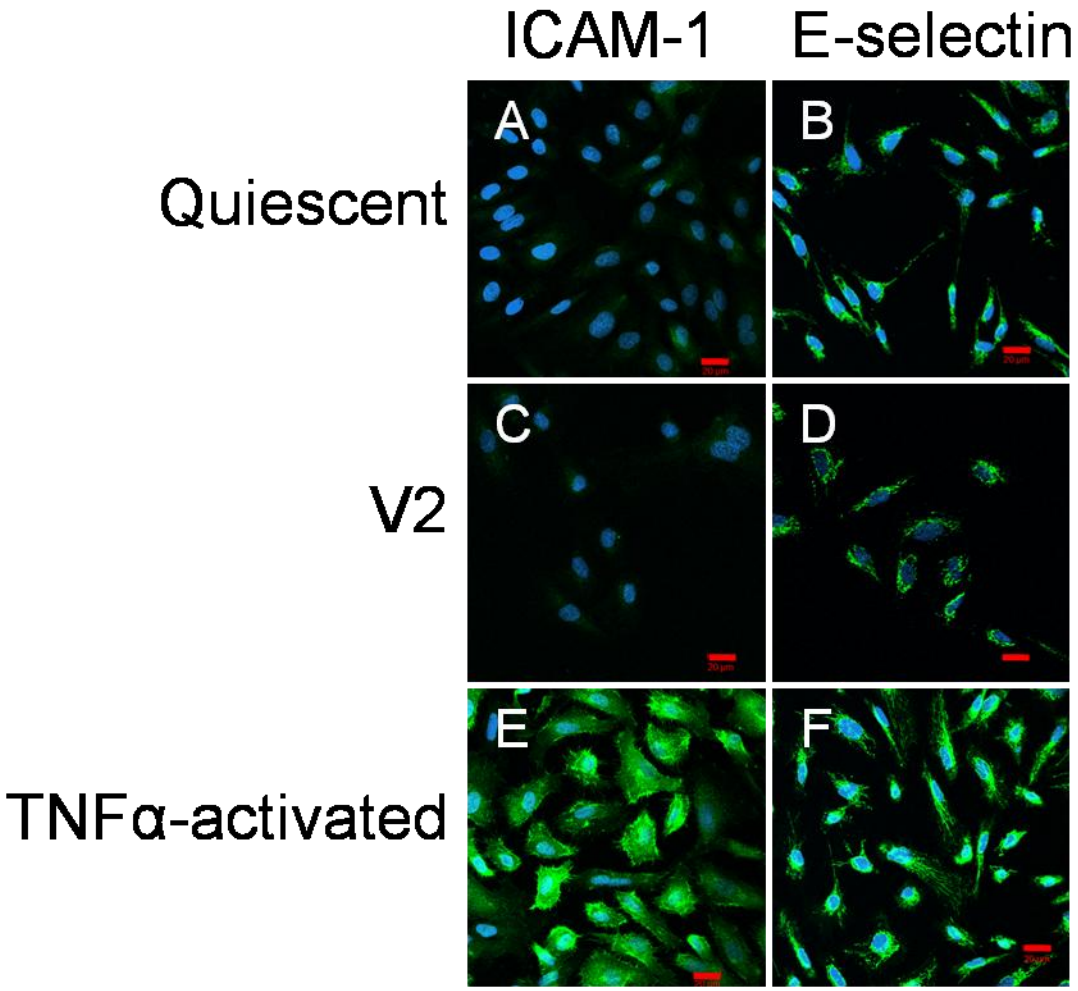

Figure 3.7. Representative confocal images of HUVECs cultured on protein polymer **V2**. Cells that were cultured on fibronectin-coated slides without TNFα stimulation (A & B) maintained a quiescent phenotype. Activation was achieved with the addition of TNFα to the culture medium (E&F). HUVEC activation or quiescence was compared to that on V2-coated slides (C & D). Markers of HUVEC activation were ICAM1-1 (A,C, and E) and E-selectin (B,D, and F). Red bars signify 20um.

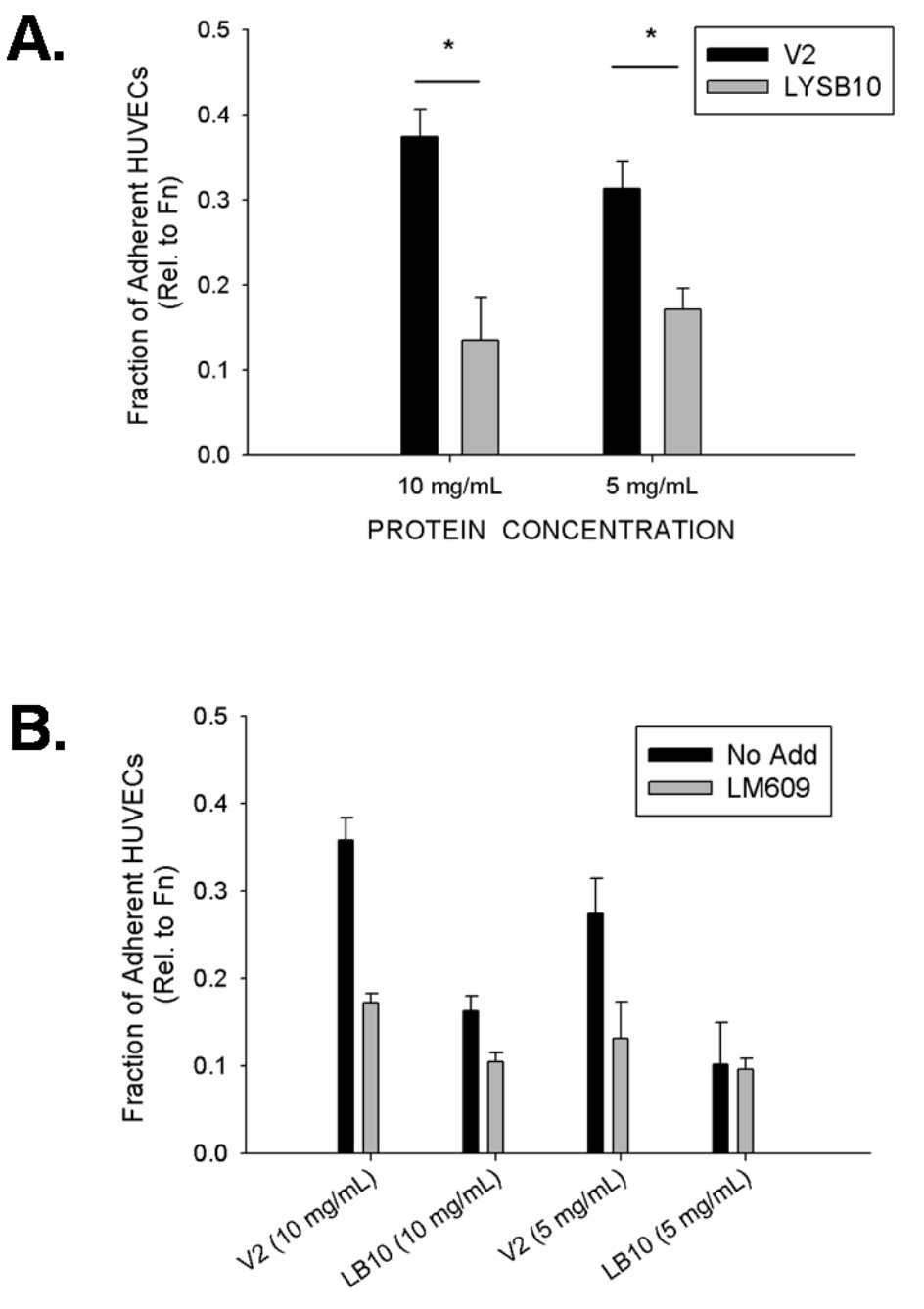

Figure 3.8. (A) HUVEC adhesion on genipin-crosslinked V2 and LysB10 hydrogels**. (B)** Integrin specificity was examined with the LM609 antibody. Cells were treated with LM609 (50 ug/mL) antibody for 30 minutes prior to seeding. 50 ug/mL fibronectin adsorbed onto polystyrene served as a positive control, and all data was normalized to this control. Data represent one of three similar experiments, with each condition run in quadruplicate. * $p<0.05$

3.4 DISCUSSION

In the present study, we sought to design a second generation elastin-mimetic triblock copolymer with the ability to guide endothelial cell behavior while maintaining the elastomeric properties of the protein polymer. Adhesion-promoting sequences, ligand density and clustering, and ELP morphology were manipulated in order to tailor material properties. To this end, a ligand isolated from pro-angiogenic, extracellular matrix–associated protein CCN1 was cloned into the central, hydrophilic domain of **LysB10**. Actin and vinculin staining confirmed that adherent cells were well-spread on the **V2** substrates. It was found that increasing densities of adsorbed **V2** protein polymer induced increased HUVEC adhesion. In particular, a density of at least 40 pmol/cm^2 was required to effectively influence endothelial cell adhesion onto modified substrates. To place this value in perspective, recent work by Tirrell and colleagues using RGD-incorporated elastin analogs documented a ligand density of approximately 2.4 pmol/cm^2 for maximal HUVEC adhesion [237, 243, 244]. This difference in surface concentration can be attributed to the ligand-receptor interactions on the cell surface. The RGD sequence, which engages multiple integrins on the endothelial cell surface ($\alpha_5\beta_1$ and $\alpha_v\beta_3$) is more efficient than the V2 ligand, which is solely dependent on integrin $\alpha_v\beta_3$ [253-255]. Similarly, adsorbed fibronectin is more effective as an adhesive coating because of its ability to target numerous integrin binding sites [256].

To determine whether **V2** was capable of modulating endothelial cell function in an integrin-dependent manner, or whether nonspecific electrostatic interactions were primarily responsible for cell behavior, blocking studies were performed. First, incubation of LM609 antibody with HUVECs eliminated their adhesion to **V2**-coated surfaces. As previously mentioned, this $\alpha_v\beta_3$integrin specificity has been well-documented in previous studies with the V2 sequence [203]. Vitronectin served as a positive control, as it utilizes $\alpha_v\beta_3$ as the primary binding site on the endothelial cell surface [257]. Furthermore, the soluble 20 amino acid V2

sequence, when incubated with HUVECs, also muted cell adhesive response to the **V2-**coated substrates, while the scrambled version did not affect HUVEC adhesion. This work confirms the ability to specifically modulate endothelial cell behavior on elastin-like protein polymers by tailoring their primary sequence.

Integrin-mediated cellular functions occur via diverse mechanisms. Previous studies have shown that the density of ECM proteins regulates cell adhesion, spreading, and migration speed. However, differences in experimental protocols and surface chemistry have resulted in a range of reported values for the minimal surface concentration required for cell adhesion and spreading. For example, Underwood and Bennet have demonstrated that a vitronectin density of 450 fmol/cm^2 and fibronectin density of 140 fmol/cm^2 is sufficient in inducing maximal cell adhesion [258]. Massia and Hubbell have reported that a minimal RGD peptide density of 10 fmol/cm^2 is required for fibroblast cell spreading and focal contact and stress fiber formation on glass [259]. In contrast, Patel et al have demonstrated a higher RGD peptide density ranging from 0.2-3 pmol/cm^2 for robust endothelial cell adhesion and spreading on interpenetrating polymer networks [260].

The multimeric structure of native ECM molecules such as fibronectin, a dimer with dual adhesion sites, and tenascin-C, which presents six repeats of cell adhesion domains, suggests that ligand clustering as well as ligand density regulates cell signaling [251]. Several studies have shown that the clustering of ligand-bound integrin receptors is essential in propagating intracellular signaling for proper cell function. For example, $\alpha_v\beta_3$ integrins can undergo affinity maturation, resulting in the recruitment of $\alpha_v\beta_3$ to focal adhesions in the cell periphery [261]. Nanoscale arrangement of RGD peptides has revealed that peptides presented as one peptide per molecule are poor substrates for fibroblast adhesion, while peptides presented in clusters of nine peptides per molecule or higher induce comparable cell attachment to matrix proteins [262]. Cell migration and spreading are dependent on this clustering mechanism as well.

It has been reported that endothelial cells increase the activation and ligation of $\alpha_v\beta_3$, while decreasing the activation and ligation of $\alpha_5\beta_1$, in order to facilitate migration for vascular wound healing [263, 264]. Integrin $\alpha_v\beta_3$, in turn, has been shown to interact with several transmembrane and membrane-associated proteins in an "outside-in" signaling mechanism important to cell mobility [265]. For example, vitronectin, a multivalent ligand, is able to increase integrin avidity, which leads to the propagation of intracellular signaling events, ultimately resulting in focal adhesion sites, cell adhesion, and migration [266, 267]. Given the role of the V2 sequence in binding to $\alpha_v\beta_3$, it is not surprising that the **V2** protein polymer was able to regulate HUVEC migration. This functionality is particularly useful when applied to vascular tissue engineering, as the migration of vascular cells can facilitate vascular wall regeneration and promote endothelialization of a graft or stent.

Adhesive strength and ligand surface density are critical factors in endothelial cell motility. In particular, previous results from experiments and mathematical modeling have shown that cell migration rates have a biphasic dependence on the surface density of ligands and cell attachment strength [260, 268, 269]. At low adhesiveness, the cell cannot form strong and stable adhesions at the leading edge to allow traction to pull itself forward. At high adhesiveness, the trailing edge of the cell cannot be released [270, 271]. Furthermore, growth factors and other chemotactic agents can influence the dynamics of the cytoskeleton leading to cell motility. For example, controlled release of sphingosine 1-phosphate, vascular endothelial growth factor, and basic fibroblast growth factor have been proven to promote endothelial cell migration by increasing lamellipodia formation and extension in the leading edge of the cell [272-274].

Many tissue engineering applications require the use of three-dimensional scaffolds and porous coatings. Therefore, we also explored ligand presentation in a three-dimensional environment, seeding HUVECs onto **LysB10** and **V2** hydrogels. The lysine residues within the protein polymers were crosslinked with genipin, a cytocompatible chemical crosslinker, in order

to stabilize the intermolecular, physical crosslinks within the elastin-like network [275-280]. While the **LysB10** hydrogel presented a relatively non-adherent surface to cells, **V2** continued to be able to support cell adhesion, at both 5 mg/mL and 10 mg/mL formulations. It is interesting to note, however, that cell adhesion was lower on the 10 mg/mL **V2** hydrogel than on its passively adsorbed **V2** counterpart. This phenomenon is most likely due to the differences in ligand presentation between a passively adsorbed **V2** molecule, and one that is suspended within the three-dimensional hydrated polymer network. In particular, both physical and chemical crosslinking of the plastic domains in the **V2** hydrogel impart a strain on the entire **V2** molecule, limiting any conformationally favorable mobility within the cell-binding sequence for receptor-ligand recognition. Although the exact three-dimensional structure of the V2 active site is poorly understood in the literature, mutational analysis has identified that the aspartate residue, as well as two cysteine residues flanking the sequence, are critical in binding to the $\alpha_v\beta_3$ receptor [203]. Other studies with integrins and phage display analysis of $\alpha_v\beta_3$ binding sites have suggested that two cysteine residues flanking the core binding sequence may form disulfide bonds to present the binding site as a loop, which would increase binding affinity [206-208]. If a tertiary looped structure is involved in V2 presentation to the integrin binding site, any conformational strain upon the V2 sequence would limit cell adhesion.

Integrin specificity is critical in directing cell fates such as migration, proliferation, and differentiation, as different integrins trigger specific signaling pathways [265, 281]. Thus, a major disadvantage of short peptides such as RGD, which binds multiple integrins, is their inability to elicit specific cell responses based on defined intracellular pathways. In contrast, the ability of V2 to target $\alpha_v\beta_3$ provides a unique approach to facilitating robust endothelial cell adhesion, focal adhesion assembly, and migration. In particular, this CCN1-mimetic ligand has been shown to promote neovascularization and angiogenesis, and is therefore an ideal biomolecule in vascular tissue engineering and wound healing applications [186-190]. While V2 does act as

an endothelial cell adhesion ligand, further experiments need to be performed to evaluate its effectiveness in binding other cell types. For instance, although integrin $\alpha_v\beta_3$ is highly expressed in angiogenic endothelial cells, it is also expressed on leukocytes.

3.5 CONCLUSION

Integration of biologic and structural functions of the extracellular matrix provides a robust design strategy for generating biomaterials that stimulate arterial wall regeneration. Therefore, the long-term goal encompassing this work was to utilize a biomolecular engineering approach that introduced cell-adhesive peptide motifs within a bio-inspired recombinant elastin-like protein polymer in order to elicit an integrin-mediated cellular response.

The **LysB10** triblock copolymer provides a versatile, non-fouling platform for engineering bioactive ligands mimicking the functions of the extracellular matrix. The ability to precisely control ligand presentation is an important design parameter, and ultimately directs cell fates such as adhesion, migration, focal adhesion assembly, spreading, proliferation, and differentiation. Thus, endothelial cell adhesion, migration, and morphology were evaluated as markers of surface functionality on the recombinant protein polymers. The improved biological activity of **V2** engineered surfaces compared to **LysB10** alone can be attributed to enhanced binding of integrin $\alpha_v\beta_3$. This approach of conveying specificity may provide a robust biomolecular strategy to elicit directed biological responses. In addition, integrin-specific biomimetic surfaces utilizing recombinant peptides of matrix molecules often exhibit lower immunogenicity and higher stability than the whole proteins. Ultimately, the generation of modified protein polymers presents a clinically relevant approach to promoting endothelialization of vascular tissue-engineered scaffolds and coatings.

CHAPTER 4

Chemical conjugation of cell-binding domain to elastin-mimetic protein polymer

4.1 INTRODUCTION

Recently, we reported a new class of recombinant elastin-mimetic protein polymer for the purpose of designing materials as small-diameter vascular grafts [14]. Synthetic grafts have been known to fail *in vivo* due to compliance mismatch between the grafts and surrounding arterial tissue [2-5]. Therefore, researchers have explored the potential of incorporating scaffolds with more extensible proteins such as elastin, a key structural element in native vasculature [87]. While native elastin's intrinsic insolubility has limited its use in biomedical applications, structural and sequence analyses of tropoelastin have determined that pentapeptide repeat motifs similar to VPGVG exhibit elastomeric behavior with features that are consistent with native elastin, including a mobile backbone and the presence of β turns [247, 248]. Consequently, elastin-like protein polymer **LysB10** was designed with the capability of physical and chemical crosslinks, and was shown to display a range of elastomeric properties that more closely match those of the native artery [14, 222-225]. This amphiphilic triblock copolymer (ABA) consisting of hydrophobic (A) and hydrophilic (B) domains was synthesized such that phase separation of the more hydrophobic blocks occurred in water under physiologically relevant conditions to form virtual crosslinks, while the hydrophilic domains remained non-crosslinked and solvated by the aqeous environment [218, 219]. The introduction of lysine residues enabled chemical crosslinking to stabilize the resulting hydrogel. This multiblock system results in structural polymorphism and the potential for a wide range of functional responses, including mechanical and biological performance. Thus, elastin-like

protein copolymers (ELPs) represent a unique class of thermoreversible hydrogels for soft tissue engineering applications.

The generation of protein polymers that mimic native structural proteins and adopt the characteristics of the arterial wall offers a unique approach to develop a vascular graft. Several investigators have endeavored to minimize graft failure due to thrombosis and intimal hyperplasia by mimicking the biologic responsiveness of the native vasculature. In particular, the poor patency rates of synthetic polymers have motivated strategies to functionalize the luminal surface of grafts in order to promote endothelialization of the material surface [7, 9, 11, 12, 26-29, 31, 32, 34, 249, 250].

While genetic engineering has allowed researchers to recombinantly express elastin polypeptides with cell-binding domains and other bioactive ligands to direct cellular behavior, chemical immobilization of short peptides to a recombinant protein polymer presents several advantages. Genetic cloning and recombinant protein expression is a time-intensive and expensive process, and therefore, is not an ideal tool for screening a wide range of bioactive domains. The synthesis of short peptides with functionalized endgroups does offer a more versatile approach for biomaterial testing. Furthermore, chemical synthesis offers the possibility of incorporating ligands that cannot be processed via the biosynthetic machinery.

A number of surface modification techniques have been developed in order to impart further biofunctionality to a material. For example, substrates used for studying cell behavior are prepared by adsorbing extracellular matrix proteins and their bioactive derivatives onto surfaces. This method results in a heterogeneous population of molecules and adsorption states on the surface due to possible unfolding events and conformational differences [282-285]. Presentation of bioadhesive motifs can be more tightly controlled with covalent tethering of biomolecules onto a biomaterial [286, 287]. This approach frequently involves reactions between the side chains of

amino acids and activated surface functional groups. The most popular but least specific method is coupling to the amino group of a lysine residue, which reacts efficiently with a number of functional groups, including aldehydes and activated carboxylic acids. Another reactive side group, the thiol side chain on cysteine, can be utilized in conjugation reactions to form disulfide bonds. However, disulfide formation is a fully reversible reaction through the use of standard reducing agents, and surfaces which have been RGD functionalized via disulfide formation lack stability [288, 289].

A major drawback to the approaches discussed above is that it is extremely difficult to control the bioconjugation reaction in such a way that only one specific linker between the protein and the target is created. For instance, if a bioactive ligand contains amino acids with similar reactive side groups at a critical integrin-binding site, chemical conjugation to a functionalized surface may lead to loss of bioactivity. Selective ligation chemistries have been developed in order to resolve the problems that arise with nonspecific covalent linkages. In this work, we have utilized maleimide-thiol chemistry for surface biofunctionalization. The high degree of specificity and reactivity of sulfhydryl groups with maleimide moieties to form stable thioether bonds has been exploited extensively in the field of bioconjugate chemistry for the construction of immobilized antibodies, enzymes, and peptide-conjugate haptens [290-293]. Maleimide reacts approximately 1000 times faster with thiols than with amines at neutral pH and below, and this reaction is widely used for conjugation of cysteine-containing peptide and proteins [294-296].

The RGD sequence was utilized in this study as a model peptide conjugate. The RGD sequence has been identified in many ECM proteins, including fibronectin, vitronectin, fibrinogen, von Willebrand factor, and collagen, and binds to numerous integrins, notably alpha5beta1 and alphavbeta3 [162]. As a result of its ability to promote cell adhesion, proliferation, migration, and survival in an integrin-dependent manner, the sequence is most

often employed for promoting cellular responsiveness on otherwise bioinert substrates. A wide range of polymers and hydrogels have been derivatized with the RGD peptide. These materials include polymers such as PEG hydrogels [297, 298], polyacrylamide [260, 299], poly(2-hydroxyethyl methacrylate) [300, 301], poly(lactic acid-co-lysine) [302] [303], poly(propylene fumarate) [304-306], polyurethanes [307-309], and more natural materials, including collagen [310-312], fibrin [182, 250], hyaluronic acid [313, 314], alginate [315, 316], dextran [317, 318], elastin-like proteins [230, 311, 319], and silk-like proteins [320].

The aim of this study was to develop a strategy for chemoselective ligation of bioactive peptides to the recombinant elastin hydrogel **LysB10**. In particular, the carboxylic acid functional group on glutamic acid residues along the **LysB10** polymer chain was utilized to chemically modify the recombinant protein polymer. It was hypothesized that the synthesis of thiolated **LysB10** along with an RGD conjugate functionalized with a terminal maleimide group would provide an effective conjugation scheme for spatial presentation and localization of bioactive ligands on the **LysB10** surface. Moreover, this controlled peptide presentation onto the functionalized hydrogel surface would stimulate vascular cell adhesion and growth. In this chapter, we outline the chemistry used for modifying **LysB10** with the RGD ligand, and illustrate increased cellular interaction on **LysB10**-RGD hydrogels, utilizing endothelial cells and mesenchymal stem cells as model cell types. This work is the first step in creating a synthetic ECM with ELPs for vascular tissue engineering applications.

4.2 MATERIALS AND METHODS

Reagents, Antibodies, and Cells

The synthesis and characterization of the RGD-maleimide linker (Scheme 4.2) is described in Appendix B, with **LysB10** protein expression and purification described in Appendix A. The chemicals N-(3-dimethylaminopropyl)-N'-ethylcarbodiimide (EDC) and cystamine dihydrochloride, and protein fibronectin were purchased from Sigma Aldrich. The reducing agent TCEP and maleimide-PEG_2-biotin linker were purchased from Pierce. Ellman's reagent and L-cysteine were procured from ThermoScientific. The sequences GRGDSP and GRGESP were synthesized by Anaspec. Fluoreporter biotin quantitation assay kit for biotinylated proteins was purchased from Molecular Probes. Porcine mesenchymal stem cells (pMSCs) were a kind gift from Dr. Steven Stice (University of Georgia). Human umbilical vein endothelial cells and EGM-2 media supplements were obtained from Clonetics, while pMSC basal media and supplements were purchased from Fisher Scientific and Invitrogen. Fibronectin solution was obtained from Sigma Aldrich. Radial migration of cells on **LysB10** surfaces was measured with the use of the Oris cell migration assembly kit, from Platypus Technologies, and calcein AM (Molecular Probes). Immunofluorescence studies were performed with mouse anti-human E-selectin and mouse anti-human ICAM-1 antibodies purchased from Millipore. Immunostaining reagents goat anti-mouse IgG antibody, streptavidin-AlexaFluor 488, phalloidin-AlexaFluor 568, and ProLong Gold antifade reagent with DAPI were all purchased from Invitrogen (Molecular Probes).

Synthesis of modified LysB10

LysB10 was chemically modified utilizing aqeous carbodiimide chemistry (Scheme 4.1) [295]. **LysB10** was dissolved at a concentration of 10mg/mL in cold phosphate-buffered saline. Cystamine (Sigma Aldrich) was added to the solution at a 20 fold molar excess over the amount

of **LysB10**. To activate the carboxylic acid groups in **LysB10,** a 5-fold molar excess of N-(3-dimethylaminopropyl)-N'-ethylcarbodiimide (EDC) over the amount of cystamine was added to the solution. The reaction was allowed to continue for 72 hours at 4°C. The cystamine-modified **LysB10** polymer was purified by dialysis. After lyophilization, the yield of the modified protein polymer was approximately 81%.

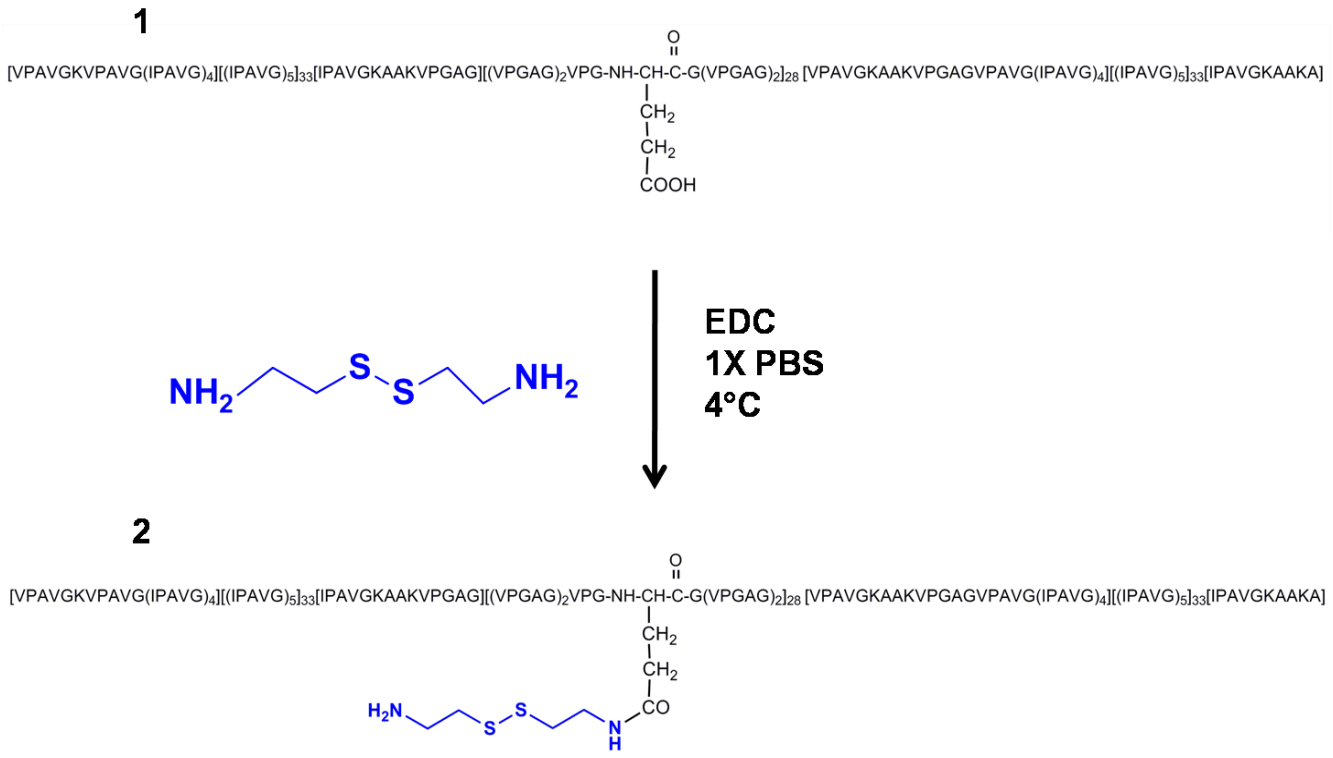

Scheme 4.1. Reaction scheme of bulk modification of LysB10 (1) molecule via glutamic acid residues. Amide bond formation is mediated by the carbodiimide through the carboxylic group of the amino acid and the amine of cystamine, resulting in thiolated **LysB10 (2).**

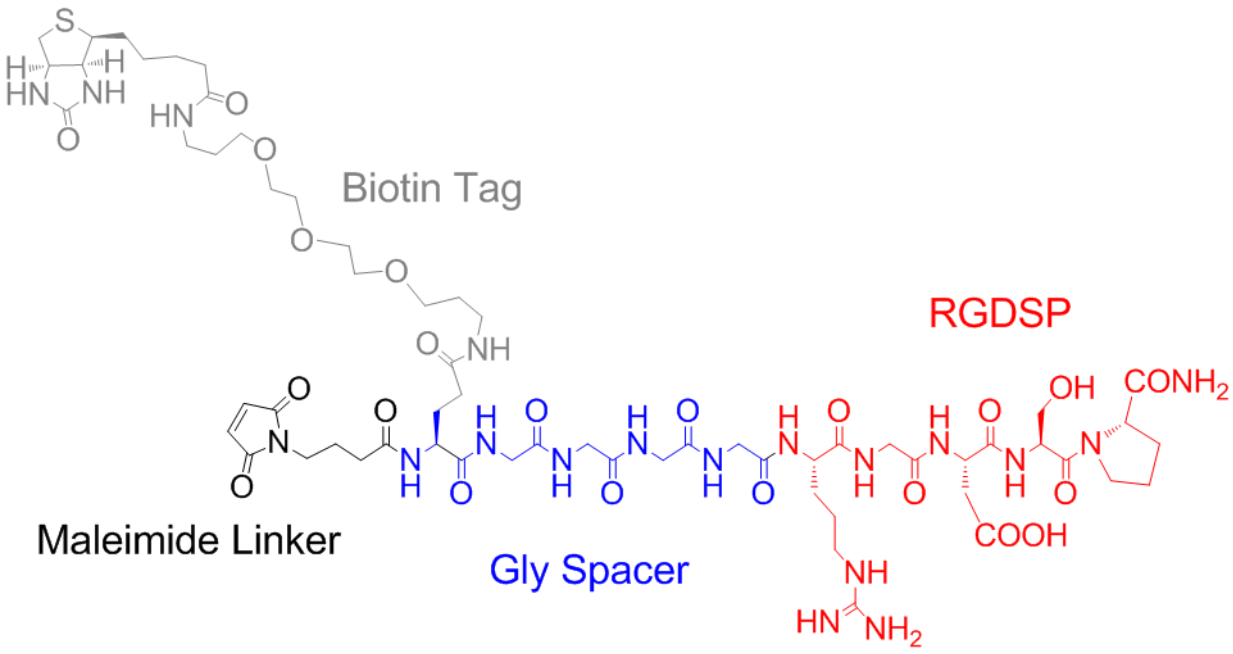

Scheme 4.2. RGD peptide linker. Peptides were generated via solid phase synthesis (see Appendix B), with key features incorporated in the design. The N-terminus of the molecule contains the thiol-reactive maleimide linker (black). Four glycine residues act as a spacer between the cell-binding RGD domain (red) and the remaining sequence to facilitate ligand-integrin presentation. A biotinyl-PEG_3 tag (gray) was incorporated into the peptide for detection of the molecule.

Hydrogel modification

Lyophilized cystamine-modified **LysB10** protein was dissolved in PBS at a 10wt% concentration. 40 uL of solution was carefully pipetted and uniformly coated into wells of a polystyrene 96-well plate at 4°C. Hydrogel formation was achieved by placing the plate at 37°C, well above the transition temperature of the protein polymer, for 1 hour. Lysine residues of the protein polymer were crosslinked with a 6 mg/mL genipin solution for 24 hours, followed by stringent PBS rinsing to remove all genipin. The thiol groups were reduced with the addition of 26mM Tris(2-carboxyethyl)phosphine (TCEP) for 6 hours. After rinsing the gels with three 20 minute PBS washes, gels were ready for conjugation and characterization experiments. Unmodified **LysB10** hydrogels were generated in a similar manner, with the exception of the reducing (TCEP) step.

Characterization of free sulfhydryl groups

Ellman's reaction was utilized to quantify the extent of thiolated **LysB10**. A cysteine standard curve was generated with 0 to 1.5 mM cysteine dilutions in a reaction buffer of 0.1 M sodium phosphate with 1 mM EDTA, pH 8.0. Ellman's reagent solution was prepared by dissolving 4 mg Ellman's reagent in 1 mL of reaction buffer. Reduced 10 mg/mL LysB10-cystamine solutions and the surfaces of a 10wt% hydrogel were reacted with Ellman's Reagent solution diluted in reaction buffer and incubated at room temperature for 15 minutes. Absorbance at 412 nm was measured in a 96-well plate. Values obtained for the standards generated a standard curve, which was then used to determine the experimental sample concentrations.

Conjugation Efficiency

Maleimide-PEG_2-biotin linker was incubated for 2 hours at room temperature to unmodified and thiol-modified **LysB10** hydrogels. 1 mg/mL, 150 ug/mL, 50 ug/mL, 25 ug/mL, 10

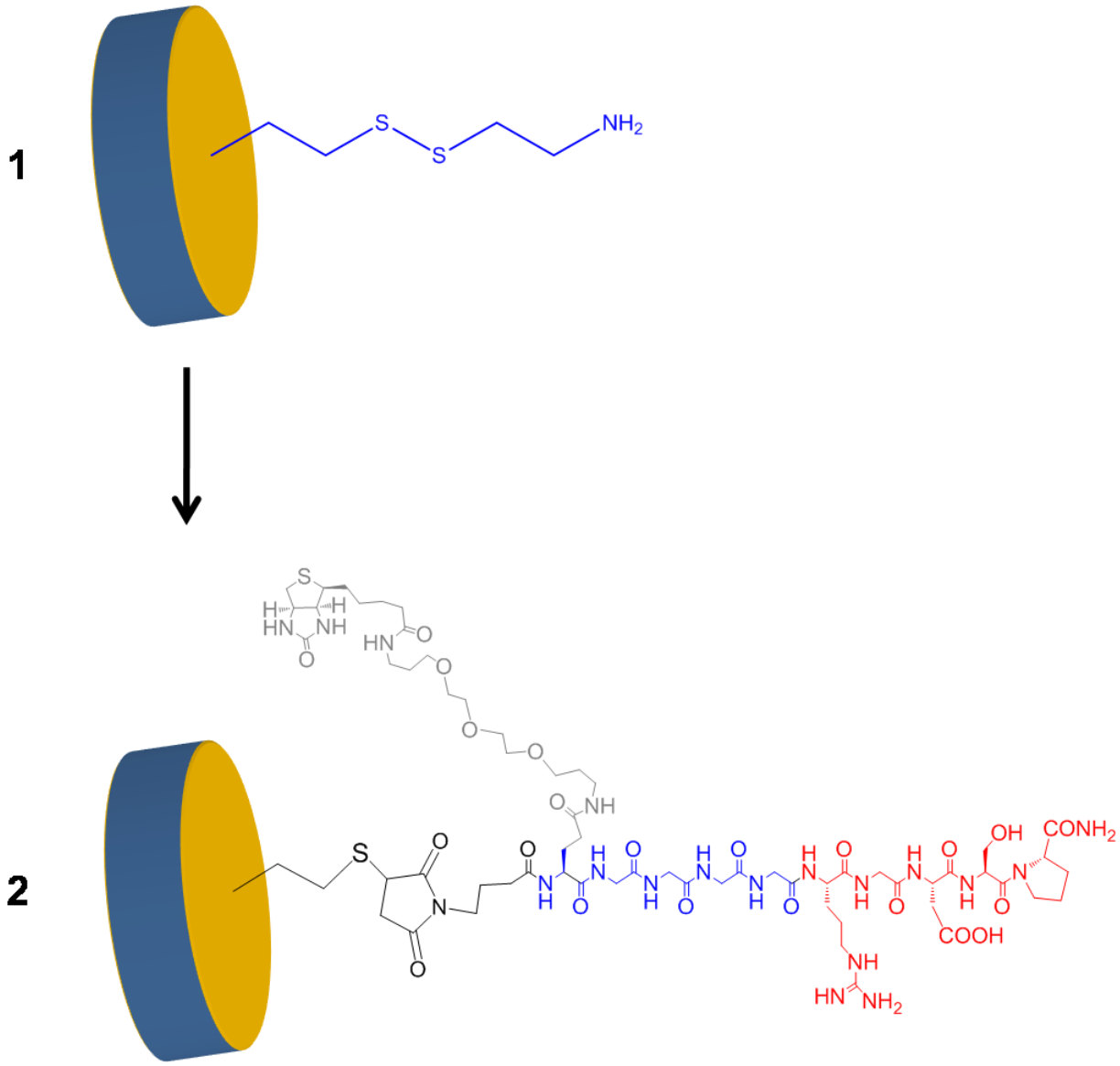

Scheme 4.3. Reaction scheme of peptide coupling to 10wt% thiolated-LysB10 hydrogel. **(1)** Hydrogel formation was achieved by placing 10wt% thiol-**LysB10** solution (Scheme 4.1) at 37°C, well above the transition temperature of the protein polymer. Lysine residues of the protein polymer were crosslinked with a 6 mg/mL genipin solution for 24 hours, followed by stringent PBS rinsing to remove all genipin. The thiol groups were reduced with the addition of 26 mM Tris(2-carboxyethyl)phosphine (TCEP) to form free sulfhydryls. **(2)** After rinsing the gels with three 20 minute PBS washes, thiol-reactive peptide linker (Scheme 4.2) was incubated for 2 hours at room temperature to form a thioether bond with the protein polymer.

ug/mL, and 5 ug/mL linker concentrations were added to hydrogel surfaces to evaluate conjugation efficiency. Upon linker grafting, daily PBS changes were performed for 5 days to remove nonspecifically-bound linker. In order to assess the moles of biotin conjugated to the **LysB10** hydrogel surface, the fluoreporter biotin quantitation assay kit (Molecular Probes) was utilized. Briefly, the kit provides a sensitive fluorometric assay for accurately determining the number of biotin labels on a protein. A standard curve was developed with known amounts of biocytin added to unmodified **LysB10** gel surfaces. Once conjugation with the model linker was demonstrated, the assay was repeated with the RGD-maleimide linker to verify results. RGD-maleimide linker synthesis and characterization is discussed in Appendix B.

Cell Studies

Thiol-modified and unmodified 10wt% **LysB10** hydrogels were formulated as described previously (hydrogel modification section). The substrates were then incubated with RGD linker solutions at room temperature for 2 hours. PBS rinsing over a 5-day period ensured complete removal of unbound peptide prior to cell studies.

Cell Adhesion and Specificity Assays

Human umbilical vein endothelial cells (HUVECs) were purchased from Clonetics and maintained in endothelial growth medium-2 (EGM-2, 2% serum, Clonetics). Porcine mesenchymal stem cells were cultured in alpha-MEM basal medium supplemented with 10% fetal bovine serum, 50U/mL penicillin, 50ug/mL streptomycin, and 2mM L-glutamine. They were kept in a humidified, 5% CO_2 environment at 37°C, and passaged every 2 days via standard culture techniques. HUVECs and pMSCS between passages 3 and 9 were used for all experiments. To begin, cells were harvested with Cell Dissociation Solution (EDTA, glycerol, sodium citrate, PBS, from Sigma) in order to maintain integrin functionality on the cell surface. After centrifugation at 220g for 5 minutes, HUVEC suspensions were prepared at a density of

200,000 cells/mL in basal medium containing 0.5% bovine serum albumin (BSA). MSCs were prepared at the same density in low-serum medium (1% serum). For peptide inhibition studies, detached cells were treated with soluble GRGDSP or GRGESP (2 mM) for 30 minutes at room temperature before plating. 100uL of the cell suspension was plated onto **LysB10** surfaces, and after incubation at 37°C for 2 hours, wells were washed three times with phosphate-buffered saline (PBS). Cell adhesion activity was evaluated with the CyQuant Cell Proliferation Assay Kit (Molecular Probes), which utilizes a fluorescent dye with strong fluorescence enhancement when bound to cellular nucleic acids (excitation/emission maxima ~480/520 nm). Briefly, after thawing frozen cells to enhance lysis, the CyQuant cell lysis buffer was added to each sample, along with CyQuant fluorescence reagent. Samples were then measured in a microplate spectrofluorometer. Results were normalized to adhesion levels on fibronectin-coated wells, which acted as the positive control.

Cell Proliferation Assay

Proliferation rates were evaluated with the CyQuant Cell Proliferation Assay Kit. Cells were seeded onto various **LysB10** gels at a density of 5,000 cells/well for 2 hours. Unbound cells were removed with media washes and substrate-bound cells were maintained in culture for another 48-hour period. Cell counts at 48 hours were compared to those at 2 hours.

Cell Migration Assay

LysB10 hydrogels with varying treatment groups (n=4) and fibronectin-coated wells were formulated in 96-well plates (black, clear bottom) provided by the manufacturer of the Oris cell migration assay FLEX kit (Platypus Technologies). Cell seeding stoppers with diameters of 2mm were placed on top of the hydrogels and wells to prevent cells from adhering to the central detection zone. Cells were harvested with Cell Dissociation Solution (EDTA, glycerol, sodium citrate, PBS, from Sigma) in order to maintain integrin functionality on the cell surface. After

centrifugation at 220g for 5 minutes, HUVEC suspensions were prepared at a density of 400,000 cells/mL in serum-free basal medium. MSCs were prepared at the same density in low-serum medium (1% fetal bovine serum). Cell suspensions were treated with 10ug/mL mitomycin C (Sigma Aldrich) in order to arrest cell proliferation. 100uL of the cell suspension was seeded onto the outer annular region of the hydrogel surfaces (30 mm^2). Cells were allowed to adhere to the seeding region for 6 hours at 37ºC, at which point the stoppers were removed to allow for migration into the central detection zone (3.14 mm^2). Several reference wells were designated, in which the stoppers remained in place until wells were read (t=0 pre-migration controls). Unbound cells were gently removed by rinsing the wells with complete media, after which all wells were filled with 150uL complete media. Cells were incubated at 37ºC for 36 hours. Quantitation of migration was performed by staining the adherent cells with Calcein AM. Briefly, wells were washed three times with PBS, after which a 2uM Calcein AM solution was added to each well and incubated for 1 hour. Migrated cells in the central detection zone were analyzed with a fluorescent plate reader. The Oris detection mask was secured to the bottom of the 96-well plate in order to prevent signal detection of the outer annular region. Therefore, any fluorescent signal detected was isolated from migratory cells in the central detection zone. Readings from the pre-migration control wells were subtracted from the post-migration wells to eliminate noise due to background. Data was normalized to the fibronectin positive control.

Immunofluorescence Studies

Fluorescent staining of cytoskeletal component F-actin (HUVECs and pMSCs) and cellular adhesion molecules ICAM-1 and E-selectin (HUVECs) were performed on cells cultured on **LysB10** hydrogels or RGD-conjugated **LysB10** hydrogels in polystyrene 8-well chamber slides (Nalge Nunc, International). Fibronectin controls were formulated by adsorbing 50ug/mL solutions overnight at 4°C. 200uL cell suspensions (approximately 15,000 cells/well) of HUVECs were seeded onto the slides and cultured for a period of 2 hours (for F-actin staining)

or 4 hours (for ICAM-1 and E-selectin staining) in serum-free medium. pMSCs were cultured in low-serum (1% FBS) media. To achieve HUVEC activation, 100 ng/mL of TNFα was added to cells cultured on fibronectin-coated slides for 4 hours prior to immunostaining. Subsequently, the cells were fixed in 4% paraformaldehyde (10 minutes), permeabilized with PBS containing 0.5% Triton X-100 (10 minutes), rinsed once with 100 mM glycine (10 minutes), and incubated with block buffer (PBS+/+, 0.2% Triton X-100, 6% goat serum) for 1 hour at room temperature. For F-actin staining, cells were incubated with Alexa Fluor 568-conjugated phalloidin for 30 minutes. 10ug/mL solutions of E-selectin and ICAM-1 monoclonal antibodies were incubated for 1 hour in order to evaluate HUVEC activation/quiescence states. Primary antibody incubation was followed by 45 minute incubation with 2.5 ug/mL biotinylated goat anti-mouse IgG secondary 30 minute incubation with 2.5 ug/mL streptavidin-AlexaFluor 488 tertiary. Nuclei were counterstained with Prolong Gold mounting medium containing DAPI, and the resultant staining was imaged using confocal microscopy (Emory University).

Statistical Analysis

Comparison between groups was analyzed via ANOVA and a paired, two-tailed student's t-test, with $p<0.05$ considered to be significant. Results are presented as mean ± standard deviation. Data represent characteristic results from a particular experimental run (each group run in quadruplicate), although at least three independent runs were conducted.

4.3 RESULTS

Design of the RGD peptide linker

The RGD peptide linker was designed to optimize ligand presentation to integrin receptors on the cell surface (Scheme 4.2, Appendix B). Enhanced cell adhesion has been shown for the sequence GRGDSP due to the contributions that the flanking residues make toward the overall peptide conformation and stability. Thus, this short sequence was chosen as a model ligand that would elicit a robust cellular response. Another concern in the peptide design was its spatial arrangement on the conjugated surface. The RGD sequence in native ECM is presented as an exposed loop of the protein. Similarly, the peptide must stand out from the artificial surface in order to interact with the crevice of the integrin receptor. Various investigators have resolved this issue by creating oligo glycine spacer lengths ranging from 2 to 12 glycines in order to distance the tether site from the RGD sequence. Based on these observations, 4 glycine residues were utilized in our peptide. An N-terminal maleimide was synthesized to facilitate covalent linkage to a thiol-modified surface. Finally, detection of the immobilized peptides was facilitated by the addition of a biotin moiety.

Chemistry

To confirm chemical modification of **LysB10**, the extent of thiol modification was first determined. Ellman's reaction was performed on reduced **LysB10**-cystamine solutions and hydrogels. Results indicated that 54.7±1.9% and 48.6±2.5% of carboxylic acids were modified, respectively. This correlates to 13 to 15 of the 28 available carboxylic groups being converted to thiol moieties in every **LysB10** molecule. Control reactions without thiol reduction were run, resulting in 0% modification.

To optimize the maleimide-thiol chemical reaction and incorporation onto modified **LysB10** gels, a wide concentration range of input RGD linker was first explored (5 ug/mL – 5 mg/mL). Passive adsorption onto unmodified **LysB10** hydrogels served as an internal control in order to distinguish between chemically conjugated linker and its adsorbed counterpart. As shown in Figure 4.1, incorporation of the peptide linker steadily increased, reaching a plateau at 1 mg/mL. While linker incorporation onto unmodified **LysB10** hydrogels was nonexistent at lower concentrations, background associated with nonspecific passive adsorption increased at the 150 ug/mL to 5 mg/mL RGD range. Thus, the 5-day PBS rinsing protocol to remove nonspecific adsorption of linker was only successful when applied to gels with low concentration linker solutions (50 ug/mL and below).

Although solid-phase conjugation requires less peptide to coat the hydrogel surface (as opposed to bulk solution phase peptide-**LysB10** modification), it is difficult to calculate peptide grafting efficiency using this methodology. However, surface densities of linker were calculated assuming a 50 nm penetration of reactants, similar to the assumption made by Mooney and colleagues [303, 315]. In this case, grafting efficiency of 50 ug/mL RGD linker solution is approximately 37%, correlating to 5 RGD peptides per **LysB10** molecule.

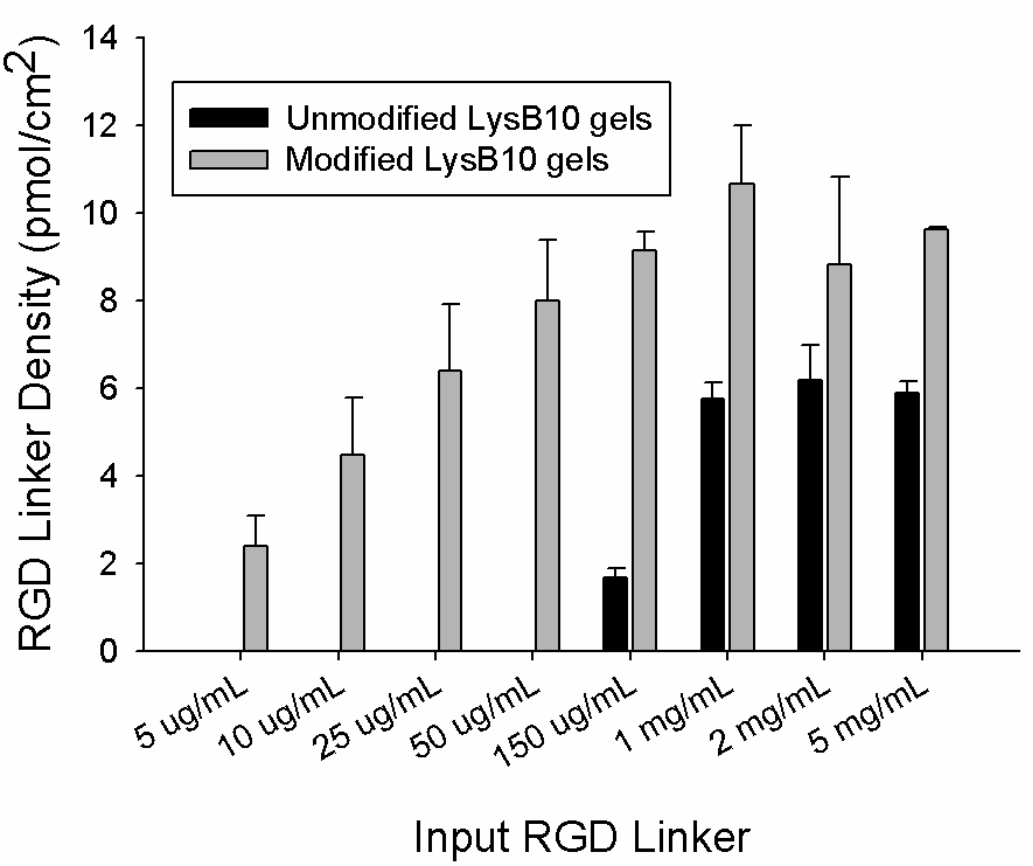

Figure 4.1. Coupled RGD peptide as a function of the amount of input peptide in surface modified LysB10. Data represent one of three similar experiments, with each condition run in quadruplicate. Peptide conjugation was assessed with the use of the biotin tag. In order to determine the moles of biotin conjugated to the **LysB10** hydrogel surface, the fluoreporter biotin quantitation assay kit was utilized.

Cell Studies

Cell Adhesion

Success of the peptide immobilization scheme was characterized by cellular response to the RGD-conjugated 10wt% **LysB10** hydrogels. Unmodified **LysB10** gels were treated with varying concentrations of RGD to compare cellular behavior between RGD adsorption and RGD conjugation on **LysB10** surfaces. A 50 ug/mL RGD linker solution was allowed to passively adsorb for 2 hours at room temperature onto polystyrene to demonstrate the bioactivity of the RGD peptide. Similarly, a 50ug/mL fibronectin solution was passively adsorbed onto polystyrene and served as the positive control against which all other data was normalized.

Cell culture experiments with HUVECs and pMSCs were utilized to illustrate enhanced ligand-receptor interactions. Data was normalized to the number of adherent cells on fibronectin-coated polystyrene (positive control). As previously mentioned, a 5-day PBS rinse period after peptide incubation was introduced into the protocol in order to remove any nonspecifically adsorbed peptides on the **LysB10** surface. Based on RGD incorporation studies (Figure 4.1), HUVEC adhesion experiments focused on four input RGD concentrations (10 ug/mL, 50 ug/mL, 150ug/mL, and 1 mg/mL). HUVECs seeded onto the RGD-coupled hydrogels attached and began spreading by 2 hours (Figure 4.2). Minimal HUVEC adhesion was observed on **LysB10** hydrogels with no RGD added. For those surfaces treated with 10 ug/mL and 50 ug/mL RGD, adhesion on thiol-modified **LysB10** was approximately 6-fold higher than that of the unmodified **LysB10**. An increase in peptide input concentration from 50 ug/mL to 1 mg/mL did not significantly increase adhesion levels, reaching a plateau at approximately 80% adhesion (compared to fibronectin positive control). However, adhesion due to nonspecific RGD adsorption on unmodified **LysB10** was doubled. The results underscore the importance of minimizing effects due to RGD adsorption on **LysB10**, while maximizing adhesion due to thiol-

reactive peptide conjugation to **LysB10**. Thus, 50 ug/mL peptide input concentrations were utilized as optimal conditions in further cell experiments.

Mesenchymal stem cell (MSC) experiments were performed in low-serum media (1% fetal bovine serum added) because of MSC sensitivity to complete serum starvation. The interaction of serum proteins with the thiol-functionalized **LysB10** surface resulted in a 1.5-fold increase in MSC attachment to non-RGD treated, thiol-modified gels compared to HUVECs. However, RGD tethering to modified **LysB10** increased MSC adhesion by a factor of 4.5 compared to MSC adhesion on non-RGD treated, modified **LysB10** alone (Figure 4.3A). Furthermore, adhesion levels on RGD-conjugated **LysB10** matched those of the positive control (fibronectin-coated polystyrene). Cell spreading was greatly enhanced on RGD-conjugated **LysB10**, with well-developed actin stress fiber networks apparent in HUVECs and pMSCs. However, on unmodified **LysB10**, cells assumed rounded morphologies, with actin molecules distributed in a nonspecific manner (Figure 4.2B-D and Figure 4.3B-D).

Cell Specificity

To ensure that improved adhesion and spreading were mediated by RGD-specific cell adhesion receptors, competitive inhibition studies were performed. Thiol-modified **LysB10** gels were treated with 50 ug/mL maleimide-PEG_2-biotin linker or 50 ug/mL RGD linker. Unmodified **LysB10** gels were treated with 50 ug/mL RGD linker and served as a control. The specificity of HUVEC and pMSC adhesion was illustrated by adding soluble GRGDSP or soluble GRGESP at 2mM to the cell solution to compete for binding sites with the RGD-coupled **LysB10** surfaces. Commercially available maleimide-PEG_2-biotin was chosen for its similarity to the RGD peptide linker, and was utilized in RGD specificity studies to examine whether the chemical conjugation reaction itself (maleimide linkage to free sulfhydryls to form a thioether bond) would affect cell adhesion. Cell attachment was significantly impaired on RGD-conjugated **LysB10** gels when

cells were incubated with GRGDSP. Quantification of the number of HUVECs and MSCs on RGD-functionalized **LysB10** revealed an 8-fold and 5-fold decrease in adhesion with soluble GRGDSP present in the seeding medium, respectively (Figure 4.4). However, cell attachment was not affected by the soluble scrambled sequence GRGESP, thereby confirming integrin-specific interaction between the cells and the RGD sequence. As expected, minimal non-specific cell adhesion was observed on unmodified **LysB10** gels and those with conjugated PEG linker (no RGD sequence).

Cell Proliferation Studies

Cell proliferation over a 48-hour period on treated hydrogels was next quantified (Figure 4.5). While unmodified **LysB10** hydrogels were not able to support adhesion and proliferation of cells, RGD-modified **LysB10** did promote a 3.5-fold increase in HUVEC density (Figure 4.5A), closely matching the proliferation rate on fibronectin-coated polystyrene. Proliferation rate was lower for pMSCs seeded onto RGD-grafted **LysB10** (approximately two-fold increase), while the positive control (fibronectin) supported a three-fold increase (Figure 4.5B).

Radial Migration Studies

Radial migration is a key factor in endothelialization of a biomaterial surface. To evaluate the ability of treated **LysB10** gels to modulate cell migration, HUVECs were seeded onto an outer annulus area and monitored for motility into an inner radial zone over a 36 hour period. Calcein AM staining of the migrated cells enabled fluorescent measurement of the number of migrated cells into the detectable inner zone, which was normalized against the number of migrated cells on fibronectin-coated polystyrene (Figure 4.6A). RGD-conjugated **LysB10** was able to stimulate a significantly higher number of HUVECs (74% of Fn control) to cross to the inner detection zone than its unmodified **LysB10** hydrogels (6-fold increase), $p<0.05$.

Similarly, an important characteristic of mesenchymal stem cells is that they migrate to sites of tissue injury as a result of the local production of inflammatory mediators in order to modulate tissue remodeling and repair [321]. When the radial migration assay was performed with pMSCs, the RGD-conjugated **LysB10** substrate was also able to stimulate migration (57.4% of Fn control) that was significantly higher than on unmodified **LysB10** (10-fold increase), $p<0.05$. As expected, the non-adherent **LysB10** surface prevents cell spreading, and thus, is unable to promote a directional migratory response (Figure 4.6B).

HUVEC Activation State

Finally, the functional state of an endothelial cell monolayer determines its ability to act as a thromboresistant barrier for blood-contacting material applications. Therefore, the success of an endothelialized surface is dependent on either activation or quiescence of adherent endothelial cells. To monitor endothelial phenotype, HUVECs were assessed with immunofluorescence staining of the cellular adhesion molecules ICAM-1 and E-selectin (Figure 4.7). Cells that were cultured on fibronectin-coated polystyrene and maintained in culture overnight in serum-free media assumed a quiescent state, with little ICAM-1 and E-selectin expression on the cell surface. Activation of HUVECs was achieved by adding 100ng/mL TNFα to the media for 4 hours. The positive and negative controls were compared to those cells adherent for 4 hours in serum-free media on RGD-conjugated **LysB10**. Limited ICAM-1 and E-selectin staining was observed. Thus, endothelial cells are not only able to adhere, spread, proliferate, and migrate on RGD-grafted **LysB10** substrates, but can maintain the phenotype necessary to limit platelet adhesion.

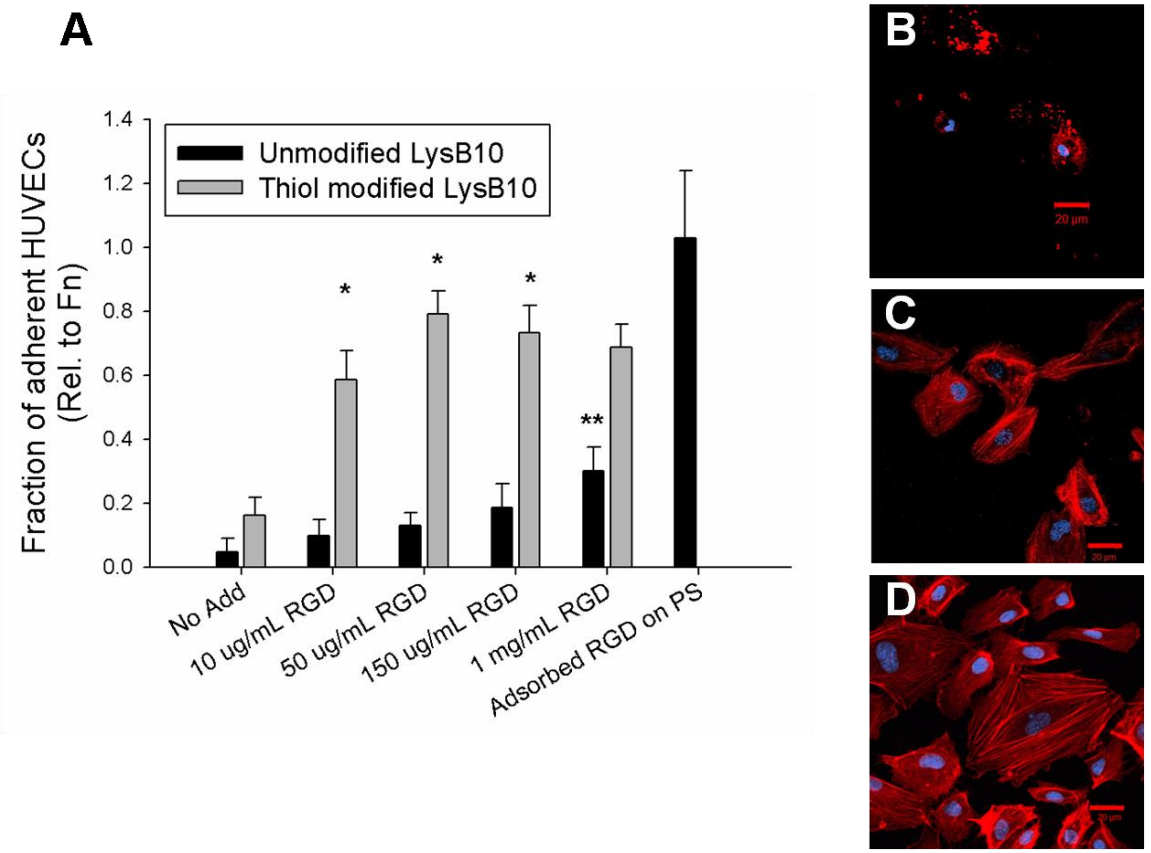

Figure 4.2. (A) HUVEC adhesion to varying LysB10 hydrogel surfaces after 2 hours. 50 ug/mL fibronectin adsorbed to polystyrene served as a positive control, and all data was normalized to this control. Data represent one of three similar experiments, with each condition run in quadruplicate. *p<0.01 compared to unmodified LysB10-RGD at the same concentration. **p<0.05 compared to unmodified LysB10-no add control. Representative confocal images of HUVECs cultured on LysB10 gels are shown, with red bars representing 20um. 10 wt% unmodified LysB10 with adsorbed 50 ug/mL RGD linker **(B),** modified LysB10 with conjugated 50 ug/mL RGD linker **(C),** along with fibronectin-coated glass **(D).** Fluorescently labeled actin is visualized in red.

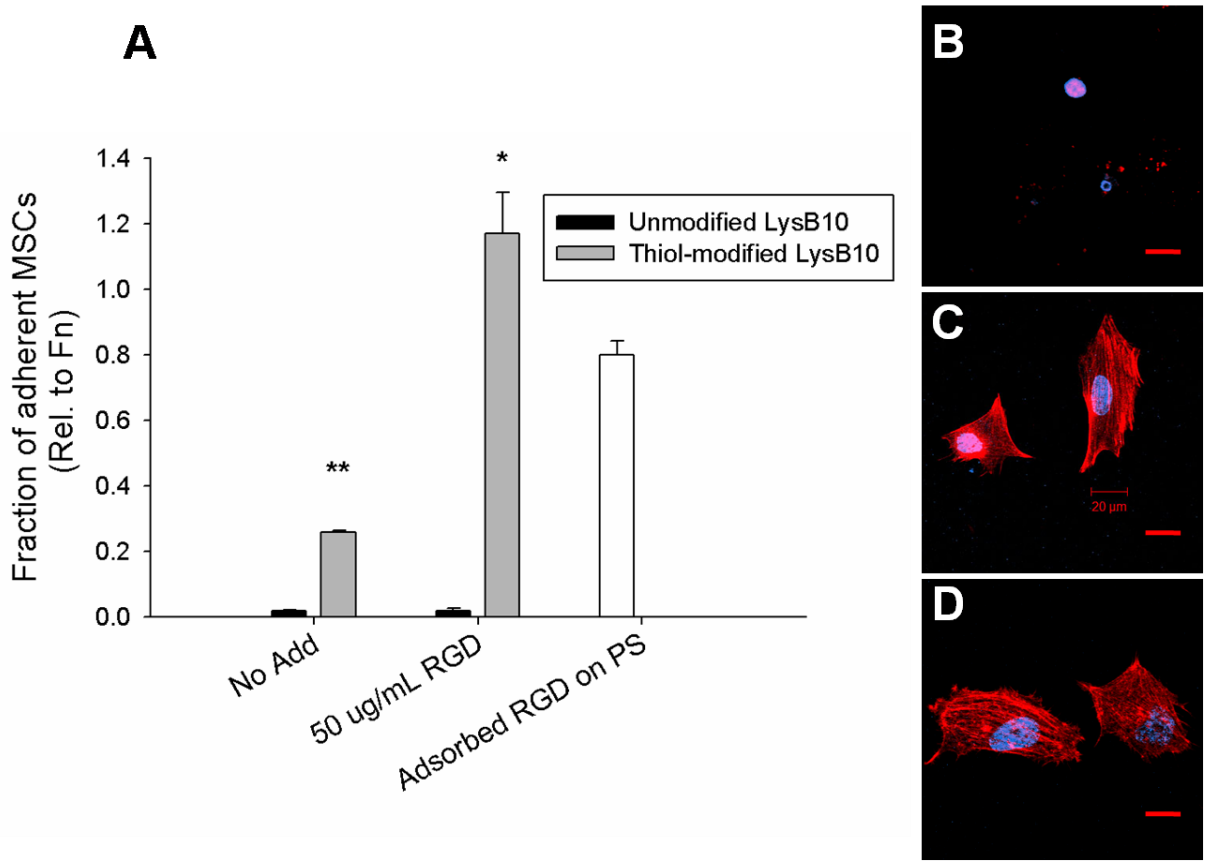

Figure 4.3. (A) pMSC adhesion to varying LysB10 hydrogel surfaces after 2 hour assay. 50 ug/mL fibronectin adsorbed to polystyrene served as a positive control, and all data was normalized to this control. Data represent one of three similar experiments, with each condition run in quadruplicate. *p<0.05 compared to thiol-modified LysB10-no add. **p<0.05 compared to unmodified LysB10-no add control. Representative confocal images of pMSCs cultured on LysB10 gels are shown, with red bars representing 20um. 10 wt% unmodified LysB10 with adsorbed 50 ug/mL RGD linker **(B),** modified LysB10 with conjugated 50 ug/mL RGD linker **(C),** along with fibronectin-coated glass **(D).** Fluorescently labeled actin is shown in red.

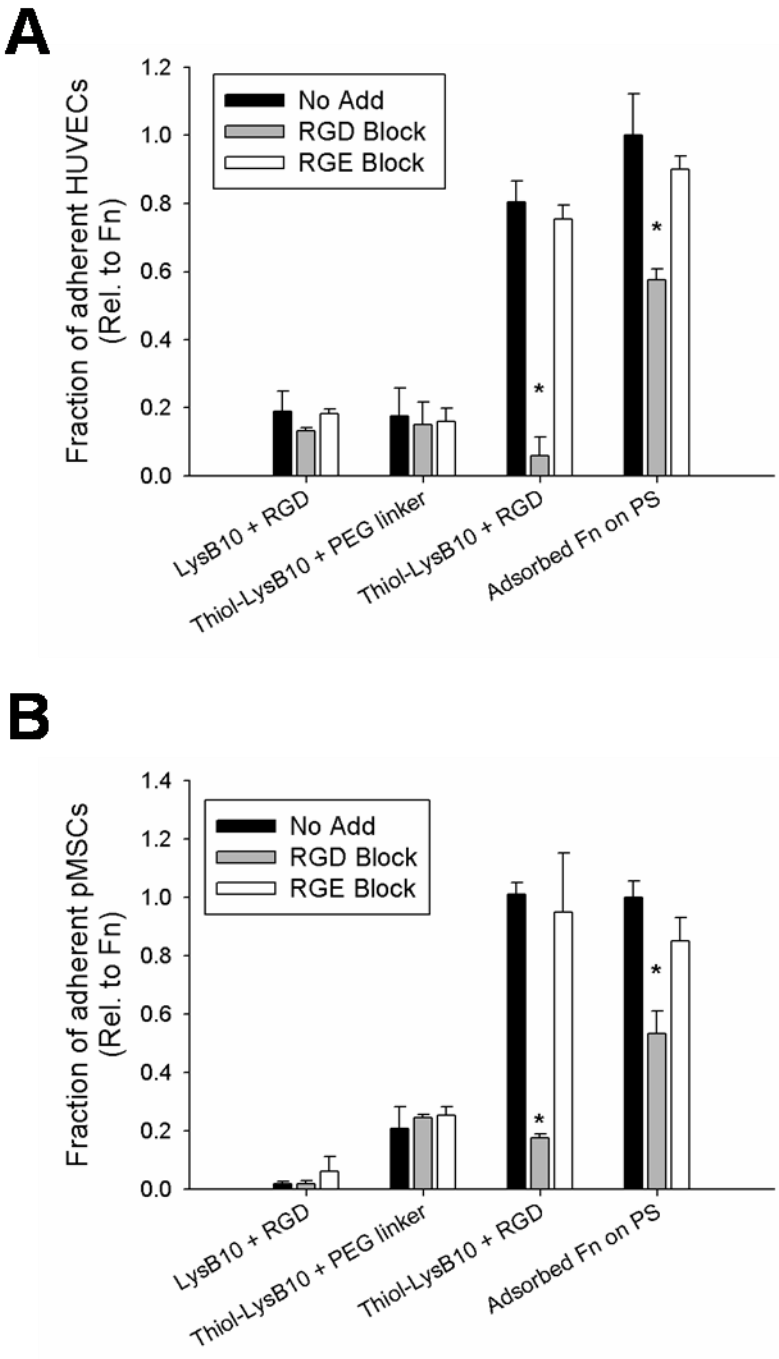

Figure 4.4. HUVEC **(A)** and pMSC **(B)** adhesion and specificity to treated LysB10 hydrogel surfaces. Adhesion on RGD-conjugated LysB10 gels is sequence-specific. Cells were treated with soluble GRGDSP (2 mM) and soluble GRGESP peptide (2 mM) for 30 minutes prior to plating. All data was normalized to the fibronectin, no add control. Data represent one of three similar experiments, with each condition run in quadruplicate. ***** $p<0.05$ compared to no-add treatment group.

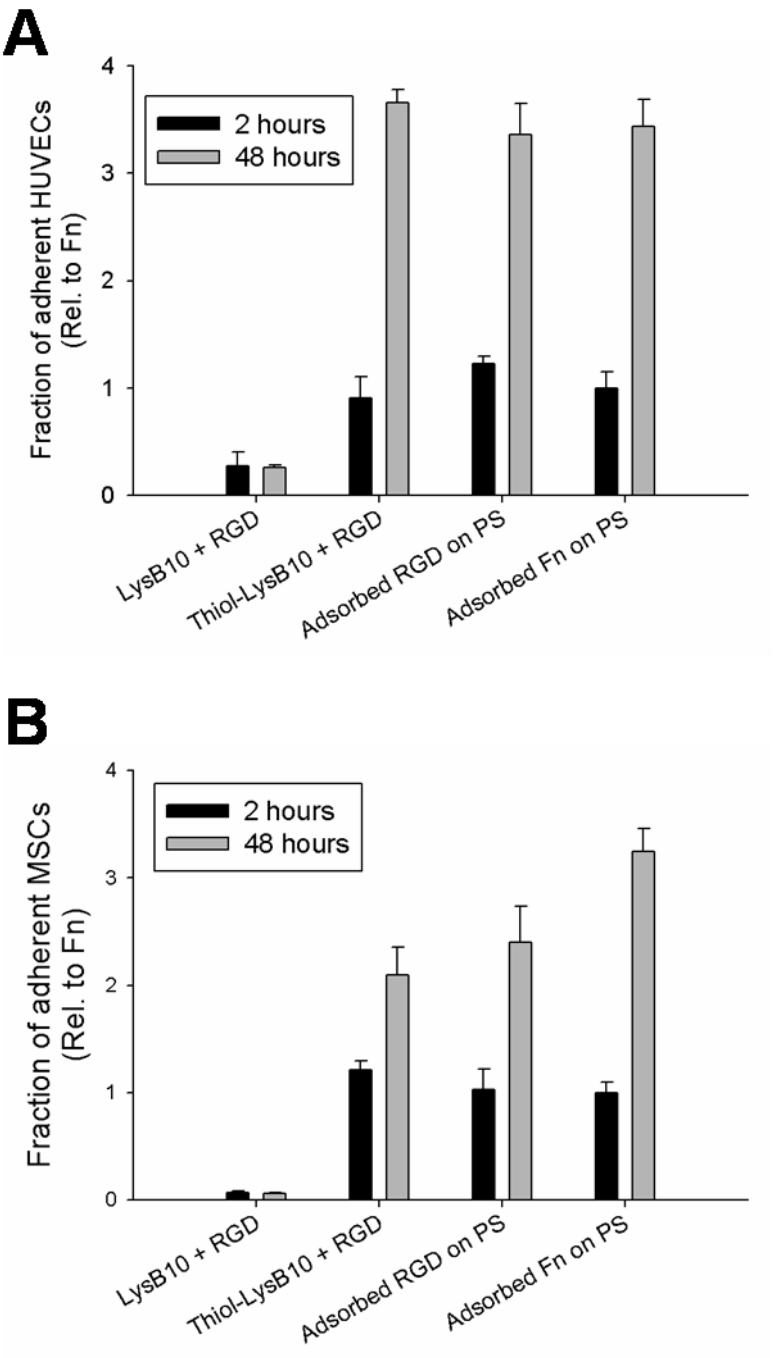

Figure 4.5. Proliferation rate of (A) HUVECs and (B) pMSCs over a 48 hour period. Cells were seeded onto various LysB10 gels at a density of 5,000 cells/well for 2 hours. Unbound cells were removed with media washes and substrate-bound cells were maintained in culture for another 48-hour period. All cell counts were normalized to the 2-hour adhesion value on fibronectin-coated polystyrene. Cell counts at 48 hours were compared to those at 2 hours for each treatment group.

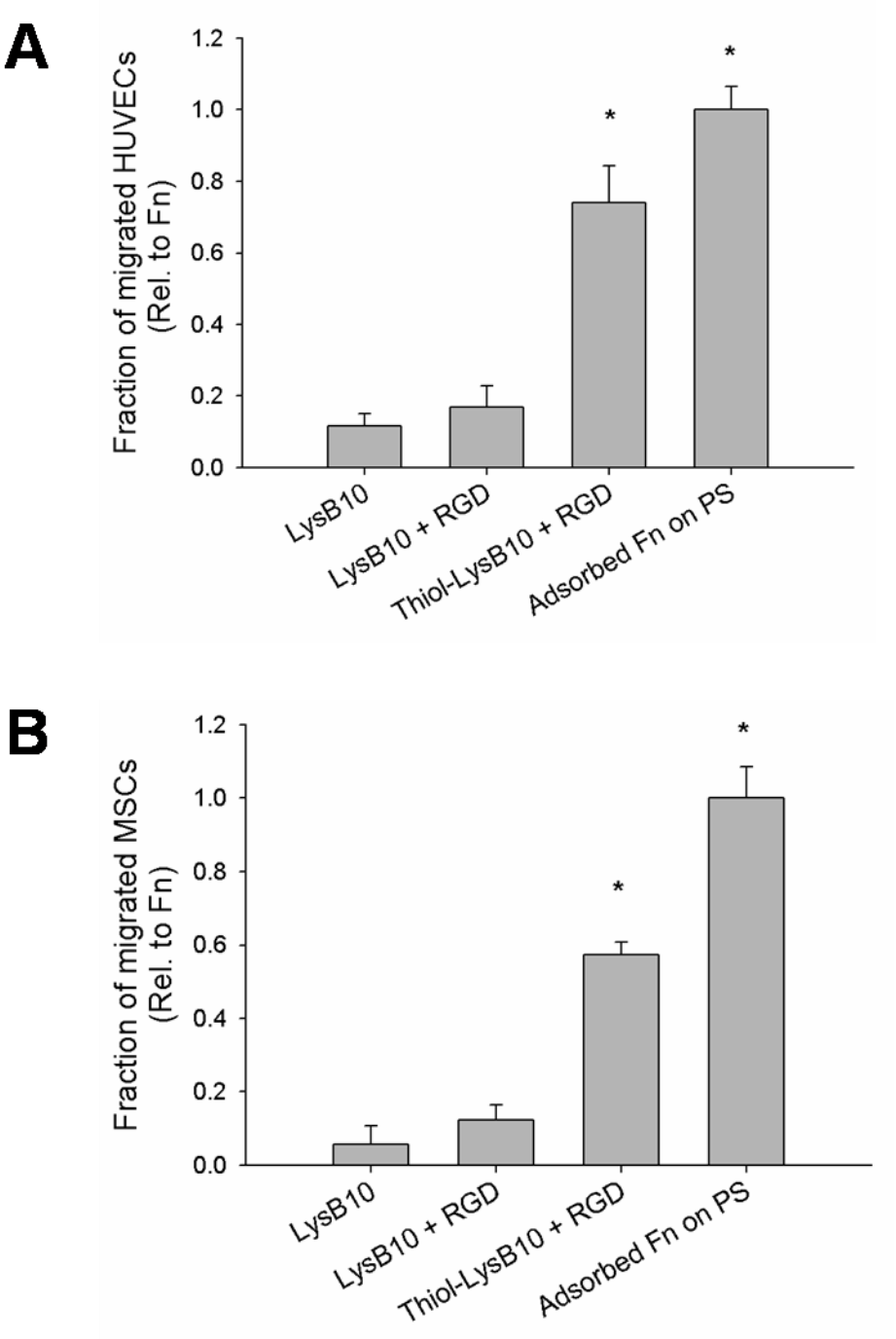

Figure 4.6. Radial migration assay of HUVECs **(A**) and pMSCs **(B).** Cells were seeded onto an outer annulus area and monitored for motility into an inner radial zone over a 36-hour period. Quantitation was achieved with fluorescent measurement of the number of migrated cells into the detectable inner zone, which was normalized against the number of migrated cells on fibronectin-coated polystyrene .*p<0.05 compared to non-RGD treated, unmodified **LysB10**.

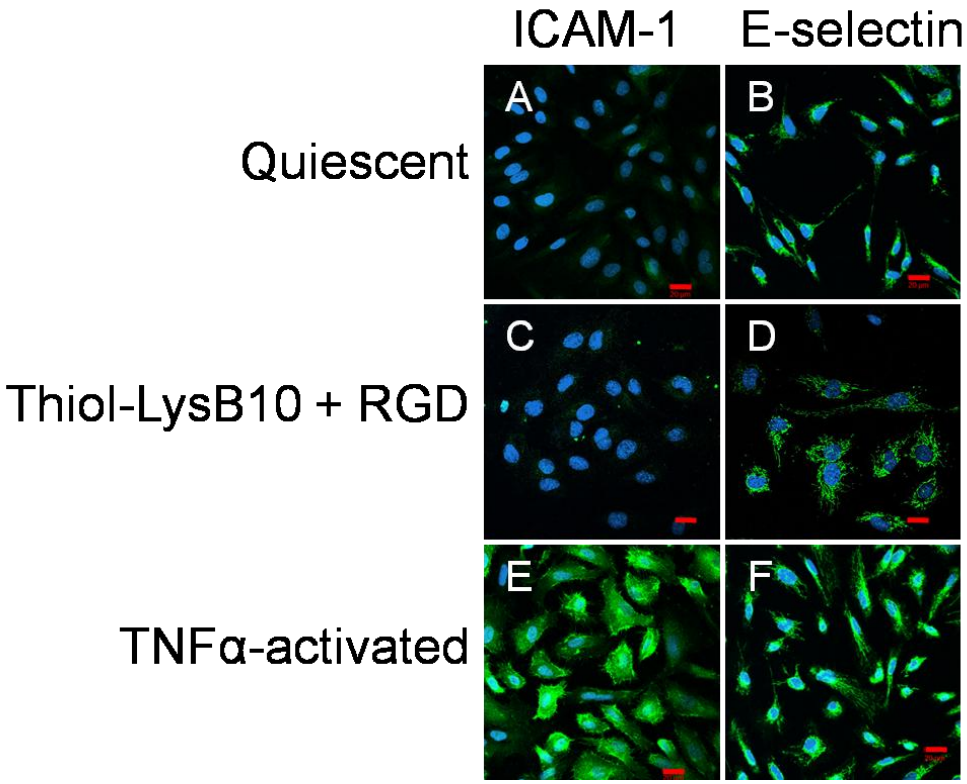

Figure 4.7. Representative confocal images of HUVECs cultured on various substrates. Cells that were cultured on fibronectin-coated slides without TNFα stimulation (**A & B**) maintained a quiescent phenotype. Activation was achieved with the addition of TNFα to the culture medium (**E&F**). HUVEC activation or quiescence was compared to that on RGD-conjugated LysB10 films (**C & D**). Markers of HUVEC activation were ICAM1-1 (**A,C, and E**) and E-selectin (**B,D, and F**). Red bars signify 20um.

4.4 DISCUSSION

Many tissue engineering applications require the use of three-dimensional scaffolds and porous coatings. Therefore, we explored ligand presentation in a three-dimensional environment, seeding HUVECs onto RGD-modified 10wt% **LysB10** gels. The lysine residues within the protein polymers were crosslinked with genipin, a cytocompatible chemical crosslinker, in order to stabilize the intermolecular, physical crosslinks within the elastin-like network [275-280].. Chemical conjugation was utilized to covalently couple the cell adhesion peptide GRGDSP to the surface of elastin-like protein polymer hydrogels. This chemistry successfully modulated biological interactions on ELPs, as illustrated with HUVECs and pMSCs. This work is the first step in creating a model synthetic ECM for vascular tissue engineering applications, using ELPs as the base material, with which ligand presentation may be varied in a controlled manner.

There are some caveats associated with the use of maleimide-thiol chemistry. In particular, nonspecific covalent linkages between a thiol-containing sequence (one that contains cysteine) and the thiolated **LysB10** can disrupt the bioactivity of the peptide. To date, however, the majority of short cell-adhesive peptides, including the sequences RGD, REDV, IKVAV and GFOGER, do not contain cysteine residues.

In order to functionalize the **LysB10** molecule, the carboxylic acid groups on the 28 glutamic acid residues were first modified to incorporate free sulfhydryls. The efficiency of the chemical reaction resulted in 48.6% conversion (13-14 modified carboxylic acids per **LysB10** molecule). Further conjugation of varying input peptide-maleimide linker concentrations onto 10wt% **LysB10** hydrogels resulted in an increase in peptide surface density that reached a plateau at 11 pmol/cm^2 (8 RGD moieties per **LysB10** molecule). This apparent limit in grafting efficiency may be due to steric hindrance of multiple bulky ligands immobilized onto the **LysB10**

backbone. Ultimately, HUVEC adhesion studies demonstrated that a peptide density of 8 pmol/cm^2 was sufficient in promoting robust cellular behavior.

Integrin-mediated cellular functions occur via diverse mechanisms. Previous studies have shown that the density of ECM proteins regulates cell adhesion, spreading, and migration speed. However, differences in experimental protocols and surface chemistry and roughness have resulted in a range of reported values for the minimal surface concentration required for cell adhesion and spreading. For example, Massia and Hubbell have reported that a minimal RGD peptide density of 10 fmol/cm^2 is required for fibroblast cell spreading, focal contact, and stress fiber formation on modified glass surfaces [259]. In contrast, Patel et al have demonstrated a higher RGD peptide density ranging from 0.2-3 pmol/cm^2 on an interpenetrating polymer network coating for robust endothelial cell adhesion and spreading [260]. Our own cell studies were performed on RGD-conjugated **LysB10** hydrogels, with grafting densities ranging from 4 to 12 pmol/cm^2. It was found that 8 pmol/cm^2 RGD grafting elicited maximal cell adhesion while minimizing peptide adsorption effects.

The multimeric structure of native ECM molecules such as fibronectin, a dimer with dual adhesion sites, and tenascin-C, which presents six repeats of cell adhesion domains, suggests that ligand clustering as well as ligand density regulates cell signaling [251] . Several studies have shown that the clustering of ligand-bound integrin receptors is essential in propagating intracellular signaling for proper cell function. For example, alphavbeta3 integrins can undergo affinity maturation, resulting in the recruitment of alphavbeta3 to focal adhesions in the cell periphery [261]. Nanoscale arrangement of RGD peptides has revealed that peptides presented as one peptide per molecule are poor substrates for fibroblast adhesion, while peptides presented in clusters of nine peptides per molecule or higher induce comparable cell attachment to matrix proteins [262]. Cell migration and spreading are dependent on this clustering mechanism as well. Peptide chemistry with thiolated-**LysB10** resulted in 5 RGD peptides

grafted per **LysB10** molecule (8 pmol/cm^2), which was sufficient in stimulating HUVEC and MSC adhesion, spreading, proliferation, and migration.

Adhesive strength and ligand surface density are critical factors in endothelial cell motility. The chemoselective ligation of RGD to thiolated-**LysB10** was shown to stimulate an increase in HUVEC radial migration across the hydrogel surfaces. Further optimization of migration rate may be achieved by modulating RGD grafting density. In particular, previous results from experiments and mathematical modeling have shown that cell migration rates display a biphasic dependence on the surface density of ligands and cell attachment strength [260, 268, 269]. At low adhesiveness, the cell cannot form strong and stable adhesions at the leading edge to allow traction to pull itself forward. At high adhesiveness, the trailing edge of the cell cannot be released [270, 271]. For example, work with RGD-grafted IPNs by Patel et al demonstrated that endothelial cell migration speed was relatively high on 0.2 pmol/cm^2 RGD treated surfaces and decreased as peptide density increased to 3 pmol/cm^2 . Moreover, growth factors and other chemotactic agents have been shown to influence the dynamics of the cytoskeleton leading to cell motility. Controlled release of sphingosine 1-phosphate, vascular endothelial growth factor, and basic fibroblast growth factor have been proven to promote endothelial cell migration by increasing lamellipodia formation and extension in the leading edge of the cell [272-274].

Integrin specificity is critical in directing cell fates such as migration, proliferation, and differentiation, as different integrins trigger specific signaling pathways. Thus, a major disadvantage of short peptides such as RGD, which binds multiple integrins, is their inability to elicit specific cell responses based on defined intracellular pathways. This lack of specificity results in non-discriminatory attachment of cells to RGD-coated surfaces. These concerns can be addressed in multiple ways. For example, in order to promote alpha5beta1-mediated adhesion, both the RGD sequence in the 10th type III repeat of fibronectin as well as its synergy

site, the PHSRN sequence in the 9th type III repeat domain, are required to be presented together [164]. Another peptide with increased integrin affinity and selectivity is the sequence REDV, which binds to the integrin alpha4beta1, and thus, is capable of cellular interaction with leukocytes, endothelial cells, and some muscle and fibroblast cell lines, but not with platelets [168].

4.5 CONCLUSION

The results of this study demonstrate that chemical conjugation of a bioactive ligand via maleimide-thiol chemistry is a viable means of functionalizing surfaces of elastin-like hydrogels. HUVEC and MSC adhesion, actin fiber formation, proliferation, radial migration, and HUVEC activation states were characterized in order to evaluate the efficacy of RGD-functionalized **LysB10**. To our knowledge, this study is the first report of direct chemical ligation of moieties onto the surfaces of recombinant elastin-mimetic protein polymer hydrogels.

CHAPTER 5

Incorporation of matrix protein fibronectin into ELP blends and its application to cell-seeded vascular constructs

5.1 INTRODUCTION

Biomimetic materials that recapitulate the complex mechanical and biochemical cues in load-bearing tissues are of significant interest in regenerative medicine and tissue engineering applications. One approach in generating suitable materials is to mirror the multiscale structural hierarchy of the extracellular matrix itself. Thus, proper selection and assembly of scaffolds that replicate the anatomic features of the tissue of interest is vital in promoting tissue integration and directing cellular behavior.

The functional importance of normal physiologic responses of the vascular wall in controlling thrombosis and inflammation has guided attempts to closely mimic the native arterial wall in the design of a new generation of vascular prostheses. These features include the structural components collagen and elastin, which are responsible for a fatigue-resistant tissue with long-term durability [20, 322]. In this study, we utilized elastin-like protein polymer (ELP) **LysB10,** which displays a range of elastomeric properties that more closely match those of the native artery [14]. This amphiphilic triblock copolymer (ABA) consisting of hydrophobic (A) and hydrophilic (B) domains was synthesized such that phase separation of the more hydrophobic blocks occurs in water under physiologically relevant conditions to form virtual crosslinks, while the hydrophilic domains remain non-crosslinked and solvated by the aqeous environment [218, 219]. The introduction of lysine residues enabled chemical crosslinking to stabilize the hydrogel. This multiblock system results in structural polymorphism and the potential for a wide range of functional responses, including mechanical and biological performance. We have previously demonstrated the ability of elastin-mimetic triblock copolymers to be used as non-thrombogenic

hydrogel coatings on the luminal surface of ePTFE prostheses [15, 221]. Further biocompatibility studies on ELPs have revealed long-term *in vivo* biostability and minimal inflammatory responses, which makes **LysB10** an ideal candidate for a structural component of engineered tissues and as a biocompatible surface coating [14, 15, 221, 323]. Thus, elastin-mimetic protein copolymers represent a unique class of thermoreversible hydrogels for soft tissue engineering applications.

LysB10 is a relatively bioinert material, and therefore requires further functionalization in order to allow for integration at the cell-material interface. Once again, we take inspiration from the native extracellular matrix by utilizing an ECM-associated protein. Fibronectin is an adhesive glycoprotein secreted by cells to form a fibrillar matrix, and regulates a number of cell functions via intracellular signaling pathways, including cell cycle progression, migration, differentiation, and assembly of other ECM components [156-158]. Unlike short peptide adhesive sequences, fibronectin contains multiple sites for functional engagement. The monomeric fibronectin molecule is 220kDa, but the functional unit exists as a disulfide-crosslinked heterodimer. The RGD and synergy cell-binding sequences interact directly with integrins on the cell surface, while binding sites for heparin, collagen, and fibrin molecules modulate the microenvironment around the cells [159].

Several investigators have endeavored to minimize graft failure due to thrombosis and intimal hyperplasia by mimicking the biologic responsiveness of the native vasculature. In particular, the poor patency rates of synthetic polymers have motivated strategies to promote endothelialization of the material surface and cellularization of a vascular construct [7, 9, 11, 12, 26-29, 31, 32, 34, 249, 250]. The endothelial lining in the native vasculature not only serves as a protective, thromboresistant barrier between blood and the surrounding tissue, but also controls vessel tone, platelet activation and leukocyte adhesion. In addition, mesenchymal stem cells have recently emerged as a promising therapeutic modality for tissue regeneration and repair. Mesenchymal stem cells (MSCs) are multipotent adult stem cells that can differentiate into a

number of cell types, including skeletal muscle cells, vascular endothelial cells, smooth muscle cells, and cardiomyocytes [324-328]. Interest has been raised by the observation that MSCs display immunomodulatory capacities that can be harnessed for vascular tissue engineering [321, 329-332].

We postulate that biologically inspired structures produced from synthetic or molecularly engineered collagen and elastin analogs, which recapitulate the biomechanical and biochemical features of the native extracellular matrix, provide an advanced foundation for engineering living tissue. As a case in point, we have previously reported the generation of an acellular vascular substitute consisting of a multilamellar structure formulated from integrated synthetic collagen microfibers and a recombinant elastin-like protein [333]. In this study, we further describe the fabrication and cellularization of thin lamellae consisting of continuous synthetic collagen fiber embedded within a recombinant elastin-like protein polymer matrix. Production of multilamellar structures affords flexible, protein-based composite sheets whose properties are dependent upon both the elastomeric matrix and the content and hierarchical organization of collagen fibers. The laminated geometry offers the potential to incorporate living cells at controlled spatial intervals throughout a stacked sheet, akin to cell sheet tissue engineering methods.

The goal of this study was to define the important parameters in generating an elastin-like protein polymer for soft tissue engineering. We hypothesized that optimized presentation of the fibronectin molecule would provide a system in which to display multiple bioactive domains for cellular interaction. Moreover, we anticipated that this engineered platform would promote cellularization of collagen-reinforced elastin-mimetic multilamellar constructs for vascular tissue engineering applications. We tested our hypothesis with a number of *in vitro* endpoints to determine endothelial and mesenchymal stem cell behavior.

5.2 MATERIALS AND METHODS

Reagents, Antibodies, and Cells

Fibronectin solution was obtained from Sigma Aldrich. Genipin was purchased from Wako, Inc, while Fibronectin EIA kit was procured from Takara Bio Inc. **LysB10** protein expression and purification is described in Appendix A. Porcine mesenchymal stem cells (pMSCs) were a kind gift from Dr. Steven Stice (University of Georgia). Human umbilical vein endothelial cells and EGM-2 media supplements were obtained from Clonetics, while pMSC basal media and supplements were purchased from Fisher Scientific and Invitrogen. Radial migration of cells on **LysB10** surfaces was measured with the use of the Oris cell migration assembly kit, from Platypus Technologies, and calcein AM (Molecular Probes). Immunofluorescence studies were performed with mouse anti-human E-selectin and mouse anti-human ICAM-1 antibodies purchased from Millipore. Immunostaining reagents goat anti-mouse IgG antibody, streptavidin-AlexaFluor 488, phalloidin-AlexaFluor 568, and ProLong Gold antifade reagent with DAPI were all purchased from Invitrogen (Molecular Probes). For gene expression analysis, RNeasy micro kit was obtained from Qiagen, while cDNA reverse transcription kit was procured from Applied Biosystems. GAPDH, IL-1beta, and COX-2 primers for the species S.scrofa were purchased from Applied Biosystems as well.

Percent Extractables Study

To determine the percent of potentially extractable protein polymer, 200uL of 10wt% protein solution was cast as a disk measuring 1 cm in diameter. Films were crosslinked in 0.5% glutaraldehyde or 6 mg/mL genipin solutions for 24 hours, and rinsed in ddH_20 for 12 hours, with 4 buffer changes to remove any residual crosslinker. The weight of dried samples was recorded prior to incubating the films in water at 4°C (below the inverse transition temperature). After a 7-day incubation period, the films were dried and weighed once more to determine material loss.

The mass retention was calculated with the following equation:

$$\%\, Mass\ Retention = [1 - \frac{initial\ dehydrated\ weight - final\ dehydrated\ weight}{initial\ dehydrated\ weight}] \times 100$$

Mechanical Data

10wt% and 6wt% **LysB10** solutions were loaded into 1mL syringes (diameter of 4.67mm) at 4°C, and subsequently gelled at 37°C. The tip of the syringe was removed with a sterile scalpel and the molded protein gel was extruded into room temperature PBS. The 8mm-long gel was cut into 2mm sections. Treatment gels were placed in 1mg/mL fibronectin solution for 4 hours prior to genipin crosslinking. Control gels were placed directly in 6 mg/mL genipin solution for 24 hours to enable crosslinking. Following crosslinking, samples were washed in PBS for 12 hours with 4 buffer changes. For compression loading, samples were tested using a 10 pound load cell and hydration chamber at 37°C. A preconditioning protocol was employed for **LysB10** samples that consisted of 10 cycles of 20% strain. Constructs were compressed to failure at a rate of 0.025 mm/s. Stress relaxation was measured by compressing the samples to a strain of 50% using a crosshead speed of 0.025mm/sec, and then allowing the crosshead to rest for 15 minutes or longer until the force decay is minimal or roughly .001Mpa per minute. Compressive modulus E was defined as the slope of the line at a particular strain percent.

Fibronectin Enzyme Immunoassay

An ELISA was used to determine the extent of fibronectin immobilization on **LysB10** hydrogel surfaces**.** The assay is a solid-phase EIA based on a sandwich method. **LysB10** solutions were formulated by adding lyophilized **LysB10** protein at a 10wt% or 6wt%

concentration in PBS at 4°C for 16 hours. 40 uL of solution was carefully pipetted and uniformly coated onto the EIA plate wells at 4°C. Hydrogel formation was achieved by placing the plate at 37°C, well above the transition temperature of the protein polymer, for 1 hour. Fibronectin solutions ranging from 0 to 1 mg/mL were allowed to adsorb onto the hydrogel for 6 hours at room temperature. Crosslinking was performed with a 6 mg/mL genipin solution for 24 hours, followed by stringent PBS rinsing over a 12-hour period to remove all genipin. Fibronectin antibody labeled with peroxidase was incubated in treatment wells, after which a substrate (tetramethylbenzidine) was added to react to bound peroxidase. The resulting color development and associated intensities are proportional to the amount of human fibronectin present in samples and standards. Standard curves were generated by adding known amounts of fibronectin to the immobilized antibody in each well. Absorbance was measured at 450nm.

Hydrogel formulations

Fibronectin-blended LysB10 gels

Fibronectin-**LysB10** blend solutions were formulated by adding lyophilized **LysB10** protein at a 10wt% or 6wt% concentration in appropriate dilutions of fibronectin in PBS at 4°C for 16 hours in order to ensure uniform blending. 40 uL of solution was carefully pipetted and uniformly coated into wells of a polystyrene 96-well plate at 4°C. Hydrogel formation was achieved by placing the plate at 37°C, well above the transition temperature of the protein polymer, for 1 hour. Lysine residues of the protein polymer were crosslinked with a 6 mg/mL genipin solution for 24 hours, followed by stringent PBS rinsing to remove all genipin.

Fibronectin-adsorbed LysB10 gels

LysB10 solutions were formulated by adding lyophilized **LysB10** protein at a 10wt% or 6wt% concentration in PBS at 4°C for 16 hours. 40 uL of solution was carefully pipetted and

uniformly coated into wells of a polystyrene 96-well plate at 4°C. Hydrogel formation was achieved by placing the plate at 37°C, well above the transition temperature of the protein polymer, for 1 hour. 1 mg/mL of fibronectin solution was allowed to adsorb onto the hydrogel for 6 hours at room temperature. Crosslinking was performed with a 6 mg/mL genipin solution for 24 hours, followed by stringent PBS rinsing over a 12-hour period to remove all genipin.

Cell Studies

HUVEC and MSC Adhesion

Human umbilical vein endothelial cells (HUVECs) were purchased from Clonetics and maintained in endothelial growth medium-2 (EGM-2, 2% serum, Clonetics). Porcine mesenchymal stem cells were cultured in alpha-MEM basal medium supplemented with 10% fetal bovine serum, 50U/mL penicillin, 50ug/mL streptomycin, and 2mM L-glutamine. They were kept in a humidified, 5% CO_2 environment at 37°C, and passaged every 2 days via standard culture techniques. HUVECs and pMSCS between passages 3 and 9 were used for all experiments. To begin, cells were harvested with Cell Dissociation Solution (EDTA, glycerol, sodium citrate, PBS, from Sigma) in order to maintain integrin functionality on the cell surface. After centrifugation at 220g for 5 minutes, HUVEC suspensions were prepared at a density of 200,000 cells/mL in basal medium containing 0.5% bovine serum albumin (BSA). MSCs were prepared at the same density in low-serum medium (1% serum). 100uL of the cell suspension was plated onto **LysB10** surfaces, and after incubation at 37°C for 2 hours, wells were washed three times with phosphate-buffered saline (PBS). Cell adhesion activity was evaluated with the CyQuant Cell Proliferation Assay Kit (Molecular Probes), which utilizes a fluorescent dye with strong fluorescence enhancement when bound to cellular nucleic acids (excitation/emission maxima ~480/520 nm). Briefly, after thawing frozen cells to enhance lysis, the CyQuant cell lysis buffer was added to each sample, along with CyQuant fluorescence reagent. Samples

were then measured in a microplate spectrofluorometer. Results were normalized to adhesion levels on fibronectin-coated polystyrene wells, which acted as the positive control.

Biostability Study

Non-crosslinked and genipin-crosslinked fibronectin-**LysB10** gels were allowed to incubate in 1xPBS for 1 week, with daily PBS changes. Following the 1 week incubation period, a 2 hour HUVEC adhesion assay was performed in order to evaluate possible destabilizing effects of fibronectin release from the hydrogels and the corresponding effects on HUVEC adhesion.

HUVEC and MSC Proliferation Assay

Proliferation rates were evaluated with the CyQuant Cell Proliferation Assay Kit. Cells were seeded onto various **LysB10** gels at a density of 5,000 cells/well for 2 hours. Unbound cells were removed with media washes and substrate-bound cells were maintained in culture for another 48-hour period. Cell counts at 48 hours were compared to those at 2 hours.

Cell Migration Assay

LysB10 hydrogels with varying treatment groups (n=4) and fibronectin-coated wells were formulated in 96-well plates (black, clear bottom) provided by the manufacturer of the Oris cell migration assay FLEX kit (Platypus Technologies). Cell seeding stoppers with diameters of 2mm were placed on top of the hydrogels and wells to prevent cells from adhering to the central detection zone. Cells were harvested with Cell Dissociation Solution (EDTA, glycerol, sodium citrate, PBS, from Sigma) in order to maintain integrin functionality on the cell surface. After centrifugation at 220g for 5 minutes, HUVEC suspensions were prepared at a density of 400,000 cells/mL in serum-free basal medium. Cell suspensions were treated with 10ug/mL mitomycin C (Sigma Aldrich) in order to arrest cell proliferation. 100uL of the cell suspension

was seeded onto the outer annular region of the hydrogel surfaces (30 mm^2). Cells were allowed to adhere to the seeding region for 6 hours at 37ºC, at which point the stoppers were removed to allow for migration into the central detection zone (3.14 mm^2). Several reference wells were designated, in which the stoppers remained in place until wells were read (t=0 pre-migration controls). Unbound cells were gently removed by rinsing the wells with complete media, after which all wells were filled with 150uL complete media. Cells were incubated at 37ºC for 36 hours. Quantitation of migration was performed by staining the adherent cells with Calcein AM. Briefly, wells were washed three times with PBS, after which a 2uM Calcein AM solution was added to each well and incubated for 1 hour. Migrated cells in the central detection zone were analyzed with a fluorescent plate reader. The Oris detection mask was secured to the bottom of the 96-well plate in order to prevent signal detection of the outer annular region. Therefore, any fluorescent signal detected was isolated from migratory cells in the central detection zone. Readings from the pre-migration control wells were subtracted from the post-migration wells to eliminate noise due to background. Data was normalized to the fibronectin positive control.

Immunofluorescence Studies

Fluorescent staining of cytoskeletal component F-actin and cellular adhesion molecules ICAM-1 and E-selectin were performed on cells cultured on fibronectin-adsorbed LysB10 hydrogels (see above for formulation description) in polystyrene 8-well chamber slides (Nalge Nunc, International). Fibronectin controls were formulated by adsorbing 50ug/mL solutions overnight at 4°C. 200uL cell suspensions (approximately 15,000 cells/well) of HUVECs were seeded onto the slides and cultured for a period of 2 hours (for F-actin staining) or 4 hours (for ICAM-1 and E-selectin staining) in serum-free medium. To achieve HUVEC activation, 100 ng/mL of TNFα was added to cells cultured on fibronectin-coated slides for 4 hours prior to immunostaining. Subsequently, the cells were fixed in 4% paraformaldehyde (10 minutes),

permeabilized with PBS containing 0.5% Triton X-100 (10 minutes), rinsed once with 100 mM glycine (10 minutes), and incubated with block buffer (PBS+/+, 0.2% Triton X-100, 6% goat serum) for 1 hour at room temperature. For F-actin staining, cells were incubated with Alexa Fluor 568-conjugated phalloidin for 30 minutes. 10ug/mL solutions of E-selectin and ICAM-1 monoclonal antibodies were incubated for 1 hour in order to evaluate HUVEC activation/quiescence states. 10ug/mL solutions of vinculin antibody was utilized for assessment of focal adhesion assembly. Primary antibody incubation was followed by 45 minute incubation with 2.5 ug/mL biotinylated goat anti-mouse IgG secondary 30 minute incubation with 2.5 ug/mL streptavidin-AlexaFluor 488 tertiary. Nuclei were counterstained with Prolong Gold mounting medium containing DAPI, and the resultant staining was imaged using confocal microscopy (Emory University).

Fabrication of mesenchymal stem cell-seeded, collagen fiber-reinforced elastin laminates

The generation of collagen-reinforced recombinant elastin sheets has been previously described by Caves et al in the fabrication of small-diameter vascular grafts [333]. Based on earlier work with fibronectin-immobilized hydrogels, we applied this technology further by generating mesenchymal stem cell-seeded constructs for tissue engineering. Briefly, protein fiber sheets were fabricated by winding defined collagen fiber layouts onto rectangular frames and implementing the transition temperature fiber embedding and lamination protocol (Scheme 5.1). Synthetic collagen microfibers were produced as described by Caves and colleagues [333, 334]. To arrange fibers with defined spacing and orientation, the frame translation speed, translation distance, and rotation speed were computed with a MATLAB script. An automated linear actuator (Velmex, Inc, Bloomfied, NY) and a DC gear motor translated and rotated the frames. After winding, each fiber layout was transferred onto a sheet of ultrasoft polyurethane and secured with tape. Solutions of protein polymer were prepared at 10-wt% concentration in ice-cold ddH_2O. To embed the fiber layouts, precision 50 µm thick plastic shims (Precision

Brand, Inc., Downers Grove IL) were placed around the layouts, and all embedding materials were cooled to 4°C. The protein polymer solution was distributed over the fibers and a sheet of acrylic was pressed on top of the solution. The fibers and the protein polymer solution were located within a 50 µm space, sandwiched between the acrylic sheet and polyurethane base that were separated by precision shims. The embedding assembly was incubated at 4°C for one hour to allow the protein polymer solution to hydrate the fiber layout, followed by transfer of the assembly to a 37°C incubator for 1 hour. When the polyurethane and acrylic sheets were peeled apart, the fiber layout remained embedded in a gel film of protein polymer, adherent to the polyurethane base. After a 5-minute incubation in 37°C ddH_2O, the fiber-reinforced film could be separated from the polyurethane base. The protein sheet was further sectioned into 1 centimeter by 1 centimeter square pieces. 1 mg/mL fibronectin solution was incubated on the surface of each square piece for 6 hours. Both sides of the protein sheet were treated with fibronectin, followed by genipin crosslinking (6mg/mL) for 24 hours. Residual genipin was removed with three PBS buffer changes over a 12-hour period. An additional cycle of fibronectin adsorption was added after crosslinking in order to maximize cell adhesion onto the surfaces of protein sheets.

Mesenchymal stem cells were seeded onto fibronectin-treated, fiber-reinforced protein sheets via a two-stage seeding protocol. pMSCs were seeded at a density of $1x10^5$ cells/cm^2 in 200uL complete medium (10% FBS) for 6 hours. The protein sheets were then placed in another 24-well plate and seeded a second time with pMSCs at a density of $1x10^5$ cells/cm^2 in 200uL complete medium (10% FBS) for 12 hours. The seeded sheets were transferred once again into new wells and incubated in fresh media for a period of 72 hours, or until a confluent monolayer for observed, with medium changes every two days.

Laminates consisted of a multilamellar stack of two or three, 50 µm thick layers. The layers were sandwiched between nylon meshes with 70 micron pores and incubated in culture

medium for 7 days, with medium exchanges every 2 days, in order to facilitate interlamellar bonding.

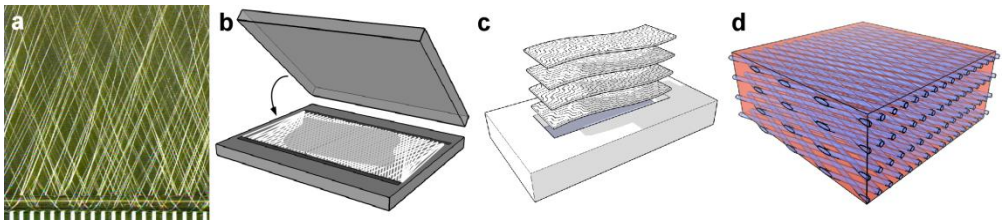

Scheme 5.1. Fabrication of a collagen microfiber reinforced elastin-like protein sheet. (**a**) Collagen microfiber is wound about rectangular frames to obtain the desired orientation and average spacing. (**b**) A cooled protein polymer solution is distributed over the microfiber layout and molded into a thin membrane. (**c**) Stacked, cell-seeded membranes are laminated by sandwich molding and 1 week incubation to form a **(d)** multilamellar composite sheet. Image modified from Caves et al.

Evaluation of MSC viability

Cell-seeded single sheets and multilamellar protein fiber sheets were incubated in 2uM Calcein AM solution for 1 hour at room temperature, and the resultant staining was imaged with confocal microscopy (Emory University).

In vitro evaluation of inflammatory response of MSCs on multilamellar protein fiber sheets: RNA isolation and real-time reverse transcriptase polymerase chain reaction

For *in vitro* studies, pMSCs were seeded onto tissue culture-treated polystyrene with and without 10 ug/mL lipopolysaccharide (LPS) added to the culture medium for 96 hours. Cell-seeded trilamellar constructs were cultured for 96 hours prior to RNA isolation as well. Medium was exchanged for all treatment groups every 2 days. Gene expression of interleukin-1beta (IL-1beta) and cyclooxygenase 2 (COX-2) was evaluated in quiescent cells, LPS-activated cells, and cell-seeded constructs (n=3).

Cells were detached and lysed with TRIzol reagent. The cell lysate for each treatment group was mixed and incubated with chloroform for 1 minute at room temperature. Phase separation was achieved by centrifuging the mixture for 15 minutes at 4°C. The top aqeous layer was collected for further RNA isolation and purification. RNA was isolated from the aqeous solution with the Qiagen RNeasy micro kit, according to the manufacturer's protocol. Complementary cDNA was generated using the high-capacity cDNA reverse transcription kit from Applied Biosystems. Thermal cycling conditions began with a 25°C incubation for 10 minutes, 37°C incubation for 120 minutes, temperature increase to 85°C for 5 seconds, and a final cooling to 4°C. The reverse transcription product was used as a template for real-time PCR analysis on the real time PCR 7900HT system (Applied Biosystems). All PCR reactions were performed in triplicate with 50 ng of cDNA per well. All primers were obtained from Applied Biosystems. The housekeeping gene glyceraldehyde-3-phosphate-dehydrogenase (GAPDH)

served as the endogenous control. Expression data was further normalized to the negative control (quiescent cells grown on tissue culture polystyrene).

Histology

Cell-seeded laminates that were maintained in culture for 1 week were cryo-sectioned as described by Nerurkar and colleagues [335]. Briefly, samples (n=3) were fixed in 4% paraformaldehdye overnight prior to flash-freezing in OCT freeze medium. Sections were incubated in hemotoxylin and eosin to visualize cell nuclei. Alcian Blue staining with Nuclear Fast read counterstain was utilized to visualize glycosaminoglycan deposition.

Statistical Analysis

Comparison between groups was analyzed via ANOVA and a paired, two-tailed student's t-test, with $p<0.05$ considered to be significant. Results are presented as mean ± standard deviation. Data represent characteristic results from a particular experimental run (each group run in quadruplicate), although at least three independent runs were conducted.

5.3 RESULTS

Genipin crosslinking of elastin-mimetic LysB10 gels

Investigations by our group have demonstrated that covalent crosslinks can enhance the mechanical stability of the elastin analog **LysB10** via the lysine residues [14]. While glutaraldyde has been effective in facilitating these covalent crosslinks, its cytotoxicity limits its applications in *in vitro* cell studies. Therefore, the naturally occurring crosslinking agent genipin was utilized to enhance intermolecular crosslinking within the **LysB10** gel, while minimizing toxicity [275-280]. As a measure of the extent of crosslinking, the percent extractable protein was examined after incubating samples at 4°C for 7 days. Below the inverse transition temperature, noncrosslinked films dissolved immediately due to disruption of physical crosslinks. After genipin and glutaraldehyde crosslinking, films retained approximately 93.5 ± 1.4% and 84.3 ± 6.2% of their mass, respectively, consistent with a high degree of chemical crosslinking.

Mechanical analysis of hydrated LysB10 hydrogels

The mechanical properties of the extracellular matrix can play a vital role in determining cell fate. In particular, cell response to substrate stiffness can influence a range of processes, including adhesion, proliferation, focal adhesion formation, migration, and differentiation potential. Therefore, in generating an elastin-mimetic for vascular tissue engineering applications, it is important to not only evaluate ligand presentation on the hydrogel surface, but to also determine its mechanical properties. Since cell deformation is one process that is thought to be important in the mechanotransduction pathway, 6wt% and 10wt% **LysB10** hydrated gels were subjected to compressive loading. Treatment groups included

noncrosslinked samples, genipin-crosslinked gels, and adsorbed fibronectin that was genipin-crosslinked onto **LysB10**.

As expected, the addition of surface-immobilized fibronectin did not interfere with the mechanical properties of **LysB10**. As seen in Figure 5.1, crosslinked samples without fibronectin behaved in a similar manner to fibronectin-crosslinked gels. Corresponding compressive moduli at various strain percents are calculated in Table 4.1. At low strain (20%), 6wt% crosslinked samples exhibit a four- to five-fold increase in compressive modulus compared to their non-crosslinked counterparts, while 10wt% crosslinked samples display a two- to three-fold increase in compressive modulus compared to their non-crosslinked counterparts. It is interesting to note that at low strain (20%), the compressive modulus of noncrosslinked 10wt% **LysB10** is equivalent to that of crosslinked 6wt% gel.

Stress relaxation was measured over a 10-minute period at 50% strain for all samples, demonstrating the viscoelastic behavior of the elastin-mimetic protein polymers. Both uncrosslinked and crosslinked 6wt% gels displayed stress relaxations of 68% of the peak stress, while crosslinked 10wt% gels displayed a 50% decrease and uncrosslinked 10wt% gels displayed 82% decrease in stress.

Characterization of fibronectin crosslinked onto LysB10 gels

To optimize incorporation onto the **LysB10** gels, a wide concentration range of fibronectin was first explored (0 to 1 mg/mL). Passive adsorption onto unmodified 6wt% and 10wt% **LysB10** hydrogels was followed by genipin crosslinking in order to covalently immobilize the fibronectin molecules in place within the context of the hydrogel surface. Quantitation of ligand density on **LysB10** surfaces was measured by means of an ELISA. As shown in Figure 5.2, incorporation of fibronectin increased in a hyperbolic manner. Furthermore, there was a

marked increase in fibronectin incorporation on 10wt% gels compared to 6wt% hydrogels at equivalent fibronectin input concentrations. This phenomenon is most likely due to an increased density of **LysB10** molecules at the surface of a 10wt% gel, which facilitates adsorption and subsequent crosslinking of adsorbed fibronectin.

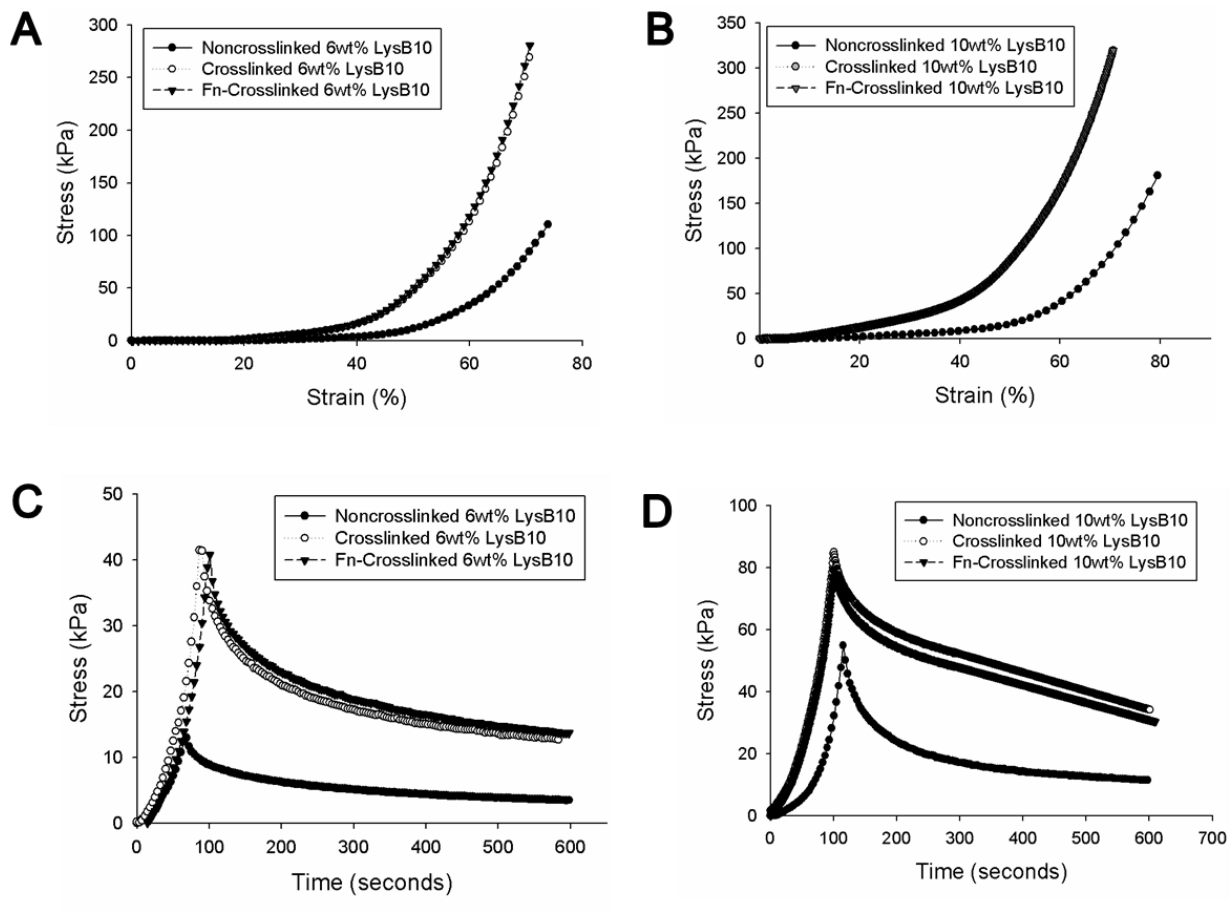

Figure 5.1. Representative mechanical behavior of LysB10 hydrogels under a compressive load. Treatment groups include noncrosslinked **LysB10**, genipin-crosslinked **LysB10**, and adsorbed fibronectin that has been genipin-crosslinked with **LysB10**. **(A)** Stress-strain behavior of 6wt% hydrogels. **(B)** Stress-strain behavior of 10wt% hydrogels. **(C)** Stress-relaxation curves of 6wt% gels at 50% strain. **(D)** Stress-relaxation curves of 10wt% gels at 50% strain.

Table 5.1. Compressive modulus (in kPa) at varying strain percents.

Strain %	6wt% (Noncrosslinked) E (kPa)	6wt% (Crosslinked) E (kPa)	6wt% (Fn-crosslinked) E (kPa)	10wt% (Noncrosslinked) E (kPa)	10wt% (Crosslinked) E (kPa)	10wt% (Fn-crosslinked) E (kPa)
20	9.2 ± 7.7	42.3	42.9 ± 5.0	44.6 ± 6.8	105.6 ± 7.1	108.8 ± 7.6
30	19.4 ± 0.4	56.5	53.4 ± 5.6	60.5 ± 9.2	143.3 ± 17.8	150.2 ± 21.1
40	48.7 ± 12.8	166.3	163.2 ± 12.7	98.3 ± 12.5	275.6 ± 10.5	278.6 ± 3.5
50	161.8 ± 18.7	504.4	509.7± 33.5	213.8 ± 17.0	605.1 ± 78.1	634.7 ± 19.5
60	321.7 ± 0.8	928.9	830.2 ± 38.8	331.8 ± 23.1	1048.9 ± 39.0	1056.6 ± 9.7

E: compressive modulus, kPa: kilopascals, Fn: fibronectin

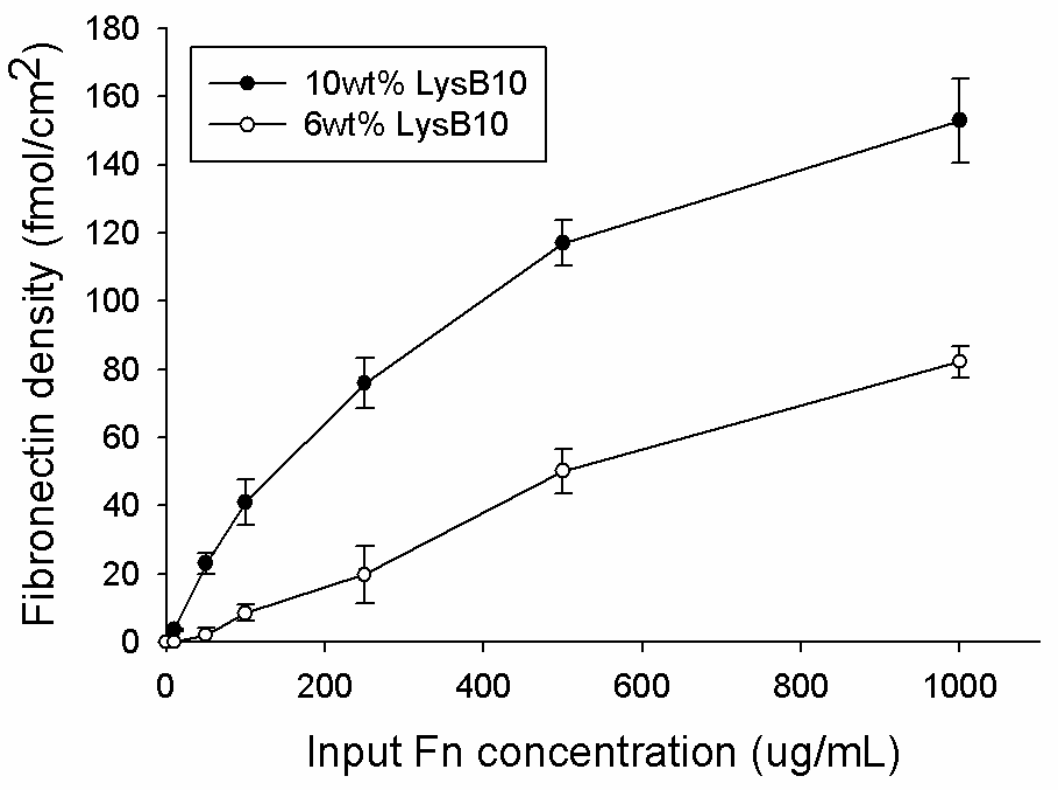

Figure 5.2. Fibronectin crosslinked onto 10wt% or 6wt% LysB10 hydrogel surfaces as a function of the amount of input protein. Data represent one of three similar experiments, with each condition run in quadruplicate. Fibronectin incorporation was assessed with the use of a fibronectin ELISA assay.

Biostability of Fibronectin-LysB10 hydrogels

Two strategies were employed in determining the bioactivity of fibronectin-**LysB10**. First, varying concentrations of fibronectin, ranging from 0.05mol% (50 ug/mL Fn) of total protein content to 0.75mol% (1 mg/mL Fn), were uniformly blended into noncrosslinked 6wt% **LysB10**. Secondly, 1 mg/mL fibronectin solution was adsorbed onto the **LysB10** hydrogel surface for 6 hours. A 50ug/mL fibronectin solution was adsorbed onto polystyrene and served as a positive control against which all data was normalized. A 2 hour HUVEC adhesion assay (Figure 5.3A) demonstrated that increasing fibronectin incorporation in **LysB10** blends incrementally increased cell adhesive response. However, the most effective formulation utilized fibronectin adsorption onto the substrate surfaces.

Chemical crosslinking of the lysine residues was previously utilized as a means of stabilizing the intermolecular physical crosslinks within **LysB10**. This crosslinking strategy was shown to improve biostability and mechanical properties of **LysB10** films. To explore the biostability and associated bioactivity of incorporated fibronectin to sustain HUVEC adhesion, non-crosslinked and genipin-crosslinked fibronectin-**LysB10** gels were allowed to incubate in PBS for 1 week, with daily PBS changes. Following the 1 week incubation period, a 2 hour adhesion assay was performed. As seen in Figure 5.3B, there were no significant differences between crosslinked and non-crosslinked Fn-**LysB10** blends. However, crosslinking of adsorbed Fn-**LysB10** gels did preserve fibronectin bioactivity, while non-crosslinked hydrogels exhibit a muted cell response due to fibronectin loss over the one week PBS incubation period.

HUVEC Proliferation

Cell proliferation over a 48-hour period on treated hydrogels was next quantified (Figure 5.4). A 750 ug/mL fibronectin solution was uniformly blended into **LysB10**, which correlated to 0.5mol% incorporation into 6wt% **LysB10** gels, and 0.33mol% of 10wt% **LysB10** gels. An additional

treatment group included the adsorption of fibronectin onto the gel surfaces. A fibronectin surface density of approximately 82 fmol/cm^2 was achieved by adsorbing 1mg/mL fibronectin onto 6wt% gels and 0.25 mg/mL fibronectin onto 10wt% gels. A maximal surface density of 153 fmol/cm^2 was achieved by adsorbing 1 mg/mL fibronectin onto 10wt% gels. All **LysB10** hydrogels were crosslinked with genipin. Adsorbed fibronectin on polystyrene served as a positive control. Results indicate that fibronectin-**LysB10** blends were able to stimulate a two-fold increase in HUVEC number, while surface immobilized fibronectin-**LysB10** supported a three-fold increase in cell number. Although proliferation rate was similar on both 10wt% and 6wt% adsorbed Fn-**LysB10** gels, there was a 24% increase in cell number on the modified 10wt% gels compared to the 6wt% hydrogels. Thus, surface modified 10wt% **LysB10** most closely matched the proliferative behavior of HUVECs on the positive control (adsorbed fibronectin on polystyrene).

HUVEC Migration

Radial migration is a key factor in endothelialization of a biomaterial surface. To evaluate the ability of treated **LysB10** gels to modulate cell migration, HUVECs were seeded onto an outer annulus area and monitored for motility into an inner radial zone over a 36 hour period. Calcein AM staining of the migrated cells enabled fluorescent measurement of the number of migrated cells into the detectable inner zone, which was normalized against the number of migrated cells on fibronectin-coated polystyrene (Figure 5.5). While unmodified **LysB10** hydrogels were unable to support cell migration, 6wt% Fn-**LysB10** gels did stimulate HUVEC motility across their surfaces. However, on 10wt% Fn-**LysB10** hydrogels, only those gels with surface-immobilized fibronectin were able to enhance HUVEC motility. In both 10wt% and 6wt% **LysB10** gels, surface treatment with fibronectin was the most effective in stimulating HUVEC migration.

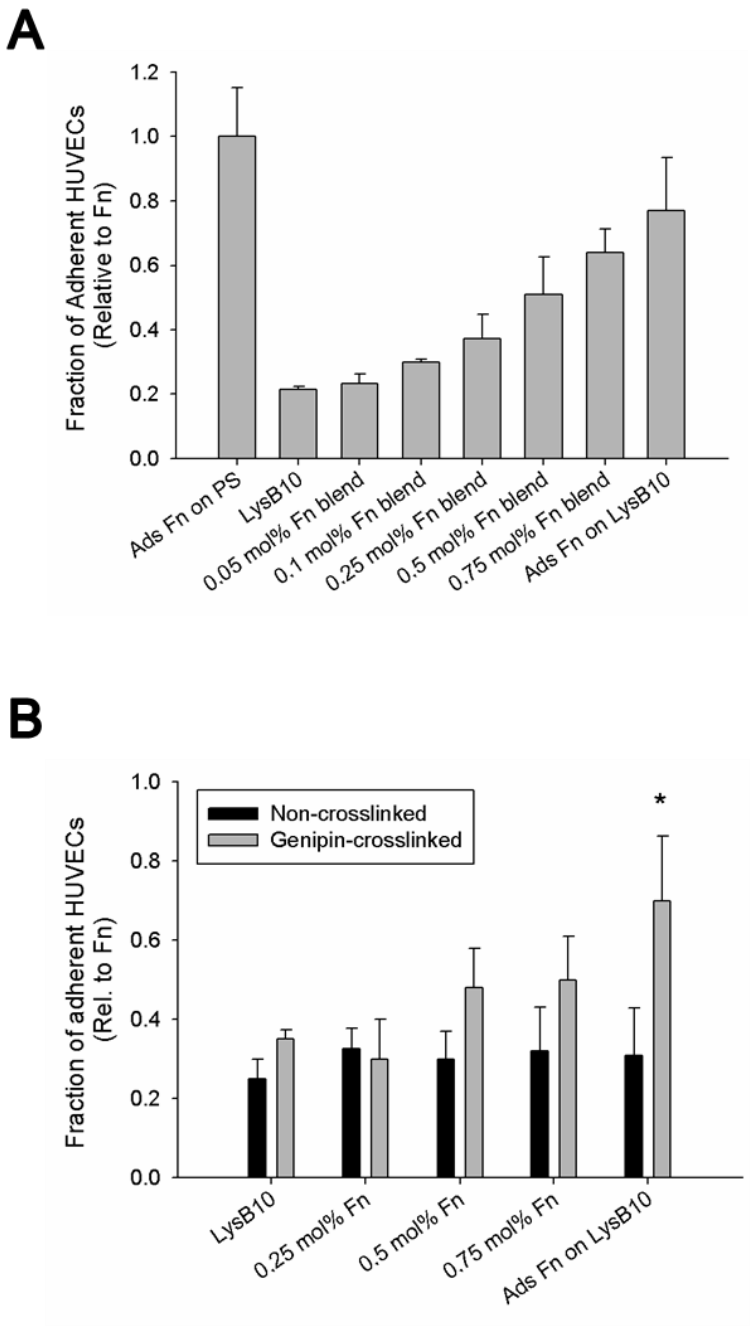

Figure 5.3. (A) 2 hour HUVEC adhesion on uniform blends of fibronectin and 6wt% LysB10, as well as surface-adsorbed fibronectin. 50 ug/mL fibronectin in PBS was allowed to adsorb to polystyrene overnight and served as a positive control. All data was normalized to this fibronectin control. **(B)** Gels were placed in PBS for 1 week prior to performing a 2 hour adhesion assay to determine their biostability and associated bioactivity. The figure above demonstrates that crosslinking of the gels preserves fibronectin bioactivity, while non-crosslinked hydrogels exhibit a muted cell response due to fibronectin loss over the 1 week PBS incubation period. * $p<0.05$ compared to non-crosslinked counterparts.

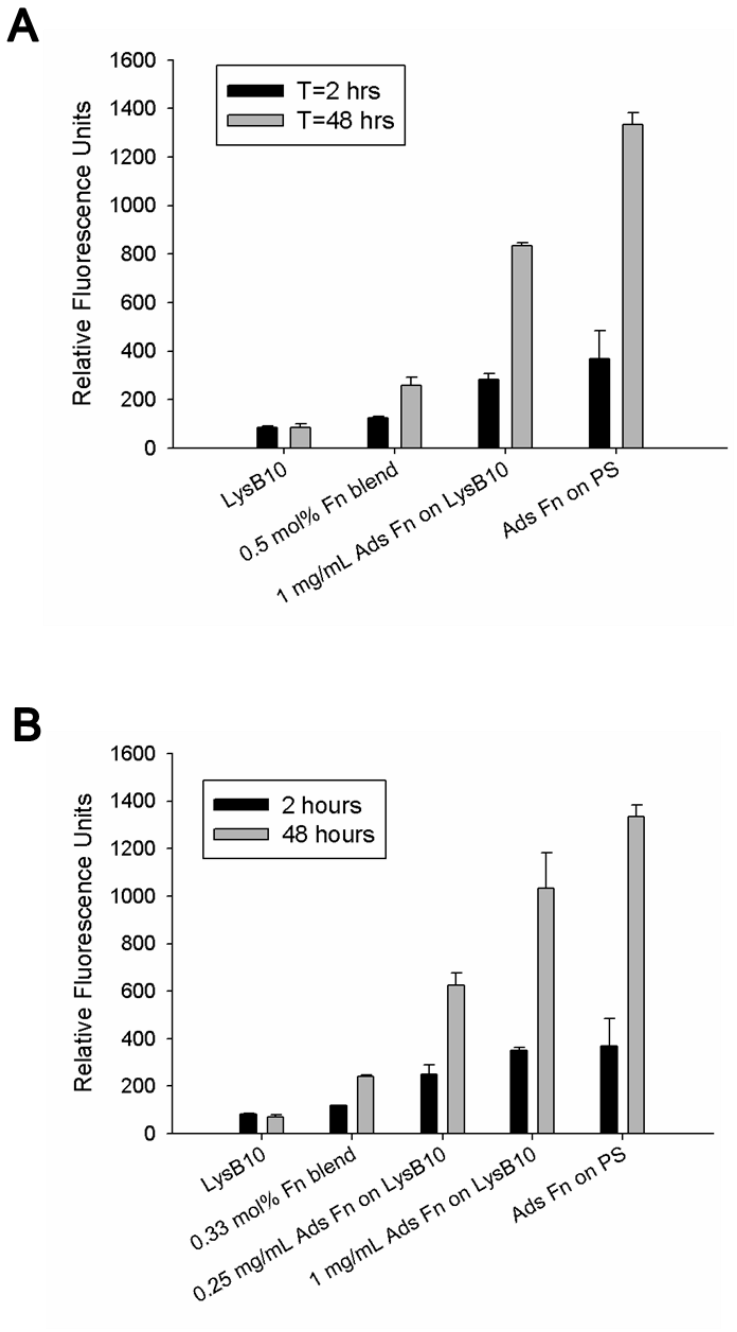

Figure 5.4. HUVEC growth on crosslinked Fn-LysB10 gels over a 48 hour period. Cells were seeded at a density of 5000 cells/well in low-serum media. After a 2 hour adhesion period, non-adherent cells were removed and complete media was added to each well. The cells that were maintained in culture for another 48 hours prior to performing the cell adhesion assay. **(A)** Cell growth over a 48 hour period on 6wt% **LysB10**-Fn gels and **(B)** 10wt% **LysB10**-Fn gels.

HUVEC Spreading

Since HUVECs assemble robust focal adhesions containing clustered integrins and intracellular structural and signaling proteins, focal adhesion assembly as well as cytoskeletal organization on the engineered interfaces was examined. In particular, two markers were chosen to further evaluate cell function: F-actin stress fibers and vinculin, a focal adhesion associated protein that functions as a linker between actin filaments and integrins (Figure 5.6). Well-developed actin stress fiber network and vinculin clustering was apparent with fibronectin-coated substrates. However, on **LysB10** alone, actin and vinculin were nonspecifically distributed throughout the few adherent cells, which assumed rounded morphologies. These results further confirm that cell adhesion is mediated through integrin-ligand binding, and that the fibronectin-coated surfaces of both 6wt% and 10wt% crosslinked gels are sufficiently robust to induce cytoskeletal organization and focal adhesion formation characteristic of well-spread cells. While a monolayer of HUVECs with characteristic “cobblestone” morphology was observed on all crosslinked Fn-**LysB10** gels and 10wt% noncrosslinked Fn-**LysB10**, unique endothelial cell morphology was observed on non-crosslinked 6wt% **LysB10** that was treated with fibronectin (Figure 5.7). Vinculin and actin staining revealed that cordlike structures and networks of elongated HUVECs were formed after 2 hours in culture, indicating tubule formation. These results suggest that both ligand density and substrate stiffness play important roles in defining endothelial cell behavior.

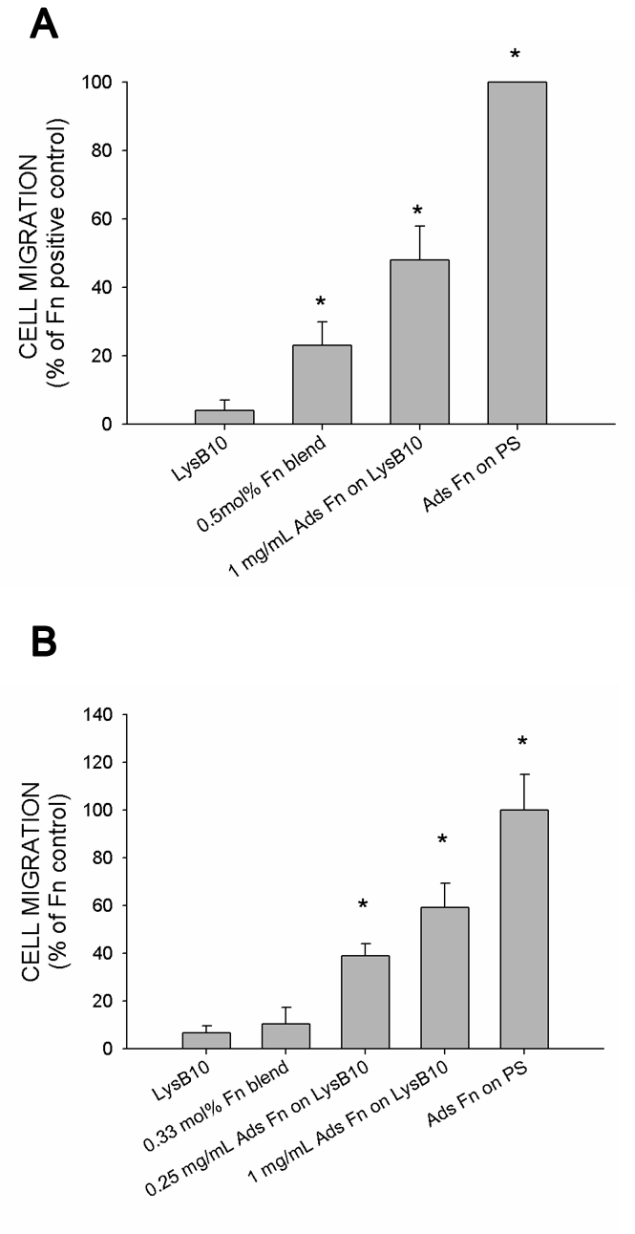

Figure 5.5. HUVEC migration into detection zone on **(A)** 6wt% crosslinked hydrogels and **(B)** 10wt% crosslinked gels. Cells were seeded onto an outer annulus area and monitored for motility into an inner radial zone over a 36-hour period. Quantitation was achieved with fluorescent measurement of the number of migrated cells into the detectable inner zone, which was normalized against the number of migrated cells on fibronectin-coated polystyrene .*$p<0.05$ compared to unmodified **LysB10**.

HUVEC Quiescence/Activation State

Further functionality of the HUVECs was assessed with immunofluorescence staining of the cellular adhesion molecules ICAM-1 and E-selectin, which are upregulated in activated HUVECs and mediate rolling of blood leukocytes in microvessels at sites of inflammation [336]. The functional state of an endothelial cell monolayer determines its ability to act as a thromboresistant barrier for blood-contacting material applications. Therefore, the success of an endothelialized surface is dependent on either activation or quiescence of the endothelial cells. Cells that were cultured on fibronectin-coated polystyrene and maintained in culture overnight in serum-free media assumed a quiescent state, with little ICAM-1 and E-selectin expression on the cell surface. Activation of HUVECs was achieved by adding 100ng/mL TNF-alpha to the media for 4 hours. The positive and negative controls were compared to those cells adherent for 4 hours in serum-free media on crosslinked Fn-**LysB10** gels. Limited ICAM-1 and E-selectin staining was observed on fibronectin-coated **LysB10** compared to the activated control. Thus, endothelial cells are not only able to adhere, proliferate, and migrate on **LysB10** substrates coated with fibronectin, but can maintain a quiescent state phenotype (Figure 5.8).

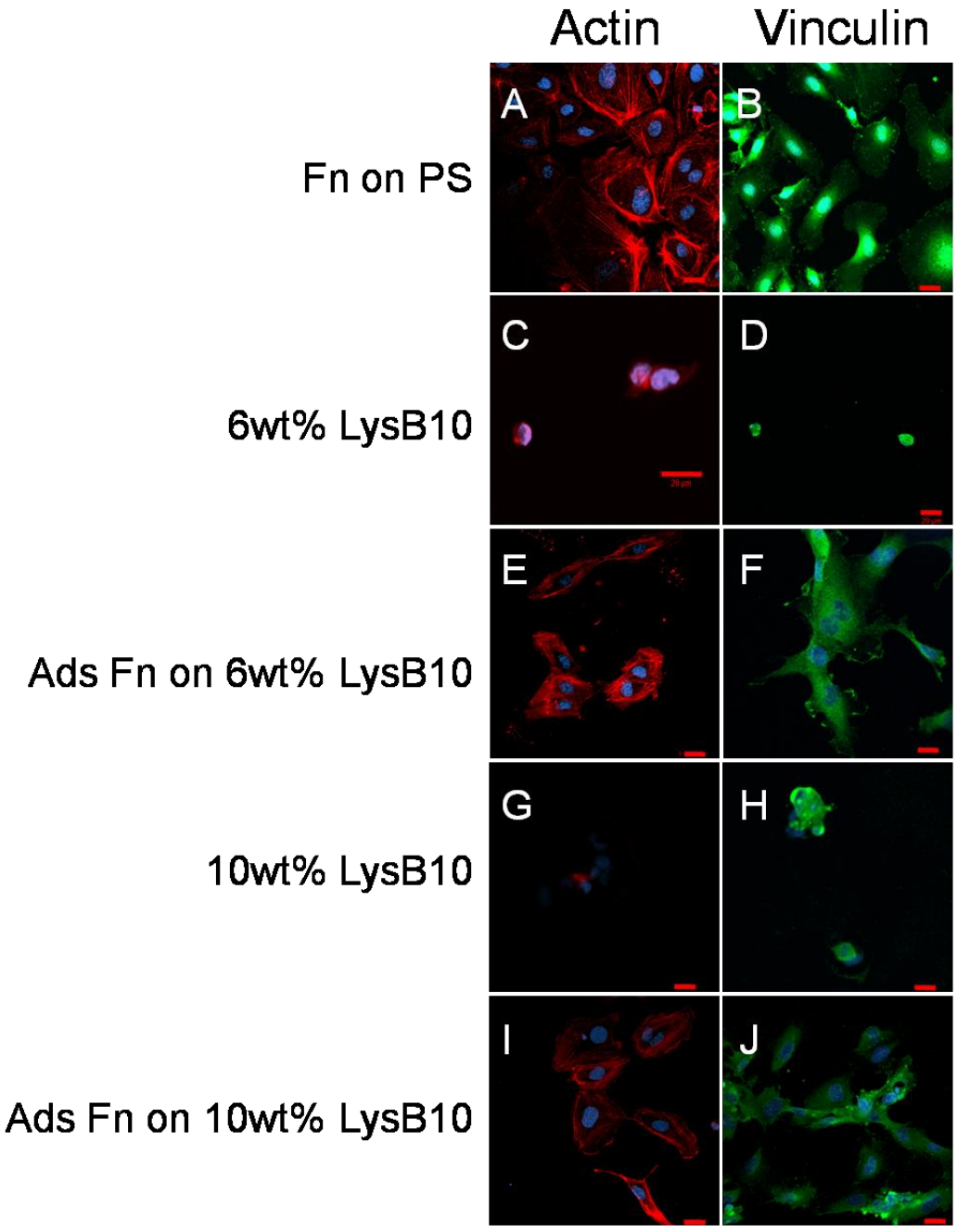

Figure 5.6. Representative confocal images of HUVECs cultured on crosslinked LysB10 gels for a period of 2 hours in serum-free media. Red bars represent 20um. 1 mg/mL fibronectin was adsorbed onto LysB10 gels and crosslinked into place with genipin. Fluorescently labeled actin is shown in red (A, C, E, G, I), while vinculin is displayed in green (B, D, F, H, J).

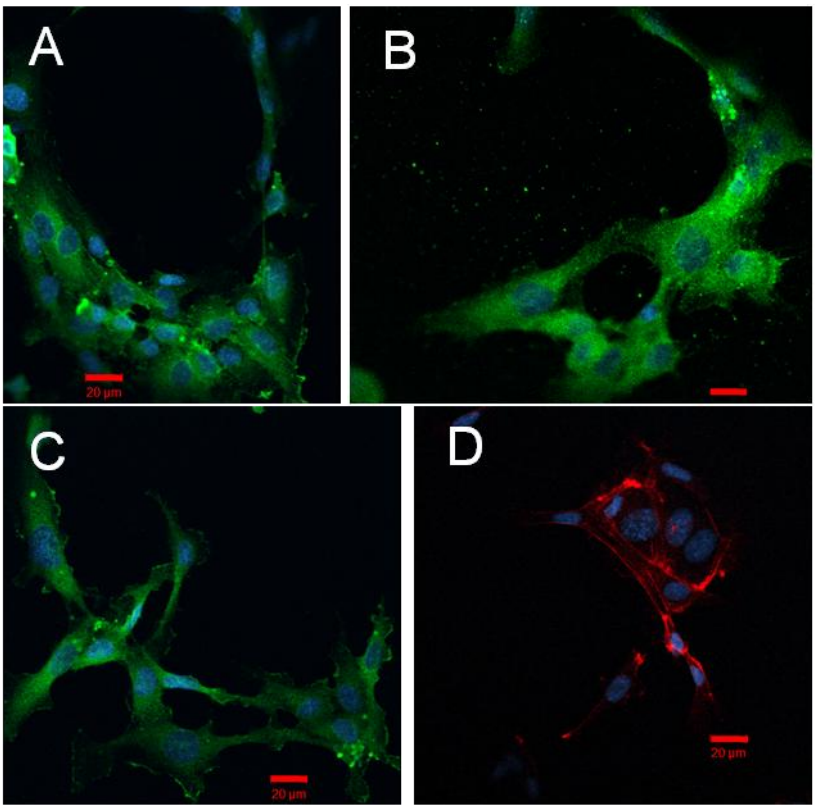

Figure 5.7. Representative confocal images of HUVECs cultured on uncrosslinked Fn-LysB10 gels for a period of 2 hours in serum-free media. Red bars represent 20um. 1 mg/mL fibronectin was adsorbed onto LysB10 gels for 6 hours prior to cell seeding. Fluorescently labeled actin is displayed in red (**D**), while vinculin is displayed in green (**A, B, C**).

Mesenchymal stem cell adhesion and proliferation on surface immobilized Fn-LysB10

Mesenchymal stem cell behavior on fibronectin-treated **LysB10** gels was determined with adhesion and proliferation assays. In particular, fibronectin density and **LysB10** density were modulated to optimize MSC response to the material properties. 1mg/mL fibronectin was surface-adsorbed onto 6wt% gels and 0.25 mg/mL fibronectin was adsorbed onto 10wt% gels, which correlated to a surface density of approximately 82 fmol/cm^2. 1 mg/mL fibronectin was adsorbed onto 10wt% gels in order to maximize surface fibronectin density at 153 fmol/cm^2. As Figure 5.9 demonstrates, hydrogel formulations without fibronectin were unable to support MSC adhesion and proliferation. While a fibronectin density of 82 fmol/cm^2 on both 6 and 10wt% **LysB10** did significantly increase adhesion and proliferation rate compared to **LysB10** alone. Maximal adhesive and proliferative responses were achieved with 10wt% gels of 153 fmol fibronectin ligand/cm^2.

Analysis of mesenchymal stem cells on collagen-fiber reinforced elastin-like sheets

Previous work in our lab has demonstrated the application of acellular collagen fiber-reinforced elastin composites in vascular graft and hernia patch engineering [333]. We sought to take this process a step further by replicating the structural hierarchy of the tissue and seeding the acellular matrix with mesenchymal stem cells. The immunomodulatory behavior of mesenchymal stem cells and their multipotency make them a promising therapeutic for tissue regeneration and an attractive cell source for a broad range of tissues.

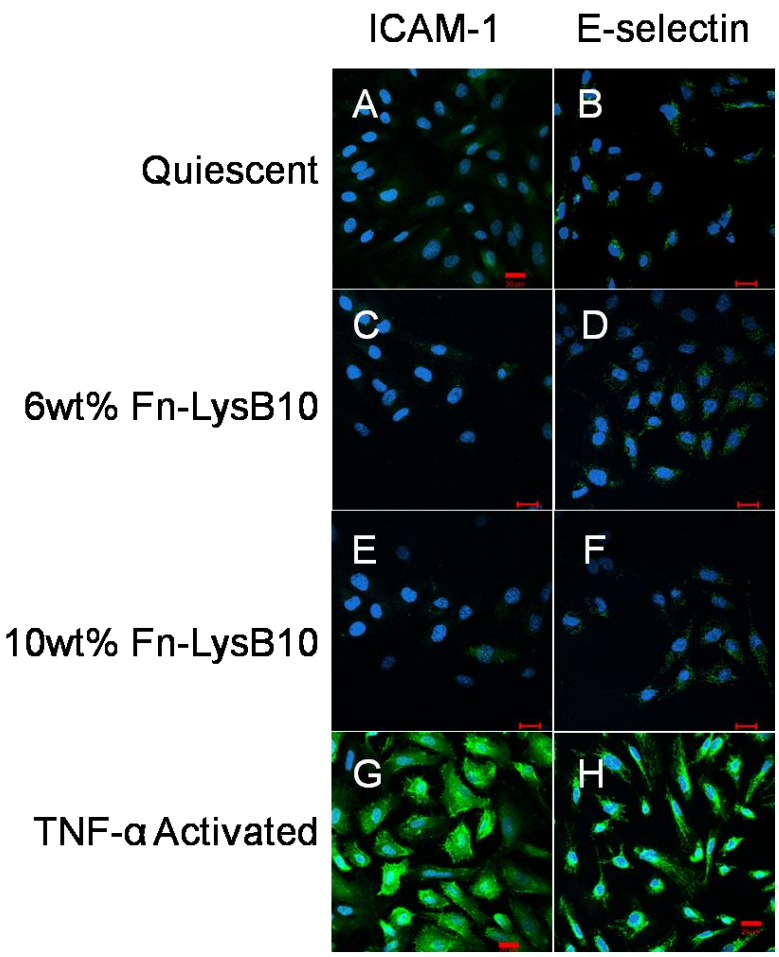

Figure 5.8. Representative confocal images of HUVECs cultured on various substrates. Cells that were cultured on fibronectin-coated slides without TNFalpha stimulation (**A & B**) maintained a quiescent phenotype. Activation was achieved with the addition of TNFalpha to the culture medium (**G & H**). HUVEC activation or quiescence was compared to that on crosslinked Fn-modified **LysB10** films (**C, D, E, & F**). Markers of HUVEC activation were ICAM1-1 (**A,C, E, & G**) and E-selectin (**B,D, F, & H**). Red bars signify 20um.

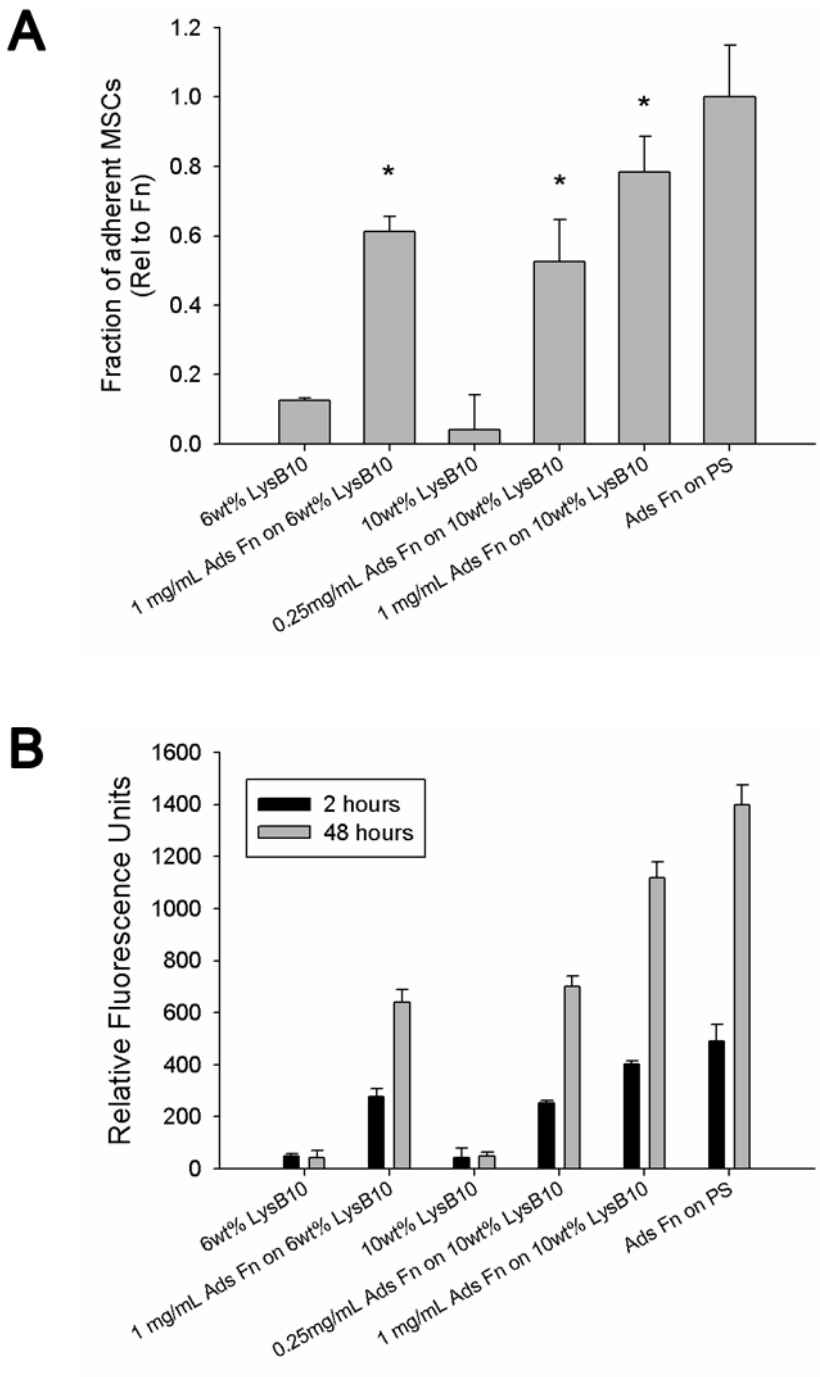

Figure 5.9. (A) pMSC 2 hour adhesion assay on crosslinked LysB10 gels with surface-immobilized fibronectin. 50 ug/mL fibronectin in PBS was allowed to adsorb to polystyrene overnight and served as a positive control. All data was normalized to this fibronectin control.*$p<0.05$ compared to LysB10-only counterparts. **(B)** pMSC proliferation over a 48-hour period on crosslinked LysB10 gels with surface-immobilized fibronectin.

Tissue constructs were formed first as 50 micron-thick single sheets of collagen fiber embedded within a thin **LysB10** film. Biofunctionalization of the protein sheet was achieved with fibronectin immobilization onto the sheet surface. MSCs were seeded onto the bioactive scaffolds, and then appositioned into multilamellar constructs. Two or three layers of the cell-seeded protein sheets were sandwiched and held together between nylon screens with 70 micron pores. These constructs were then cultured *in vitro* for one week to enable cellular matrix deposition and interlamellar bonding. After one week in culture, weak lamellar bonding was observed. Furthermore, as seen in Figure 5.10, MSCs remained viable on single protein sheets and within multilamellar constructs. While laminates remained intact in cell culture medium and PBS without external support, they were unable to withstand high shear forces during handling, during which time delamination of the layers was occasionally observed. Interlamellar bonding will be improved by increasing the culture period to two weeks or longer to allow for further matrix deposition and construct maturation.

Histological analysis of cells cultured for 72 hours on the surfaces of single protein sheets revealed a uniform, dense cell layer at the scaffold surface, with no infiltration through the thickness of the films (Figure 5.11A). No glycosaminoglycan deposition was observed at the cell-sheet interface (Figure 5.11 B). After trilayer formation and one-week culture period (Figure 5.11C), the cell layers fused in the contacting region between lamellae, forming a thin inter-lamellar space, but did not infiltrate through the layers. Alcian blue stain with nuclear fast red counterstain of a bilamellar construct revealed intermittent glycosaminoglycan deposition by MSCs (Figure 5.11D). However, it is evident that further construct maturation in culture is required to strengthen interlamellar adhesion and enhance matrix deposition.

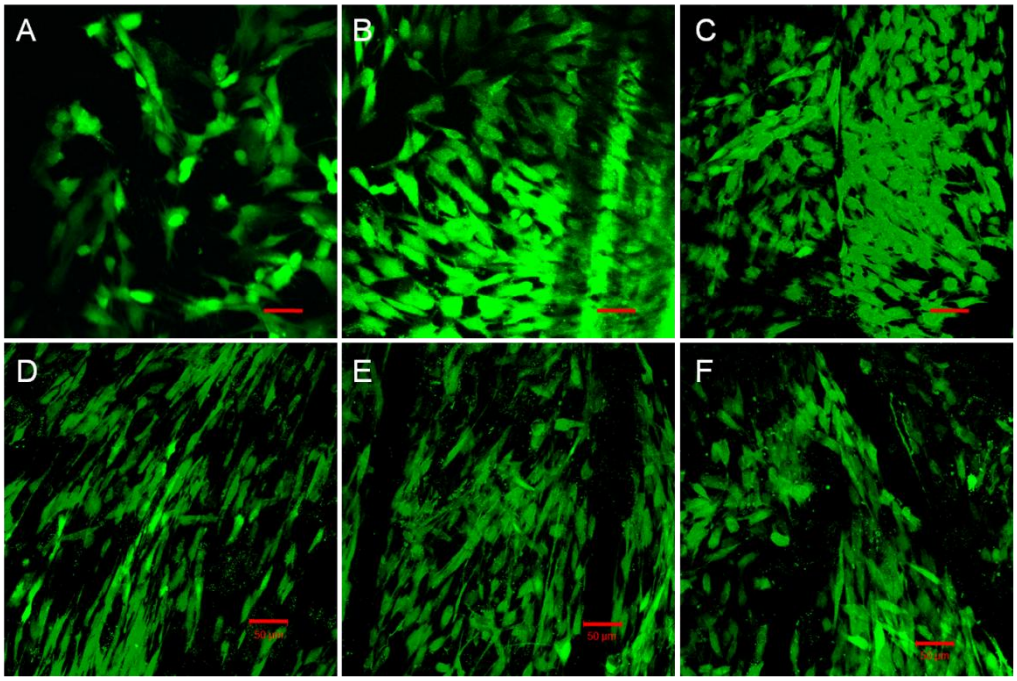

Figure 5.10. Representative confocal images of MSC viability on protein sheets. Cell-seeded constructs were incubated in Calcein AM solution for 1 hour prior to imaging. **(A)** MSC viability on 40 micron-thick single protein sheet immediately following two-stage cell seeding protocol. **(B)** MSC viability on 40 micron-thick single protein sheet after culturing to confluence. **(C)** Bilayer laminate of cell-seeded protein construct. Cell viability within a tri-lamellar construct is visualized in **(D)** top layer **(E)** middle layer and **(F) bottom** layer of construct. Red bars represent 50 microns.

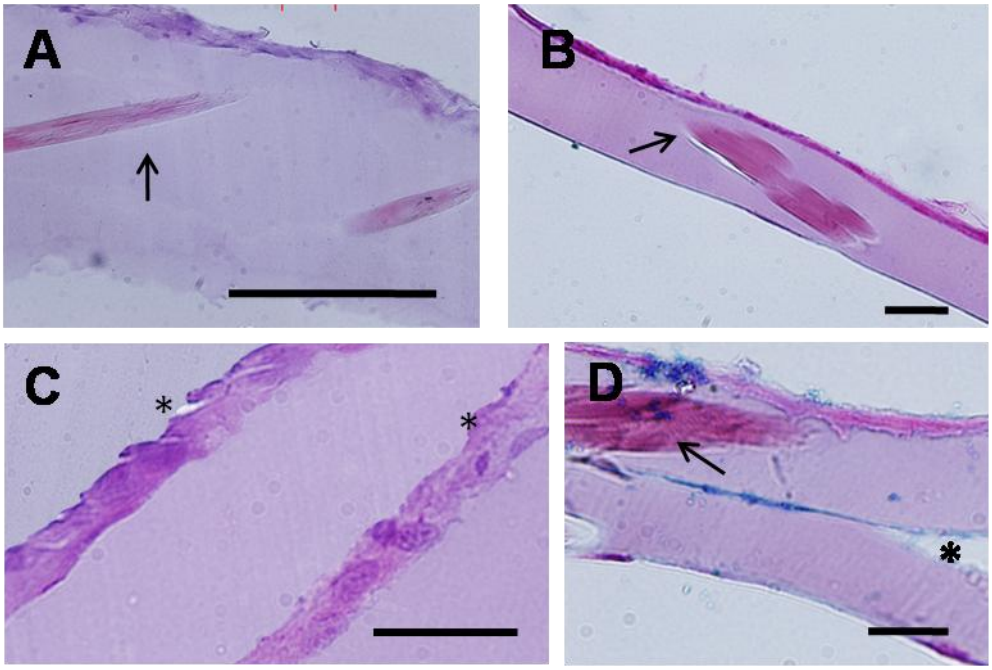

Figure 5.11. Histological analysis of MSC-seeded protein fiber sheets. Samples were cross-sectioned in order to visualize individual layer thickness and interlamellar bonding. **(A)** H&E staining of a single protein sheet retrieved after 72 hours in culture demonstrates MSC adhesion to the surface of the elastin-like sheet. **(B)** Alcian blue stain with nuclear fast red counterstain of a single sheet reveals limited glycosaminoglycan deposition. **(C)** H&E staining of a trilamellar construct after one week in culture demonstrates limited MSC infiltration through the layers, with weak interlamellar bonding. Asterisks highlight the interlamellar space. **(D)** Alcian blue stain with nuclear fast red counterstain of a bilamellar construct reveals intermittent glycosaminoglycan deposition by MSCs. Weak interlamellar adhesion is highlighted with an asterisk, where partial delamination was observed. Arrows indicate the presence of collagen fibers. Bars represent 50 microns.

In vitro evaluation of inflammatory response of MSCs on multilamellar protein sheets: Gene expression of IL-1beta and COX-2

Previous *in vivo* studies with **LysB10** and other elastin-mimetics have demonstrated their minimal inflammatory response. However, it is difficult to predict MSC behavior within a multilamellar collagen fiber-reinforced elastin-like construct. Therefore, the inflammatory response of MSCs cultured within multilamellar protein sheets was characterized using real time RT-PCR. pMSCs were seeded onto tissue culture-treated polystyrene with and without 10 ug/mL lipopolysaccharide (LPS) added to the culture medium for 96 hours. Cell-seeded trilamellar constructs were cultured for 96 hours prior to RNA isolation as well. Gene expression of interleukin-1beta (IL-1beta) and cyclooxygenase 2 (COX-2) was evaluated in quiescent cells, LPS-activated cells, and cell-seeded trilamellar constructs (n=3).

The PCR results demonstrate that expression of the COX-2 gene was similar to that of the IL-1beta gene (Figure 5.12). Furthermore, cells grown in the presence of LPS had a significantly higher expression of the inflammatory markers IL-1beta and COX-2 compared to non-activated cells (negative control). However, gene expression of cells cultured within the collagen-**LysB10** scaffolds was comparable to that of cells grown on tissue culture polystyrene (negative control). Thus, we were able to demonstrate that MSCs interspersed within the multilamellar **LysB10** constructs can maintain their anti-inflammatory phenotype.

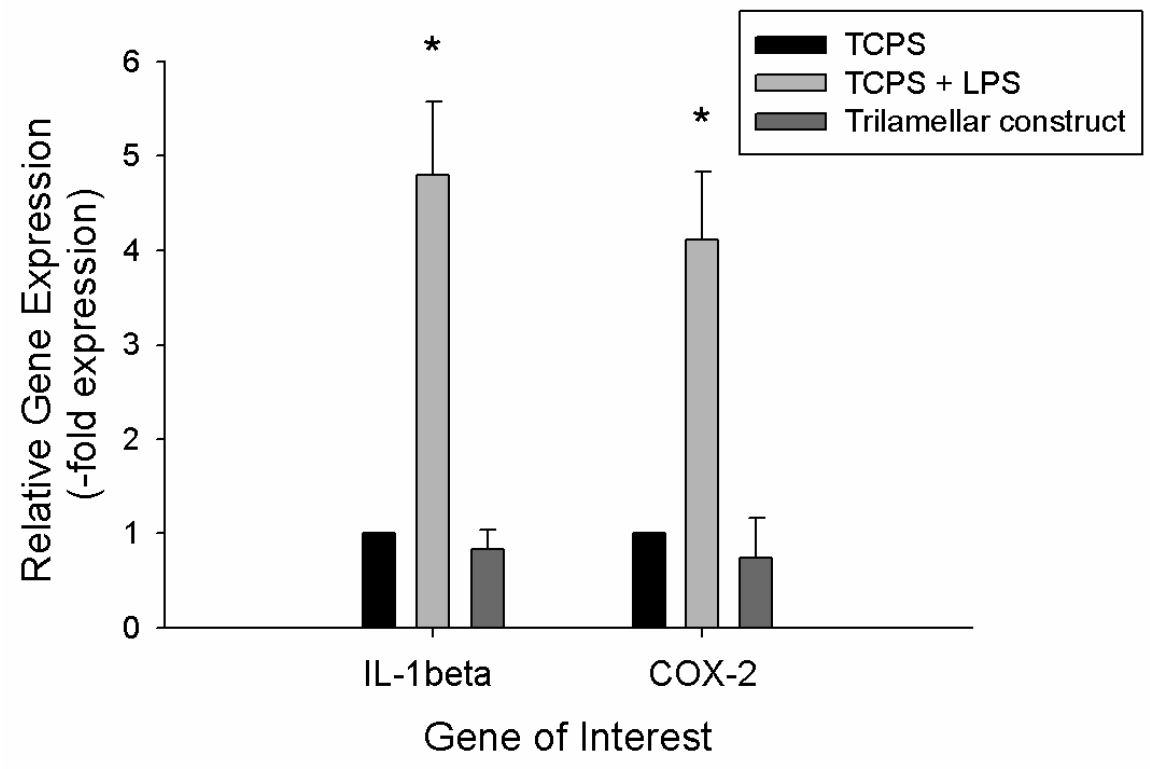

Figure 5.12. Relative interleukin 1beta and cyclooxygenase 2 gene expression by porcine mesenchymal stem cells cultured on tissue culture polystyrene (TCPS, negative control), TCPS with 10 ug/mL LPS (positive control), and cell-seeded trilamellar collagen-reinforced elastin-like sheets after 96 hours in culture. The endogenous control used was the housekeeping gene GAPDH. The expression data was normalized to the TCPS negative control. *$p<0.01$ compared to the TCPS negative control. N=3

5.4 DISCUSSION

Fibronectin-LysB10

Recently, we reported a new class of recombinant elastin-mimetic protein polymer, **LysB10**, for the purpose of designing materials for small-diameter vascular grafts [323]. The goal of this study was to add desired biological functionality to the recombinant elastin analog **LysB10** in order to enhance cell adhesion and migration to an otherwise non-adhesive substrate.

The functional importance of the endothelium in controlling thrombosis and inflammation has guided attempts to closely mimic the native arterial wall in the design of a new generation of vascular prostheses. The endothelial lining in the native vasculature not only serves as a protective, thromboresistant barrier between blood and the surrounding tissue, but also controls vessel tone, platelet activation and leukocyte adhesion. While numerous strategies exist to improve cell adhesion and retention on vascular prostheses, this study focuses on the immobilization of fibronectin on **LysB10**. Fibronectin serves as a multifunctional ligand that binds directly to cells, as well as heparin, collagen, and fibrin molecules, thereby modulating the ECM microenvironment [156-158]. Pretreatment of vascular grafts with fibronectin has been investigated by several groups in order to improve *in vitro* and *in vivo* endothelialization of graft surfaces [160]. For example, Nishibe and colleagues covalently bonded fibronectin to the luminal surface of ePTFE grafts and demonstrated accelerated transmural tissue ingrowth and neointima formation in a canine model [161]. Although there were concerns that fibronectin treatment would increase graft thrombogenicity due to platelet activation and adhesion, no significant decrease in patency was observed. On the contrary, thrombus area was significantly lower on fibronectin-coated grafts compared to untreated ePTFE grafts.

Two formulations of fibronectin-**LysB10** hydrogels were explored: (i) uniformly blended fibronectin-**LysB10** solutions that were formed into hydrogels and (ii) **LysB10** hydrogels that were surface-adsorbed with fibronectin. While both formulations with 0.75mg/mL fibronectin input concentrations were able to support similar levels of endothelial cell adhesion, the latter proved to be more effective in eliciting endothelial cell proliferation and migration. This phenomenon can be attributed to the fact that most of the bioactive epitopes in uniform fibronectin blending are hidden within the hydrogel bulk, while surface-adsorbed fibronectin allows for concentrated ligand coating at the cell-material interface over a prolonged period of time. Thus, mechanical testing, endothelial cell spreading studies, and mesenchymal stem cell characterization were conducted on surface-immobilized Fn-**LysB10** hydrogels.

The adsorption profile of fibronectin on 10wt% hydrogels was greater than that on 6wt% gels (Figure 5.2). This phenomenon is most likely due to an increased density of **LysB10** molecules at the surface of a 10wt% gel, which facilitates adsorption and subsequent crosslinking of fibronectin. Therefore, two ligand densities were chosen for cell experiments: (i) a fibronectin surface density of approximately 82 fmol/cm^2 was achieved by adsorbing 1mg/mL fibronectin onto 6wt% gels and 0.25 mg/mL fibronectin onto 10wt% gels. (ii) A maximal surface density of 153 fmol/cm^2 was achieved by adsorbing 1 mg/mL fibronectin onto 10wt% gels.

To explore the biostability and associated bioactivity of incorporated fibronectin, non-crosslinked and genipin-crosslinked fibronectin-**LysB10** gels were allowed to incubate in PBS for 1 week, with daily PBS changes. Following the 1 week incubation period, a 2 hour adhesion assay was performed. Intermolecular crosslinking with genipin is thought to occur via the primary amine groups and the C3 carbon of genipin, with subsequent dimerization produced by radical reactions [275-280] . It is important to note that crosslinking of the primary amine groups in fibronectin did not result in loss of bioactivity. In fact, crosslinking of fibronectin-adsorbed **LysB10** preserved endothelial cell adhesion, while non-crosslinked hydrogels exhibited a muted

cell response due to fibronectin loss over the one-week PBS incubation period. This suggests that the bioactive sites within the fibronectin molecule were not disrupted by crosslinking activity.

The mechanical properties of the extracellular matrix can play a vital role in determining cell fate. In particular, cell response to substrate stiffness can influence a range of processes, including adhesion, proliferation, migration, tubulogenesis, focal adhesion formation, and differentiation potential [337-340]. Therefore, in generating an elastin-mimetic for vascular tissue engineering applications, it is important to not only evaluate fibronectin ligand presentation on the hydrogel surface, but to also determine its mechanical properties and the interplay between the two factors [262, 341]. Since cell deformation is one process that is thought to be important in the mechanotransduction pathway, hydrated gels were subjected to compressive loading [342]. Previous investigations have controlled compressive moduli by varying the degree of crosslinking in polyacrylamide gels or altering collagen gel and matrigel concentrations [241, 343-347]. In a similar manner, our treatment groups included noncrosslinked samples, genipin-crosslinked gels, and adsorbed fibronectin that was genipin-crosslinked onto **LysB10**. 6wt% and 10wt% formulations were chosen in order to examine a broad range of substrate stiffness. Moreover, previous studies in our lab have utilized these two formulations in applications ranging from hydrogel coatings to composite collagen-elastin vascular grafts.

In general, cell adhesion and growth increase as substrate stiffness increases, until a threshold is reached, beyond which cell response does not vary. For example, a greater fibroblast proliferation rate has been reported on 14 kPa gels compared to 4.7 kPa gels [348]. A two-fold increase in apoptosis has also been reported on softer gels compared to stiffer ones. Thus, increases in cell number on stiff substrates can be attributed to both increased proliferation and decreased apoptosis [348]. Moreover, stiffer substrates have been reported to promote cell spreading, with the greatest degree of spreading noted on 10kPa gels, with no

further increase in spread area beyond that value [349, 350]. This observation confirms previous studies that noted increased recruitment of vinculin to adhesion sites on stiffer substrates [351].

The interplay between stiffness and adhesive ligand presentation is apparent when comparing endothelial cell proliferation on **LysB10** gels. Both crosslinked 6wt% and 10wt% Fn-**LysB10** hydrogels display relatively high compressive moduli, even at low strains (42 kPa and 106 kPa, respectively). Results in Figure 5.4 and Figure 5.5 demonstrate that an increase in compressive modulus from 42 kPa to 106 kPa, with equivalent fibronectin density presentation, does not alter endothelial cell proliferation and migration. While adhesion levels, proliferation rate, and migration are relatively constant on those substrates grafted with 82 fmol fibronectin/cm^2, a greater fibronectin density of 153 fmol/cm^2 on 10wt% gels stimulates the highest endothelial proliferation and migration rate, closely matching that of fibronectin-adsorbed polystyrene. It is difficult to predict the outcome of a higher fibronectin density on 6wt% gels, as the maximal adsorption range that could be reasonably achieved on this substrate was approximately 82 fmol/cm^2. Significantly, Underwood and Bennet have reported that a fibronectin density of 140 fmol/cm^2 is required in inducing maximal cell adhesion [258].

The formation of blood vessels from endothelial cells, or tubulogenesis, is a multistep process in which alignment of endothelial cells and generation of a patent lumen is induced by biochemical and mechanical factors [339, 352, 353]. Numerous groups have demonstrated that the formation of cordlike structures and networks of elongated cells are governed by a combination of ligand density and substrate modulus. For example, Califano and colleagues observed cord-like formation of endothelial cells on 1 kPa polyacrylamide substrates derivatized with type I collagen, while cells on 10 kPa gels formed evenly distributed monolayers [354]. However, when collagen density was decreased 100-fold, network formation was seen on 10 kPa gels as well. Similarly, Deroanne and colleagues have reported the formation of cordlike structures on 17 kPa matrigel while cells on 75 kPa gels formed a monolayer [355]. Our own

morphological observations confirm previous reports that a decrease in mechanical resistance is sufficient to switch endothelial cell patterning from a monolayer to differentiated tube-like structures. As seen in Figures 5.6 and 5.7, a decrease in compressive modulus from 42kPa (crosslinked 6wt% gels) to approximately 9 kPa does trigger formation of elongated cells and the assembly of tube-like structures.

The interplay between substrate stiffness and ligand presentation also directs mesenchymal stem cell behavior. Mesenchymal stem cells have emerged as a promising therapeutic modality for tissue regeneration and repair. Mesenchymal stem cells are multipotent adult stem cells that can differentiate into a number of cell types, including osteoblasts, chondrocytes, skeletal muscle cells, vascular endothelial cells, and cardiomyocytes [321, 324-326]. They are ideal for tissue engineering applications in that they are able to adhere and expand in culture. Moreover, MSCs have been shown to display immunosuppressive properties. Although the molecular mechanisms are not completely understood, numerous studies have revealed that MSCs avoid allorecognition and interfere with dendritic cell and T-cell function [252, 328, 331]. Similarities of porcine MSCs with their human counterparts make them ideal candidates for *in vitro* studies and preclinical investigations, and have contributed to enhanced wound healing, angiogenesis, myocardial viability, and bone formation, to name a few applications [332]. Rowlands and colleagues have found that the attachment of MSCs on polyacrylamide gels is dependent not only on gel stiffness, but also on the type of ECM molecule presented on the surface of the gel [345]. In general, stiffer gels supported higher cell adhesion and proliferation than softer ones (range explored was 0.7 kPa to 80 kPa), with similar proliferation rates on gels of 25 kPa and higher. Moreover, at 25 kPa and higher, fibronectin-coated gels supported the highest number of adherent MSCs, with collagen I, laminin, and collagen IV coatings supporting adhesion to a lesser degree. Our studies of MSC behavior on

Fn-**LysB10** gels yielded similar results to those of endothelial cells, with maximal adhesive and proliferative responses achieved with crosslinked 10wt% gels of 153 fmol fibronectin ligand/cm^2.

Although the controlled differentiation of mesenchymal stem cells is outside the scope of this study, other investigators have utilized substrate stiffness to direct MSC differentiation as well. In particular, Engler and colleagues, along with Rowlands et al., have shown that lineage specification can be directed by tuning the elasticity of the matrix [344, 345]. For example, elastic moduli of collagen I-coated polyacrylamide ranging from 0.1-1 kPa simulated that of the brain, moduli of 8-17 kPa mimicked that of muscle, and moduli greater than 34 kPa was comparable to that of collagenous bone. Using these guidelines, the investigators were able to demonstrate MSC differentiation into neurogenic, myogenic, and osteogenic precursors when cultured on gels of the appropriate elasticity.

Cell Sheet Engineering

Collagen and elastin networks contribute to highly specialized biomechanical responses in numerous tissues and species. Specifically, acellular composite sheets were previously produced with properties that ranged over 13-fold in elongation to break (23 - 314%), six-fold in Young's modulus (5.3 to 33.1 MPa), and more than two-fold in tensile strength (1.85 to 4.08 MPa), exceeding that of a number of native human tissues, including urinary bladder, pulmonary artery, and aorta [333]. Consequently, Caves et al. demonstrated the application of collagen fiber-reinforced **LysB10** composites in vascular graft and hernia patch engineering [333]. Based on improved cellular response to fibronectin-coated **LysB10**, we sought to take this process a step further by replicating the structural hierarchy of native tissue and seeding the acellular matrix with mesenchymal stem cells. The laminated geometry offers the potential to incorporate living cells at controlled spatial intervals throughout a stacked sheet, similar to cell sheet tissue engineering methods.

While mesenchymal stem cells remained viable within the bilamellar and trilamellar constructs, the one week culture period limited ECM deposition within the interlamellar space, and resulted in weak interlamellar bonding. Delamination of the constructs can be addressed in a number of ways. Increase in culture time can facilitate cellular infiltration through the lamellae and allow for extracellular matrix production to strengthen interlamellar bonding. Furthermore, the addition of sodium ascorbate has been utilized by L'Heureux and colleagues to accelerate cell-secreted matrix production [356].

After examining MSC viability, we evaluated the inflammatory potential of collagen-reinforced **LysB10** trilamellar scaffolds intended for use in stem cell engineering of tissues. Gene expression of the inflammatory markers interleukin-1beta (IL-1beta) and cyclooxygenase 2 (COX-2) demonstrated that MSCs interspersed within the multilamellar constructs were able to maintain their anti-inflammatory phenotype [320]. These results confirm previous observations that protein polymer blocks composed of VPGVG, VPGKG, VPGEG, IPAVG, and VPAVG induce minimal inflammatory and allergic reactions [232, 357, 358]. While antibodies can be raised against peptides derived from the hydrolysis of native elastin, neither VPGVG nor VPAVG peptides are among the recognized sequences [359]. Further biocompatibility studies on **LysB10** have revealed long-term *in vivo* biostability and minimal inflammatory responses, which makes it an ideal candidate for structural components of engineered tissues and biocompatible surface coatings [14].

Three-dimensional reconstruction of functional tissues with cell sheet technology has been extensively explored. For example, the temperature-responsive polymer poly(N-isopropylacrylamide) (PIPAAm) enables culturing of cells and facilitates the harvest of confluent cells as intact sheets [360, 361]. Promising applications of this technology have been the layering of mesenchymal stem cell sheets for the development of tissue-engineered cardiac patches as well as the creation of organ-like tubular structures [329, 362]. Other investigators

have utilized prolonged culture periods of up to ten weeks and the addition of media supplements to stimulate increased matrix deposition of cultured cells onto polymer scaffolds in order to generate mechanically-robust cell sheets [54, 356]. The use of collagen fibers and elastin-mimetic recombinant proteins allows greater independent control of scaffold properties, including compliance, resilience, strength, and anisotropy, than those tissue engineered constructs which rely on direct assembly of cultured cell sheets. The layering of two to three individual cell sheets has provided the groundwork for future investigations, in which three-dimensional tissues will be comprised of eight to ten cell sheets.

CHAPTER 6

CONCLUSION AND FUTURE DIRECTIONS

Previous studies in our lab generated the elastin-like protein polymer **LysB10**, which was designed with the capability of physical and chemical crosslinks, and was shown to display a range of elastomeric properties that more closely matched those of the native artery. Several investigators have endeavored to not only emulate the mechanical properties of the vasculature, but to also mimic the biologic responsiveness of the blood vessel. In particular, the poor patency rates of vascular grafts composed of synthetic polymers have motivated strategies to functionalize the luminal surface of grafts in order to promote endothelialization, and thereby limit thrombosis and inflammation. Consequently, this dissertation addresses three approaches to modulating cellular behavior on elastin-mimetic analogs with the goal of promoting vascular wall healing and tissue regeneration: (1) genetic engineering of elastin-like protein polymers (ELPs) with cell-binding domains, (2) biofunctionalization of elastin-like protein polymers via chemoselective ligation of bioactive ligands, and (3) incorporation of matrix protein fibronectin for engineering of cell-seeded multilamellar collagen-reinforced elastin-like constructs.

Chapter 3. Genetic engineering of elastin-mimetic protein polymer with cell-binding domains. The development of genetic and recombinant protein engineering has enabled the synthesis of bio-inspired protein polymers composed of repetitive amino acid sequences and peptide blocks, whose structural complexity impart specific mechanical, chemical, and biologic properties. The most significant impact of this strategy is the capacity to introduce precise changes in the amino acid sequence to modulate properties of the entire protein network. This

"bottom-up" approach to materials design enables researchers to finely modulate the nanostructure of a material in order to influence its bulk properties

In the present study, we sought to design a second generation elastin-mimetic triblock copolymer with the ability to guide endothelial cell behavior while maintaining the elastomeric properties of the protein polymer. Adhesion-promoting sequences, ligand density, presentation, and clustering, and ELP morphology were manipulated in order to tailor material properties. To this end, an alphavbeta3-associated ligand isolated from a pro-angiogenic, extracellular matrix–associated protein CCN1 was cloned into the central, hydrophilic domain of **LysB10**. The long-term goal encompassing this work was to utilize a biomolecular engineering approach that introduced cell-adhesive peptide motifs within a bio-inspired recombinant elastin-like protein polymer in order to elicit an integrin-mediated cellular response. The ability to precisely control ligand presentation is an important design parameter, and ultimately directs cell fates such as adhesion, migration, focal adhesion assembly, spreading, proliferation, and differentiation. Thus, endothelial cell adhesion, migration, and morphology were evaluated as markers of surface functionality on the recombinant protein polymers. The improved biological activity of **V2** engineered surfaces compared to **LysB10** alone can be attributed to enhanced binding of integrin alphavbeta3. This approach of conveying integrin specificity provides a robust biomolecular strategy to elicit directed biological responses on the biomaterial interface. In particular, the generation of modified protein polymers presents a clinically relevant approach to promoting endothelialization of vascular tissue-engineered scaffolds and coatings.

CCN1 is a matrix-associated protein known to play a critical role in vascular tissue regeneration and wound healing. This 40 kDa heparin-binding protein displays pro-angiogenic activities, including endothelial cell adhesion, migration, proliferation, and tubule formation [191]. The protein also promotes migration and adhesion of circulating endothelial progenitor cells (EPCs), while inducing them to secrete various growth factors and chemokines to remodel the

vascular wall [194]. Consequently, future studies will evaluate the ability of the V2 sequence to encourage EPC adhesion and migration within the context of the elastomeric recombinant protein polymer.

The ability of **V2** polymer to ultimately facilitate endothelialization and vascular wall regeneration must be demonstrated *in vivo*. We have previously coated ePTFE grafts with thin ELP hydrogel layers and defined non-thrombogenicity with an *ex vivo* baboon shunt model [15]. However, characterization of the extent of endothelialization and tissue integration will require *in vivo* studies as well as *in vitro* experiments that incorporate shear stress as a factor of endothelial cell retention. Two approaches can be taken to evaluate the utility of V2 as an appropriate biomaterial for generating clinically durable vascular substitutes; (1) The generation of a non-thrombogenic acellular conduit will stimulate *in situ* arterial wall regeneration by displaying cell-binding sites and matrix assembly motifs for migration and proliferating vascular wall cells that are repopulating the construct, and (2) fabrication of endothelial cell-seeded constructs will promote accelerated vascular tissue regeneration via increased endothelial cell retention.

Chapter 4. Chemical conjugation of cell-binding domain to elastin-mimetic protein polymer. While genetic engineering has allowed researchers to recombinantly express elastin polypeptides with cell-binding domains and other bioactive ligands to direct cellular behavior, chemical immobilization of short peptides to a recombinant protein polymer offers several advantages. Genetic cloning and recombinant protein expression is a time-intensive and expensive process, and therefore, is not an ideal tool for screening a wide range of bioactive domains. The synthesis of short peptides with functionalized endgroups does offer a more versatile approach for biomaterial testing. Furthermore, chemical synthesis offers the possibility

of incorporating ligands that cannot be processed via the biosynthetic machinery. Finally, peptide conjugation onto a polymer scaffold allows modulation of ligand presentation that is independent of the recombinant protein polymer.

The aim of this study was to develop a strategy for chemoselective ligation of bioactive peptides to the recombinant elastin hydrogel **LysB10**. In particular, the carboxylic acid functional group on glutamic acid residues along the **LysB10** polymer chain was utilized to chemically modify the recombinant protein polymer. It was hypothesized that the synthesis of thiolated **LysB10** along with an RGD conjugate functionalized with a terminal maleimide group would provide an effective conjugation scheme for spatial presentation and localization of bioactive ligands on the **LysB10** surface. Moreover, this controlled peptide presentation onto the functionalized hydrogel surface would stimulate cell adhesion and growth. This work is the first step in creating a model synthetic ECM for vascular tissue engineering applications, using ELPs as the base material, with which ligand presentation may be varied in a controlled manner. Although cellular behavior onto modified scaffolds was studied in the two-dimensional setting in this dissertation, many tissue engineering applications require the use of cells embedded within a three-dimensional matrix for tissue regeneration. In the future, examination of these integrin-specific interactions in a three-dimensional environment will be an important first step towards these applications.

The results of this study demonstrated that chemical conjugation of a bioactive ligand via maleimide-thiol chemistry is a viable means of functionalizing surfaces of elastin-like hydrogels. HUVEC and MSC adhesion, actin fiber formation, proliferation, radial migration, and HUVEC activation states were characterized in order to evaluate the efficacy of RGD-functionalized **LysB10**. To our knowledge, this study is the first report of direct chemical ligation of moieties onto the surfaces of recombinant elastin-mimetic protein polymer hydrogels.

While RGD served as a proof-of-concept ligand for biofunctionalization chemistry, future studies will exploit the bioactivity of other ligands in enhancing endothelial and mesenchymal stem cell behavior on ELP surfaces. For example, while RGD lacks integrin specificity, cyclic RGD has been found to enhance alphavbeta3 integrin binding [165]. Moreover, the cyclic derivative has been known to lead to higher shear stress cell detachment resistance compared to linear peptides . In order to promote alpha5beta1-mediated adhesion, both the RGD sequence in the 10th type III repeat of fibronectin as well as its synergy site, the PHSRN sequence in the 9th type III repeat domain, are required to be presented together [164]. Another peptide with increased integrin affinity and selectivity is the sequence REDV, which binds to the integrin alpha4beta1, and thus, is capable of cellular interaction with leukocytes, endothelial cells, and some muscle and fibroblast cell lines, but not with platelets [169].

Although beyond the scope of this dissertation, future studies will also explore the behavior of smooth muscle cells on ELP derivatives, and their ability to simulate the medial layer of native vasculature. Moreover, the potential of mesenchymal stem cells to differentiate into a vascular phenotype for graft engineering has been explored by a few investigators, with mixed results. Consequently, controlled presentation of bioactive ligands on elastin-like protein polymers may further elucidate the mechanisms that mediate mesenchymal stem cell differentiation pathways. Ultimately, the contribution of cell-seeding of various cell types onto an elastin-like vascular construct will be validated *in vivo* for restoration of a physiologic vascular wall.

Chapter 5. Incorporation of matrix protein fibronectin into elastin-mimetic protein polymer blends and their application to cell-seeded vascular constructs. While numerous strategies exist to improve cell adhesion and retention on vascular prostheses, this study

focused on the immobilization of fibronectin on **LysB10**. Fibronectin serves as a multifunctional ligand that binds directly to cells, as well as heparin, collagen, and fibrin molecules, thereby modulating the ECM microenvironment. Pretreatment of vascular grafts with fibronectin has been investigated by several groups in order to improve *in vitro* and *in situ* endothelialization of graft surfaces. Consequently, in generating an elastin-mimetic for vascular tissue engineering applications, we found that fibronectin immobilization via amine crosslinking onto **LysB10** enabled endothelial cell adhesion, proliferation, migration, and spreading, and mesenchymal stem cell adhesion and proliferation. Moreover, we found that the interplay between matrix stiffness and ligand presentation influenced a number of cell processes, including adhesion, proliferation, migration, tubulogenesis, and focal adhesion formation.

Three-dimensional reconstruction of functional tissues with cell sheet technology has been extensively explored for use in tissue regeneration. Moreover, collagen and elastin networks have been shown to contribute to highly specialized biomechanical responses in numerous tissues and species. Previous investigations in the Chaikof lab have demonstrated the application of acellular collagen fiber-reinforced **LysB10** composites in vascular graft [333] and hernia patch engineering [in press]. Based on improved cellular response to fibronectin-coated **LysB10**, we sought to take this process a step further by replicating the structural hierarchy of native tissue and seeding the acellular matrix with mesenchymal stem cells. The laminated geometry offered the potential to incorporate multipotent cells at controlled spatial intervals throughout a stacked sheet, similar to cell sheet tissue engineering methods.

After examining tissue structure and function with viability studies, histological analysis, and *in vitro* inflammatory responses, we found that cell-seeded multilamellar collagen-reinforced **LysB10** scaffolds demonstrated enhanced biological properties, as well as previously reported mechanical stability. The use of collagen fibers and elastin-mimetic recombinant proteins allows greater independent control of scaffold properties, including compliance, resilience, strength,

and anisotropy, than those tissue engineered constructs which rely on direct assembly of cultured cell sheets. While the layering of two to three individual cell sheets has provided much of the groundwork, future investigations will rely upon the construction of three-dimensional tissues comprised of eight to ten cell sheets. This scale-up process will undoubtedly require further exploration of multiple factors, including the thickness of multilamellar units, diffusion limitations, and stimulation of angiogenesis within the matrix.

While *in vitro* experiments that expose the constructs to physiological shear stress will further optimize and validate the use of cell-seeded collagen-fiber reinforced, elastin-mimetic constructs for vascular tissue engineering, *in vivo* implantation of the vascular tissue replacement will ultimately determine the patency of the composite vascular graft. Preliminary work conducted by other members in the Chaikof lab has explored the use of acellular vascular substitutes in a porcine carotid artery model. Further optimization to improve the patency rate of acellular and cellularized vascular substitutes will be dependent on a number of factors, including inflammatory responses, cell and tissue integration, mesenchymal stem cell differentiation, and shear-stress induced responses at the blood-material interface.

APPENDIX A

Table A.1. Coding sequences of oligonucleotide cassettes employed for the construction of crosslinkable protein triblocks

Elastic-like Block

Val	**Pro**	**Gly**	**Ala**	**Gly**	**Val**	**Pro**	**Gly**	**Ala**	**Gly**	**Val**	**Pro**	**Gly**	**Glu**	**Gly**	**Val**	**Pro**	**Gly**
GTT	CCA	GGT	CGA	GGC	GTA	CCG	GGT	GCT	GGC	GTT	CCG	GGT	GAA	GGT	GTT	CCA	GGC
Ala	**Gly**	**Val**	**Pro**	**Gly**	**Ala**	**Gly**											
GCA	GGT	GTA	CCG	GGT	GCG	GGT											

Plastic-like Block

Ile	**Pro**	**Ala**	**Val**	**Gly**	**Ile**	**Pro**	**Ala**	**Val**	**Gly**	**Ile**	**Pro**	**Ala**	**Val**	**Gly**	**Ile**	**Pro**	**Ala**
ATT	CCG	GCT	GTT	GGT	ATC	CCA	GCT	GTT	GGT	ATC	CCA	GCT	GTT	GGC	ATT	CCG	GCT
Val	**Gly**	**Ile**	**Pro**	**Ala**	**Val**	**Gly**											
GTA	GGT	ATC	CCG	GCA	GTG	GGC											

Lysine Insert

Ile	**Pro**	**Ala**	**Val**	**Gly**	**Lys**	**Ala**	**Ala**	**Lys**	**Val**	**Pro**	**Gly**	**Ala**	**Gly**
ATT	CCA	GCT	GTT	GGT	AAG	GCG	GCC	AAG	GTT	CCA	GGT	GCA	GGC

Modified Lysine Adaptor

Val	**Pro**	**Ala**	**Val**	**Gly**	**Lys**	**Val**	**Pro**	**Ala**	**…..**	**Ile**	**Pro**	**Ala**	**Val**	**Gly**	**Lys**	**Ala**	**Ala**
GTT	CCA	GCT	GTT	GGT	AAG	GTT	CCA	GCT	…...	ATT	CCA	GCT	GTT	GGT	AAG	GCG	GCC
Lys	**Ala**	**Stop**															
AAG	GCG	TAA															

A.2 Synthesis of a recombinant elastin-mimetic triblock protein polymer LysB10

Genetic engineering, expression, purification, and characterization of the elastin-mimetic protein polymer, designated **LysB10,** has been described elsewhere. Briefly, the flanking 75 kDa endblocks of the protein polymer contained 33 repeats of the hydrophobic pentapeptide sequence $[IPAVG]_5$, and the central 58 kDa midblock consisted of 28 repeats of the elastic, hydrophilic sequence $[(VPGAG)_2VPGEG(VPGAG)_2]$. Additional sequences between blocks and at the C terminus include the residues [KAAK], which along with the N-terminal amine provide amino groups for chemical crosslinking.

The protein polymer sequence is contained in a single contiguous reading frame within the plasmid pET24-a, which was used to transform the *E. coli* expression strain BL21(DE3). Fermentation was performed at 37°C in Circle Grow (QBIOgene) medium supplemented with kanamycin (50 µg/mL) in a 100 L fermentor at the Bioexpression and Fermentation Facility, University of Georgia. Cultures were incubated under antibiotic selection for 24 hr at 37°C. Isolation of the **LysB10** consisted of breaking the cells with freeze/thaw cycles and sonication, a high speed centrifugation (20,000 RCF, 40 min, 4°C) with 0.5% poly(ethyleneimine) to precipitate nucleic acids, and a series of alternating warm/cold centrifugations. Each cold centrifugation (20,000 RCF, 40 min, 4°C) was followed by the addition of NaCl to 2M to precipitate the protein polymer as it incubated for 25 min at 25°C. This was followed by warm centrifugation (9500 RCF, 15 min, 25) and resuspension of the pellet in cold, sterile PBS on ice for 10 to 20 min. After 6 to 10 cycles, when minimal contamination was recovered in the final cold centrifugation, the material was subject to a warm centrifugation, resuspended in cold sterile PBS, dialyzed, and lyophilized. Lyophilized protein was resuspended in sterile molecular grade water at 1 mg/mL and endotoxin levels were assessed according to manufacturer instructions using the Limulus Amoebocyte Lysate (LAL) assay (Cambrex).

APPENDIX B

Protocol for solid phase peptide synthesis

Synthesis scale: 0.4 mmol.

Resin Used: Fmoc derivatized Rink amide resin that generates C-terminal amide. Loading capacity: 0.45 mmol/g. Amount of resin used 1 g.

1. Resin swelling: Weigh out 1 g of the resin; wash the resin with 20 mL dichloromethane for 5 min and drain. Repeat 3 times.

2. Wash with 20 ml N,N-dimethylformamide (DMF) for 5 min and drain. Repeat 3 times.
3. Fmoc Deprotection: Add 10 mL of 25% piperidine in DMF; Shake for 10 min and drain. Wash with 20 mL DMF and repeat once.
4. Wash the resin with 20 mL DMF for 1 min and drain. Repeat 4 times.
5. Prepare amino acid solution for coupling reaction.

   5 mL of 1.6 mmol amino acid (4.0 eq) in DMF
   5 mL of 1.6 mmol 2-(1H-benzotriazole-1-yl)-1,1,3,3,-tetramethyluronium hexafluorphosphate (HBTU) in DMF (4.0 eq)
   5 mL of 1.6 mmol HOBT in DMF (4.0 eq)
   5 mL of 2.4 mmol diisopropylethylamine (DIEA) in DMF (6.0 eq)
   Mix amino acid and HBTU solution followed by HOBT and DMF. Add DIEA, shake for 3 min to preactivate the carboxylic acid.
6. Add mixture from step 5 to the resin. Agitate the resin for 40 min and drain.
7. Wash the resin twice with 20 mL DMF and repeat steps 5 and 6 one more time to ensure complete reaction.
8. Repeat 3-7 for subsequent amino acids.
9. Finally to cleave the peptide from resin, wash the resin once with 20 mL DCM and agitate the resin with 25 mL of TFA cocktail (95 % TFA, 2 % TIPS, 3 % water)

Peptides used for synthesis: F-moc protected proline, serine, aspartic acid, glycine, arginine, glutamic acid(biotinyl-PEG), 3-maleimidopropionic acid.

Solid phase peptide synthesis consists of assembling amino acids from the C-terminal to the N-terminal. The a-carboxyl group is attached via an acid-labile linker to a solid support resin. The amino terminal end of the amino acid is protected by a base-labile Fmoc (9-fluorenylmethoxycarbonyl) protecting group while the side chains are protected by acid labile groups such at tertiary-butyl (tBu). After the first amino acid is loaded onto the resin, the Fmoc group is removed using piperidine (deprotection). A kaiser test is then performed to confirm that

all the Fmoc protecting groups are removed. The next Fmoc amino acid is then attached to the growing peptide by activation of its carboxyl group (coupling). A kaiser test is then performed to confirm that complete coupling has occurred on all the free amines on the resin. This cycle of deprotection/coupling continues until the peptide is completely synthesized. The peptide is then cleaved from the resin and side chain protection groups are removed using trifluoroacetic acid (TFA).

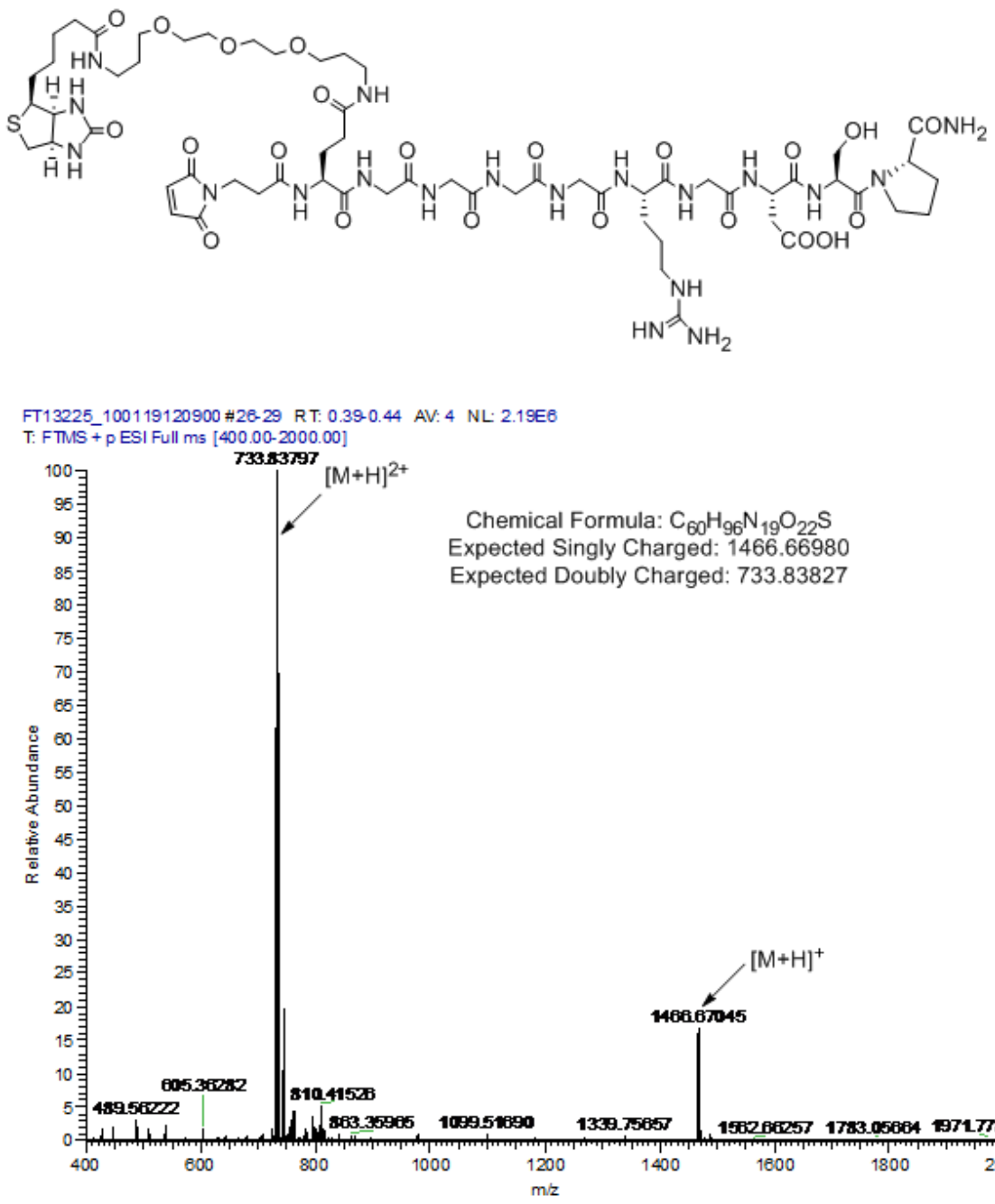

Figure B.1. Mass spectrometry analysis confirms successful synthesis of a pure peptide, with no other by-products present.

REFERENCES

1. Association, A.H. *Heart Disease and Stroke Statistics - 2008 Update*. May 2nd, 2010]; Available from: http://www.americanheart.org/presenter.jhtml?identifier=1928.

2. Abbott, W.M., et al., *Effect of compliance mismatch on vascular graft patency.* J Vasc Surg, 1987. **5**(2): p. 376-82.

3. Conte, M.S., *The ideal small arterial substitute: a search for the Holy Grail?* FASEB J, 1998. **12**(1): p. 43-5.

4. Greisler, H.P., *Interactions at the blood/material interface.* Ann Vasc Surg, 1990. **4**(1): p. 98-103.

5. Wittemore, A.D., Kent, K.C., Donaldson, M.C., Couch, N.P., Mannick, J.A., *What is the proper role of polytetrafluoroethylene grafts in infrainguinal reconstruction?* J Vasc Surg, 1989. **10**: p. 299-305.

6. Meinhart, J.G., et al., *Clinical autologous in vitro endothelialization of 153 infrainguinal ePTFE grafts.* Ann Thorac Surg, 2001. **71**(5 Suppl): p. S327-31.

7. Greisler, H.P., et al., *Biointeractive polymers and tissue engineered blood vessels.* Biomaterials, 1996. **17**(3): p. 329-36.

8. Clagett, G.P., et al., *Platelet reactivity in vivo in dogs with arterial prostheses seeded with endothelial cells.* Circulation, 1984. **69**(3): p. 632-9.

9. Gosselin, C., et al., *ePTFE coating with fibrin glue, FGF-1, and heparin: effect on retention of seeded endothelial cells.* J Surg Res, 1996. **60**(2): p. 327-32.

10. Herring, M.B., et al., *Seeding arterial prostheses with vascular endothelium. The nature of the lining.* Ann Surg, 1979. **190**(1): p. 84-90.

11. Hubbell, J.A., et al., *Endothelial cell-selective materials for tissue engineering in the vascular graft via a new receptor.* Biotechnology (N Y), 1991. **9**(6): p. 568-72.

12. Seifalian, A.M., et al., *Improving the clinical patency of prosthetic vascular and coronary bypass grafts: the role of seeding and tissue engineering.* Artif Organs, 2002. **26**(4): p. 307-20.

13. Doi, K. and T. Matsuda, *Enhanced vascularization in a microporous polyurethane graft impregnated with basic fibroblast growth factor and heparin.* J Biomed Mater Res, 1997. **34**(3): p. 361-70.

14. Sallach, R.E., et al., *Elastin-mimetic protein polymers capable of physical and chemical crosslinking.* Biomaterials, 2009. **30**(3): p. 409-22.

15. Jordan, S.W., et al., *The effect of a recombinant elastin-mimetic coating of an ePTFE prosthesis on acute thrombogenicity in a baboon arteriovenous shunt.* Biomaterials, 2007. **28**(6): p. 1191-7.

16. Berger, P.B., et al., *Frequency of early occlusion and stenosis in a left internal mammary artery to left anterior descending artery bypass graft after surgery through a median sternotomy on conventional bypass: benchmark for minimally invasive direct coronary artery bypass.* Circulation, 1999. **100**(23): p. 2353-8.

17. McKee, J.A., et al., *Human arteries engineered in vitro.* EMBO Rep, 2003. **4**(6): p. 633-8.

18. Verma, S., et al., *Should radial arteries be used routinely for coronary artery bypass grafting?* Circulation, 2004. **110**(5): p. e40-6.

19. Kannan, R.Y., et al., *Current status of prosthetic bypass grafts: a review.* J Biomed Mater Res B Appl Biomater, 2005. **74**(1): p. 570-81.

20. Humphrey, J.D., *Mechanics of the arterial wall: review and directions.* Crit Rev Biomed Eng, 1995. **23**(1-2): p. 1-162.

21. Weinberg, C.B. and E. Bell, *A blood vessel model constructed from collagen and cultured vascular cells.* Science, 1986. **231**(4736): p. 397-400.

22. Bhattacharya, V., et al., *Enhanced endothelialization and microvessel formation in polyester grafts seeded with CD34(+) bone marrow cells.* Blood, 2000. **95**(2): p. 581-5.

23. Chen, L., et al., *[Dual cell seeding to improve cell retention on polytetrafluoroethylene grafts].* Zhonghua Wai Ke Za Zhi, 2003. **41**(2): p. 143-5.

24. Fields, C., et al., *Evaluation of electrostatically endothelial cell seeded expanded polytetrafluoroethylene grafts in a canine femoral artery model.* J Biomater Appl, 2002. **17**(2): p. 135-52.

25. Griese, D.P., et al., *Isolation and transplantation of autologous circulating endothelial cells into denuded vessels and prosthetic grafts: implications for cell-based vascular therapy.* Circulation, 2003. **108**(21): p. 2710-5.

26. Kapfer, X., W. Meichelboeck, and F.M. Groegler, *Comparison of carbon-impregnated and standard ePTFE prostheses in extra-anatomical anterior tibial artery bypass: a prospective randomized multicenter study.* Eur J Vasc Endovasc Surg, 2006. **32**(2): p. 155-68.

27. Nishibe, T., et al., *Effects of fibronectin bonding on healing of high porosity expanded polytetrafluoroethylene grafts in pigs.* J Cardiovasc Surg (Torino), 2001. **42**(5): p. 667-73.

28. Randone, B., et al., *Dual role of VEGF in pretreated experimental ePTFE arterial grafts.* J Surg Res, 2005. **127**(2): p. 70-9.

29. Krijgsman, B., et al., *An assessment of covalent grafting of RGD peptides to the surface of a compliant poly(carbonate-urea)urethane vascular conduit versus conventional biological coatings: its role in enhancing cellular retention.* Tissue Eng, 2002. **8**(4): p. 673-80.

30. Walluscheck, K.P., et al., *Improved endothelial cell attachment on ePTFE vascular grafts pretreated with synthetic RGD-containing peptides.* Eur J Vasc Endovasc Surg, 1996. **12**(3): p. 321-30.

31. Greisler, H.P., et al., *Biomaterial pretreatment with ECGF to augment endothelial cell proliferation.* J Vasc Surg, 1987. **5**(2): p. 393-9.

32. Gray, J.L., et al., *FGF-1 affixation stimulates ePTFE endothelialization without intimal hyperplasia.* J Surg Res, 1994. **57**(5): p. 596-612.

33. Greisler, H.P., Wise, D., Trantolo, D., Altobelli, D., et al., *Regulation of vascular graft healing by induction of tissue incorporation.*, in *Human biomaterials applications*, D. Wise, Editor. 1996, Humana Press: Totowa, NJ. p. 227.

34. Greisler, H.P., et al., *Enhanced endothelialization of expanded polytetrafluoroethylene grafts by fibroblast growth factor type 1 pretreatment.* Surgery, 1992. **112**(2): p. 244-54; discussion 254-5.

35. Zilla, P., M. Deutsch, and J. Meinhart, *Endothelial cell transplantation.* Semin Vasc Surg, 1999. **12**(1): p. 52-63.

36. Hedeman Joosten, P.P., et al., *Thrombogenesis of different cell types seeded on vascular grafts and studied under blood-flow conditions.* J Vasc Surg, 1998. **28**(6): p. 1094-103.

37. Pearson, J.D., *Endothelial cell function and thrombosis.* Baillieres Best Pract Res Clin Haematol, 1999. **12**(3): p. 329-41.

38. Rotmans, J.I., et al., *In vivo cell seeding with anti-CD34 antibodies successfully accelerates endothelialization but stimulates intimal hyperplasia in porcine arteriovenous expanded polytetrafluoroethylene grafts.* Circulation, 2005. **112**(1): p. 12-8.

39. Reynolds, M.M., et al., *Nitric oxide releasing polyurethanes with covalently linked diazeniumdiolated secondary amines.* Biomacromolecules, 2006. **7**(3): p. 987-94.

40. Taite, L.J., et al., *Nitric oxide-releasing polyurethane-PEG copolymer containing the YIGSR peptide promotes endothelialization with decreased platelet adhesion.* J Biomed Mater Res B Appl Biomater, 2008. **84**(1): p. 108-16.

41. Hashi, C.K., et al., *Antithrombogenic property of bone marrow mesenchymal stem cells in nanofibrous vascular grafts.* Proc Natl Acad Sci U S A, 2007. **104**(29): p. 11915-20.

42. Hoerstrup, S.P., et al., *Functional growth in tissue-engineered living, vascular grafts: follow-up at 100 weeks in a large animal model.* Circulation, 2006. **114**(1 Suppl): p. I159-66.

43. Iwai, S., et al., *Biodegradable polymer with collagen microsponge serves as a new bioengineered cardiovascular prosthesis.* J Thorac Cardiovasc Surg, 2004. **128**(3): p. 472-9.

44. Izhar, U., et al., *Novel synthetic selectively degradable vascular prostheses: a preliminary implantation study.* J Surg Res, 2001. **95**(2): p. 152-60.

45. Kim, B.S. and D.J. Mooney, *Engineering smooth muscle tissue with a predefined structure.* J Biomed Mater Res, 1998. **41**(2): p. 322-32.

46. Mooney, D.J., et al., *Stabilized polyglycolic acid fibre-based tubes for tissue engineering.* Biomaterials, 1996. **17**(2): p. 115-24.

47. Pektok, E., et al., *Degradation and healing characteristics of small-diameter poly(epsilon-caprolactone) vascular grafts in the rat systemic arterial circulation.* Circulation, 2008. **118**(24): p. 2563-70.

48. Wake, M.C., P.K. Gupta, and A.G. Mikos, *Fabrication of pliable biodegradable polymer foams to engineer soft tissues.* Cell Transplant, 1996. **5**(4): p. 465-73.

49. Greisler, H.P., et al., *Dacron inhibition of arterial regenerative activities.* J Vasc Surg, 1986. **3**(5): p. 747-56.

50. Yu, T.J. and C.C. Chu, *Bicomponent vascular grafts consisting of synthetic absorbable fibers. I. In vitro study.* J Biomed Mater Res, 1993. **27**(10): p. 1329-39.

51. Yu, T.J., D.M. Ho, and C.C. Chu, *Bicomponent vascular grafts consisting of synthetic absorbable fibers: Part II: In vivo healing response.* J Invest Surg, 1994. **7**(3): p. 195-211.

52. Mooney, D.J., et al., *Design and fabrication of biodegradable polymer devices to engineer tubular tissues.* Cell Transplant, 1994. **3**(2): p. 203-10.

53. Fidkowski, C., et al., *Endothelialized microvasculature based on a biodegradable elastomer.* Tissue Eng, 2005. **11**(1-2): p. 302-9.

54. Niklason, L.E., et al., *Functional arteries grown in vitro.* Science, 1999. **284**(5413): p. 489-93.

55. Shum-Tim, D., et al., *Tissue engineering of autologous aorta using a new biodegradable polymer.* Ann Thorac Surg, 1999. **68**(6): p. 2298-304; discussion 2305.

56. Fu, P., et al., *Effects of basic fibroblast growth factor and transforming growth factor-beta on maturation of human pediatric aortic cell culture for tissue engineering of cardiovascular structures.* ASAIO J, 2004. **50**(1): p. 9-14.

57. Shinoka, T., et al., *Creation of viable pulmonary artery autografts through tissue engineering.* J Thorac Cardiovasc Surg, 1998. **115**(3): p. 536-45; discussion 545-6.

58. Watanabe, M., et al., *Tissue-engineered vascular autograft: inferior vena cava replacement in a dog model.* Tissue Eng, 2001. **7**(4): p. 429-39.

59. Shin'oka, T., Y. Imai, and Y. Ikada, *Transplantation of a tissue-engineered pulmonary artery.* N Engl J Med, 2001. **344**(7): p. 532-3.

60. Shin'oka, T., et al., *Midterm clinical result of tissue-engineered vascular autografts seeded with autologous bone marrow cells.* J Thorac Cardiovasc Surg, 2005. **129**(6): p. 1330-8.

61. Matsumura, G., et al., *Evaluation of tissue-engineered vascular autografts.* Tissue Eng, 2006. **12**(11): p. 3075-83.

62. Ennett, A.B., D. Kaigler, and D.J. Mooney, *Temporally regulated delivery of VEGF in vitro and in vivo.* J Biomed Mater Res A, 2006. **79**(1): p. 176-84.

63. Guan, J., J.J. Stankus, and W.R. Wagner, *Biodegradable elastomeric scaffolds with basic fibroblast growth factor release.* J Control Release, 2007. **120**(1-2): p. 70-8.

64. Alberts, B., Bray, D., Lewis, J., Raff, M., Roberts, K., Watson, J., *Molecular Biology of the Cell*. 3rd ed, ed. G.S. Anderson M. 1994, New York: Garland Publishing.

65. Buttafoco, L., et al., *Electrospinning of collagen and elastin for tissue engineering applications.* Biomaterials, 2006. **27**(5): p. 724-34.

66. Ottani, V., M. Raspanti, and A. Ruggeri, *Collagen structure and functional implications.* Micron, 2001. **32**(3): p. 251-60.

67. Nicolas, F.L. and C.H. Gagnieu, *Denatured thiolated collagen. II. Cross-linking by oxidation.* Biomaterials, 1997. **18**(11): p. 815-21.

68. Habermehl, J., et al., *Preparation of ready-to-use, stockable and reconstituted collagen.* Macromol Biosci, 2005. **5**(9): p. 821-8.

69. Charulatha, V. and A. Rajaram, *Influence of different crosslinking treatments on the physical properties of collagen membranes.* Biomaterials, 2003. **24**(5): p. 759-67.

70. Brinkman, W.T., et al., *Photo-cross-linking of type I collagen gels in the presence of smooth muscle cells: mechanical properties, cell viability, and function.* Biomacromolecules, 2003. **4**(4): p. 890-5.

71. Elbjeirami, W.M., et al., *Enhancing mechanical properties of tissue-engineered constructs via lysyl oxidase crosslinking activity.* J Biomed Mater Res A, 2003. **66**(3): p. 513-21.

72. Orban, J.M., et al., *Crosslinking of collagen gels by transglutaminase.* J Biomed Mater Res A, 2004. **68**(4): p. 756-62.

73. Hirai, J. and T. Matsuda, *Self-organized, tubular hybrid vascular tissue composed of vascular cells and collagen for low-pressure-loaded venous system.* Cell Transplant, 1995. **4**(6): p. 597-608.

74. Nerem, R.M. and A.E. Ensley, *The tissue engineering of blood vessels and the heart.* Am J Transplant, 2004. **4 Suppl 6**: p. 36-42.

75. Nerem, R.M. and D. Seliktar, *Vascular tissue engineering.* Annu Rev Biomed Eng, 2001. **3**: p. 225-43.

76. Baguneid, M., et al., *Shear-stress preconditioning and tissue-engineering-based paradigms for generating arterial substitutes.* Biotechnol Appl Biochem, 2004. **39**(Pt 2): p. 151-7.

77. L'Heureux, N., et al., *In vitro construction of a human blood vessel from cultured vascular cells: a morphologic study.* J Vasc Surg, 1993. **17**(3): p. 499-509.

78. Seliktar, D., et al., *Dynamic mechanical conditioning of collagen-gel blood vessel constructs induces remodeling in vitro.* Ann Biomed Eng, 2000. **28**(4): p. 351-62.

79. Cummings, C.L., et al., *Properties of engineered vascular constructs made from collagen, fibrin, and collagen-fibrin mixtures.* Biomaterials, 2004. **25**(17): p. 3699-706.

80. Ye, Q., et al., *Fibrin gel as a three dimensional matrix in cardiovascular tissue engineering.* Eur J Cardiothorac Surg, 2000. **17**(5): p. 587-91.

81. Clark, R.A., *Fibrin glue for wound repair: facts and fancy.* Thromb Haemost, 2003. **90**(6): p. 1003-6.

82. Jockenhoevel, S., et al., *Fibrin gel -- advantages of a new scaffold in cardiovascular tissue engineering.* Eur J Cardiothorac Surg, 2001. **19**(4): p. 424-30.

83. Long, J.L. and R.T. Tranquillo, *Elastic fiber production in cardiovascular tissue-equivalents.* Matrix Biol, 2003. **22**(4): p. 339-50.

84. Swartz, D.D., J.A. Russell, and S.T. Andreadis, *Engineering of fibrin-based functional and implantable small-diameter blood vessels.* Am J Physiol Heart Circ Physiol, 2005. **288**(3): p. H1451-60.

85. Grassl, E.D., T.R. Oegema, and R.T. Tranquillo, *A fibrin-based arterial media equivalent.* J Biomed Mater Res A, 2003. **66**(3): p. 550-61.

86. Lillie, M.A. and J.M. Gosline, *The viscoelastic basis for the tensile strength of elastin.* Int J Biol Macromol, 2002. **30**(2): p. 119-27.

87. Patel, A., et al., *Elastin biosynthesis: The missing link in tissue-engineered blood vessels.* Cardiovasc Res, 2006. **71**(1): p. 40-9.

88. Silver, F.H., I. Horvath, and D.J. Foran, *Viscoelasticity of the vessel wall: the role of collagen and elastic fibers.* Crit Rev Biomed Eng, 2001. **29**(3): p. 279-301.

89. Silver, F.H., P.B. Snowhill, and D.J. Foran, *Mechanical behavior of vessel wall: a comparative study of aorta, vena cava, and carotid artery.* Ann Biomed Eng, 2003. **31**(7): p. 793-803.

90. Isenberg, B.C. and R.T. Tranquillo, *Long-term cyclic distention enhances the mechanical properties of collagen-based media-equivalents.* Ann Biomed Eng, 2003. **31**(8): p. 937-49.

91. Ramamurthi, A. and I. Vesely, *Evaluation of the matrix-synthesis potential of crosslinked hyaluronan gels for tissue engineering of aortic heart valves.* Biomaterials, 2005. **26**(9): p. 999-1010.

92. Stock, U.A., et al., *Dynamics of extracellular matrix production and turnover in tissue engineered cardiovascular structures.* J Cell Biochem, 2001. **81**(2): p. 220-8.

93. Daamen, W.F., et al., *Comparison of five procedures for the purification of insoluble elastin.* Biomaterials, 2001. **22**(14): p. 1997-2005.

94. Buijtenhuijs, P., et al., *Tissue engineering of blood vessels: characterization of smooth-muscle cells for culturing on collagen-and-elastin-based scaffolds.* Biotechnol Appl Biochem, 2004. **39**(Pt 2): p. 141-9.

95. Cappello, J., et al., *Genetic engineering of structural protein polymers.* Biotechnol Prog, 1990. **6**(3): p. 198-202.

96. McGrath, K.P., et al., *Chemical and biosynthetic approaches to the production of novel polypeptide materials.* Biotechnol Prog, 1990. **6**(3): p. 188-92.

97. Meyer, D.E. and A. Chilkoti, *Genetically encoded synthesis of protein-based polymers with precisely specified molecular weight and sequence by recursive directional ligation: examples from the elastin-like polypeptide system.* Biomacromolecules, 2002. **3**(2): p. 357-67.

98. Nagapudi, K., et al., *Viscoelastic and mechanical behavior of recombinant protein elastomers.* Biomaterials, 2005. **26**(23): p. 4695-706.

99. Chang, D.K., Urry, D.K., *Molecular dynamics calculations on relaxed and extended states of the polypentapeptide of elastin.* Chem Phys Letters 1988. **147**(4): p. 395-400.

100. Petka, W.A., et al., *Reversible hydrogels from self-assembling artificial proteins.* Science, 1998. **281**(5375): p. 389-92.

101. Urry, D.W., *Physical chemistry of biological free energy transduction as demonstrated by elastin protein-based polymers.* J Phys Chem B, 1997. **101**: p. 11007-11028.

102. Urry, D.W., *Five axioms for the functional design of peptide-based polymers as molecular machines and materials: principles for macromolecular assembly.* Biopolymers, 1998. **47**: p. 167-178.

103. Nagarsekar, A., et al., *Genetic engineering of stimuli-sensitive silkelastin-like protein block copolymers.* Biomacromolecules, 2003. **4**(3): p. 602-7.

104. Kwon, I.K., S. Kidoaki, and T. Matsuda, *Electrospun nano- to microfiber fabrics made of biodegradable copolyesters: structural characteristics, mechanical properties and cell adhesion potential.* Biomaterials, 2005. **26**(18): p. 3929-39.

105. Li, M., et al., *Electrospun protein fibers as matrices for tissue engineering.* Biomaterials, 2005. **26**(30): p. 5999-6008.

106. van Hest, J.C. and D.A. Tirrell, *Protein-based materials, toward a new level of structural control.* Chem Commun (Camb), 2001(19): p. 1897-904.

107. Wright, E.R., McMillan, R.A., Cooper, A., et al, *Thermoplastic elastomer hydrogels via self-assembly of an elastin-mimetic triblock polypeptide.* Advanced functional materials, 2002. **12**(2): p. 1-6.

108. Wright, E.R. and V.P. Conticello, *Self-assembly of block copolymers derived from elastin-mimetic polypeptide sequences.* Adv Drug Deliv Rev, 2002. **54**(8): p. 1057-73.

109. Barnes, C.P., et al., *Nanofiber technology: designing the next generation of tissue engineering scaffolds.* Adv Drug Deliv Rev, 2007. **59**(14): p. 1413-33.

110. Pham, Q.P., U. Sharma, and A.G. Mikos, *Electrospinning of polymeric nanofibers for tissue engineering applications: a review.* Tissue Eng, 2006. **12**(5): p. 1197-211.

111. Stankus, J.J., et al., *Fabrication of cell microintegrated blood vessel constructs through electrohydrodynamic atomization.* Biomaterials, 2007. **28**(17): p. 2738-46.

112. de Mel, A., et al., *Development of cardiovascular bypass grafts: endothelialization and applications of nanotechnology.* Expert Rev Cardiovasc Ther, 2008. **6**(9): p. 1259-77.

113. Li, D. and Y.N. Xia, *Electrospinning of nanofibers: Reinventing the wheel?* Advanced Materials, 2004. **16**(14): p. 1151-1170.

114. He, W., et al., *Fabrication and endothelialization of collagen-blended biodegradable polymer nanofibers: potential vascular graft for blood vessel tissue engineering.* Tissue Eng, 2005. **11**(9-10): p. 1574-88.

115. Kannan, R.Y., et al., *The antithrombogenic potential of a polyhedral oligomeric silsesquioxane (POSS) nanocomposite.* Biomacromolecules, 2006. **7**(1): p. 215-23.

116. Kannan, R.Y., et al., *The endothelialization of polyhedral oligomeric silsesquioxane nanocomposites: an in vitro study.* Cell Biochem Biophys, 2006. **45**(2): p. 129-36.

117. Endo, M., et al., *Thrombogenicity and blood coagulation of a microcatheter prepared from carbon nanotube-nylon-based composite.* Nano Lett, 2005. **5**(1): p. 101-5.

118. Meng, J., et al., *Improving the blood compatibility of polyurethane using carbon nanotubes as fillers and its implications to cardiovascular surgery.* J Biomed Mater Res A, 2005. **74**(2): p. 208-14.

119. Hurt, R.H., M. Monthioux, and A. Kane, *Toxicology of carbon nanomaterials: Status, trends, and perspectives on the special issue.* Carbon, 2006. **44**(6): p. 1028-1033.

120. Kim, J.Y., et al., *Decreased macrophage density on carbon nanotube patterns on polycarbonate urethane.* J Biomed Mater Res A, 2009. **88**(2): p. 419-26.

121. Dahl, S.L., et al., *Decellularized native and engineered arterial scaffolds for transplantation.* Cell Transplant, 2003. **12**(6): p. 659-66.

122. Schmidt, C.E. and J.M. Baier, *Acellular vascular tissues: natural biomaterials for tissue repair and tissue engineering.* Biomaterials, 2000. **21**(22): p. 2215-31.

123. Tamura, N., et al., *A new acellular vascular prosthesis as a scaffold for host tissue regeneration.* Int J Artif Organs, 2003. **26**(9): p. 783-92.

124. Uchimura, E., et al., *Novel method of preparing acellular cardiovascular grafts by decellularization with poly(ethylene glycol).* J Biomed Mater Res A, 2003. **67**(3): p. 834-7.

125. Courtman, D.W., B.F. Errett, and G.J. Wilson, *The role of crosslinking in modification of the immune response elicited against xenogenic vascular acellular matrices.* J Biomed Mater Res, 2001. **55**(4): p. 576-86.

126. Khor, E., *Methods for the treatment of collagenous tissues for bioprostheses.* Biomaterials, 1997. **18**(2): p. 95-105.

127. Amiel, G.E., et al., *Engineering of blood vessels from acellular collagen matrices coated with human endothelial cells.* Tissue Eng, 2006. **12**(8): p. 2355-65.

128. Cho, S.W., et al., *Small-diameter blood vessels engineered with bone marrow-derived cells.* Ann Surg, 2005. **241**(3): p. 506-15.

129. Conklin, B.S., et al., *Development and evaluation of a novel decellularized vascular xenograft.* Med Eng Phys, 2002. **24**(3): p. 173-83.

130. Conklin, B.S., et al., *Basic fibroblast growth factor coating and endothelial cell seeding of a decellularized heparin-coated vascular graft.* Artif Organs, 2004. **28**(7): p. 668-75.

131. DiMuzio, P., et al., *Development of a tissue-engineered bypass graft seeded with stem cells.* Vascular, 2006. **14**(6): p. 338-42.

132. Holdsworth, R.J., et al., *Glutaraldehyde-tanned bovine carotid artery graft for infrainguinal vascular reconstruction: 5-year follow-up.* Eur J Vasc Endovasc Surg, 1997. **14**(3): p. 208-11.

133. Kaushal, S., et al., *Functional small-diameter neovessels created using endothelial progenitor cells expanded ex vivo.* Nat Med, 2001. **7**(9): p. 1035-40.

134. McFetridge, P.S., et al., *Endothelial and smooth muscle cell seeding onto processed ex vivo arterial scaffolds using 3D vascular bioreactors.* ASAIO J, 2004. **50**(6): p. 591-600.

135. Shimizu, K., et al., *Effective cell-seeding technique using magnetite nanoparticles and magnetic force onto decellularized blood vessels for vascular tissue engineering.* J Biosci Bioeng, 2007. **103**(5): p. 472-8.

136. Voytik-Harbin, S.L., et al., *Identification of extractable growth factors from small intestinal submucosa.* J Cell Biochem, 1997. **67**(4): p. 478-91.

137. Badylak, S.F., et al., *Small intestinal submucosa: a substrate for in vitro cell growth.* J Biomater Sci Polym Ed, 1998. **9**(8): p. 863-78.

138. Huynh, T., et al., *Remodeling of an acellular collagen graft into a physiologically responsive neovessel.* Nat Biotechnol, 1999. **17**(11): p. 1083-6.

139. Marshall, S.E., et al., *An alternative to synthetic aortic grafts using jejunum.* J Invest Surg, 2000. **13**(6): p. 333-41.

140. Robotin-Johnson, M.C., et al., *An experimental model of small intestinal submucosa as a growing vascular graft.* J Thorac Cardiovasc Surg, 1998. **116**(5): p. 805-11.

141. Campbell, G.R. and G.B. Ryan, *Origin of myofibroblasts in the avascular capsule around free-floating intraperitoneal blood clots.* Pathology, 1983. **15**(3): p. 253-64.

142. Campbell, J.H., et al., *Haemopoietic origin of myofibroblasts formed in the peritoneal cavity in response to a foreign body.* J Vasc Res, 2000. **37**(5): p. 364-71.

143. Campbell, J.H., J.L. Efendy, and G.R. Campbell, *Novel vascular graft grown within recipient's own peritoneal cavity.* Circ Res, 1999. **85**(12): p. 1173-8.

144. Chue, W.L., et al., *Dog peritoneal and pleural cavities as bioreactors to grow autologous vascular grafts.* J Vasc Surg, 2004. **39**(4): p. 859-67.

145. Efendy, J.L., G.R. Campbell, and J.H. Campbell, *The effect of environmental cues on the differentiation of myofibroblasts in peritoneal granulation tissue.* J Pathol, 2000. **192**(2): p. 257-62.

146. Chen, C.H., et al., *Novel living cell sheet harvest system composed of thermoreversible methylcellulose hydrogels.* Biomacromolecules, 2006. **7**(3): p. 736-43.

147. Sekine, H., et al., *Pulsatile myocardial tubes fabricated with cell sheet engineering.* Circulation, 2006. **114**(1 Suppl): p. I87-93.

148. Yang, J., et al., *Reconstruction of functional tissues with cell sheet engineering.* Biomaterials, 2007. **28**(34): p. 5033-43.

149. L'Heureux N, D.N., Konig G, Victor B, Keire P, Wight TN, Chronos NA, Kyles AE, Gregory CR, Hoyt G, Robbins RC, McAllister TN, *Human tissue-engineered blood vessels for adult arterial revascularization.* Nature Medicine, 2006. **12**(3): p. 361-365.

150. Chan, G. and D.J. Mooney, *New materials for tissue engineering: towards greater control over the biological response.* Trends Biotechnol, 2008. **26**(7): p. 382-92.

151. Rizzi, S.C., et al., *Recombinant protein-co-PEG networks as cell-adhesive and proteolytically degradable hydrogel matrixes. Part II: biofunctional characteristics.* Biomacromolecules, 2006. **7**(11): p. 3019-29.

152. Yurchenco PD, B.D., Mecham RP, *Extracellular matrix assembly and structure*: Academic Press Inc.

153. Kleinman, H.K., D. Philp, and M.P. Hoffman, *Role of the extracellular matrix in morphogenesis.* Current Opinion in Biotechnology, 2003. **14**(5): p. 526-532.

154. Geiger, B., et al., *Transmembrane crosstalk between the extracellular matrix and the cytoskeleton.* Nat Rev Mol Cell Biol, 2001. **2**(11): p. 793-805.

155. Pankov, R. and K.M. Yamada, *Fibronectin at a glance.* J Cell Sci, 2002. **115**(20): p. 3861-3863.

156. Bourdoulous, S., et al., *Fibronectin matrix regulates activation of RHO and CDC42 GTPases and cell cycle progression.* J Cell Biol, 1998. **143**(1): p. 267-76.

157. Sakai, T., M. Larsen, and K.M. Yamada, *Fibronectin requirement in branching morphogenesis.* Nature, 2003. **423**(6942): p. 876-81.

158. Sechler, J.L. and J.E. Schwarzbauer, *Control of cell cycle progression by fibronectin matrix architecture.* J Biol Chem, 1998. **273**(40): p. 25533-6.

159. Yamada, K.M., *Cell surface interactions with extracellular materials.* Annu Rev Biochem, 1983. **52**: p. 761-99.

160. Shimada, T., et al., *Improved Healing of Small-Caliber, Long-Fibril Expanded Polytetrafluoroethylene Vascular Grafts by Covalent Bonding of Fibronectin.* Surgery Today, 2004. **34**(12): p. 1025-1030.

161. Nishibe, T., et al., *Enhanced Graft Healing of High-Porosity Expanded Polytetrafluoroethylene Grafts by Covalent Bonding of Fibronectin.* Surgery Today, 2000. **30**(5): p. 426-431.

162. Pfaff, M., *Recognition sites of RGD-dependent integrins*, in *Integrin-Ligand Interaction*, J.A.K. Eble, Klaus, Editor. 1997, R.G. Landes Company. p. 101-121.

163. Pierschbacher, M.D. and E. Ruoslahti, *Influence of stereochemistry of the sequence Arg-Gly-Asp-Xaa on binding specificity in cell adhesion.* Journal of Biological Chemistry, 1987. **262**(36): p. 17294-17298.

164. Cutler, S.M. and A.J. García, *Engineering cell adhesive surfaces that direct integrin [alpha]5[beta]1 binding using a recombinant fragment of fibronectin.* Biomaterials, 2003. **24**(10): p. 1759-1770.

165. Haubner, R., et al., *Structural and Functional Aspects of RGD-Containing Cyclic Pentapeptides as Highly Potent and Selective Integrin αVβ3 Antagonists.* Journal of the American Chemical Society, 1996. **118**(32): p. 7461-7472.

166. Xiao, Y. and G.A. Truskey, *Effect of receptor-ligand affinity on the strength of endothelial cell adhesion.* 1996. **71**(5): p. 2869-2884.

167. Blindt, R., et al., *A Novel Drug-Eluting Stent Coated With an Integrin-Binding Cyclic Arg-Gly-Asp Peptide Inhibits Neointimal Hyperplasia by Recruiting Endothelial Progenitor Cells.* J Am Coll Cardiol, 2006. **47**(9): p. 1786-1795.

168. Drumheller, P.D. and J.A. Hubbell, *Polymer Networks with Grafted Cell Adhesion Peptides for Highly Biospecific Cell Adhesive Substrates.* Analytical Biochemistry, 1994. **222**(2): p. 380-388.

169. Humphries, M.J., et al., *Identification of an alternatively spliced site in human plasma fibronectin that mediates cell type-specific adhesion.* The Journal of Cell Biology, 1986. **103**(6): p. 2637-2647.

170. Plouffe, B.D., et al., *Peptide-Mediated Selective Adhesion of Smooth Muscle and Endothelial Cells in Microfluidic Shear Flow.* Langmuir, 2007. **23**(9): p. 5050-5055.

171. Colombi, M., et al., *Matrix Assembly Induction and Cell Migration and Invasion Inhibition by a 13-Amino Acid Fibronectin Peptide.* Journal of Biological Chemistry, 2003. **278**(16): p. 14346-14355.

172. Capadona, J.R., et al., *Surface-Nucleated Assembly of Fibrillar Extracellular Matrices.* Advanced Materials, 2005. **17**(21): p. 2604-2608.

173. Durbeej, M., *Laminins.* Cell and Tissue Research, 2010. **339**(1): p. 259-268.

174. Hirano, Y., et al., *Cell-attachment activities of surface immobilized oligopeptides RGD, RGDS, RGDV, RGDT, and YIGSR toward five cell lines.* Journal of Biomaterials Science, Polymer Edition, 1993. **4**: p. 235-243.

175. Olbrich, K.C., et al., *Surfaces modified with covalently-immobilized adhesive peptides affect fibroblast population motility.* Biomaterials, 1996. **17**(8): p. 759-764.

176. Massia SP, H.J., *Covalent surface immobilization of Arg-Gly-Asp- and Tyr-Ile-Gly-Ser-Arg-containing peptides to obtain well-defined cell-adhesive substrates.* Anal Biochem. , 1990. **187**(2): p. 292-301.

177. Massia, S.P., S.S. Rao, and J.A. Hubbell, *Covalently immobilized laminin peptide Tyr-Ile-Gly-Ser-Arg (YIGSR) supports cell spreading and co-localization of the 67-kilodalton laminin receptor with alpha-actinin and vinculin.* Journal of Biological Chemistry, 1993. **268**(11): p. 8053-8059.

178. Jun, H.-W. and J.L. West, *Modification of polyurethaneurea with PEG and YIGSR peptide to enhance endothelialization without platelet adhesion.* Journal of Biomedical Materials Research, 2005. **72B**(1): p. 131-139.

179. Jun, H.-W. and J.L. West, *Endothelialization of Microporous YIGSR/PEG-Modified Polyurethaneurea.* Tissue Engineering, 2005. **11**(7-8): p. 1133-1140.

180. Tashiro, K., et al., *A synthetic peptide containing the IKVAV sequence from the A chain of laminin mediates cell attachment, migration, and neurite outgrowth.* Journal of Biological Chemistry, 1989. **264**(27): p. 16174-16182.

181. Schense, J.C. and J.A. Hubbell, *Cross-Linking Exogenous Bifunctional Peptides into Fibrin Gels with Factor XIIIa.* Bioconjugate Chemistry, 1998. **10**(1): p. 75-81.

182. Schense, J.C., et al., *Enzymatic incorporation of bioactive peptides into fibrin matrices enhances neurite extension.* Nat Biotech, 2000. **18**(4): p. 415-419.

183. Reyes, C.D. and A.J. García, *alpha_{<FONT SIZE='-1'>2</FONT>}beta_{<FONT SIZE='-1'>1</FONT>} integrin-specific*

collagen-mimetic surfaces supporting osteoblastic differentiation. Journal of Biomedical Materials Research Part A, 2004. **69A**(4): p. 591-600.

184. Knight, C.G., et al., *The Collagen-binding A-domains of Integrins α1β1 and α2β1Recognize the Same Specific Amino Acid Sequence, GFOGER, in Native (Triple-helical) Collagens.* Journal of Biological Chemistry, 2000. **275**(1): p. 35-40.

185. Hinek, A., *Biological roles of the non-integrin elastin/laminin receptor.* Biol Chem, 1996. **377**: p. 471-480.

186. Babic, A.M., et al., *CYR61, a product of a growth factor-inducible immediate early gene, promotes angiogenesis and tumor growth.* Proceedings of the National Academy of Sciences of the United States of America, 1998. **95**(11): p. 6355-6360.

187. O'Brien, T. and L. Lau, *Expression of the growth factor-inducible immediate early gene cyr61 correlates with chondrogenesis during mouse embryonic development.* Cell Growth Differ, 1992. **3**(9): p. 645-654.

188. Chen, C.-C., F.-E. Mo, and L.F. Lau, *The Angiogenic Factor Cyr61 Activates a Genetic Program for Wound Healing in Human Skin Fibroblasts.* Journal of Biological Chemistry, 2001. **276**(50): p. 47329-47337.

189. Hadjiargyrou, M., W. Ahrens, and C.T. Rubin, *Temporal Expression of the Chondrogenic and Angiogenic Growth Factor CYR61 During Fracture Repair.* Journal of Bone and Mineral Research, 2000. **15**(6): p. 1014-1023.

190. Latinkic, B.V., et al., *Promoter Function of the Angiogenic Inducer Cyr61Gene in Transgenic Mice: Tissue Specificity, Inducibility During Wound Healing, and Role of the Serum Response Element.* Endocrinology, 2001. **142**(6): p. 2549-2557.

191. Leu, S.-J., S.C.-T. Lam, and L.F. Lau, *Pro-angiogenic Activities of CYR61 (CCN1) Mediated through Integrins αvβ3 and α6β1 in Human Umbilical Vein Endothelial Cells.* Journal of Biological Chemistry, 2002. **277**(48): p. 46248-46255.

192. Mo, F.-E., et al., *CYR61 (CCN1) Is Essential for Placental Development and Vascular Integrity.* Mol. Cell. Biol., 2002. **22**(24): p. 8709-8720.

193. Xie, D., et al., *Breast Cancer.* Journal of Biological Chemistry, 2001. **276**(17): p. 14187-14194.

194. Grote, K., et al., *The angiogenic factor CCN1 promotes adhesion and migration of circulating CD34+ progenitor cells: potential role in angiogenesis and endothelial regeneration.* Blood, 2007. **110**(3): p. 877-885.

195. Yang, G. and L. Lau, *Cyr61, product of a growth factor-inducible immediate early gene, is associated with the extracellular matrix and the cell surface.* Cell Growth Differ, 1991. **2**(7): p. 351-357.

196. Lau, L.F. and S.C.T. Lam, *The CCN Family of Angiogenic Regulators: The Integrin Connection.* Experimental Cell Research, 1999. **248**(1): p. 44-57.

197. Kireeva, M.L., S.C.-T. Lam, and L.F. Lau, *Adhesion of Human Umbilical Vein Endothelial Cells to the Immediate-Early Gene Product Cyr61 Is Mediated through Integrin αvβ3.* Journal of Biological Chemistry, 1998. **273**(5): p. 3090-3096.

198. Grzeszkiewicz, T.M., et al., *The Angiogenic Factor Cysteine-Rich 61 (CYR61, CCN1) Supports Vascular Smooth Muscle Cell Adhesion and Stimulates Chemotaxis through Integrin {alpha}6{beta}1 and Cell Surface Heparan Sulfate Proteoglycans.* Endocrinology, 2002. **143**(4): p. 1441-1450.

199. Schober, J.M., et al., *Identification of a Novel Integrin αMβ2 Binding Site in CCN1 (CYR61), a Matricellular Protein Expressed in Healing Wounds and Atherosclerotic Lesions.* Journal of Biological Chemistry, 2003. **278**(28): p. 25808-25815.

200. Todorovicç, V., et al., *The matrix protein CCN1 (CYR61) induces apoptosis in fibroblasts.* The Journal of Cell Biology, 2005. **171**(3): p. 559-568.

201. Leu, S.-J., et al., *Identification of a Novel Integrin α6β1 Binding Site in the Angiogenic Inducer CCN1 (CYR61).* Journal of Biological Chemistry, 2003. **278**(36): p. 33801-33808.

202. Leu, S.-J., et al., *Targeted Mutagenesis of the Angiogenic Protein CCN1 (CYR61).* Journal of Biological Chemistry, 2004. **279**(42): p. 44177-44187.

203. Chen, N., et al., *Identification of a Novel Integrin αvβ3 Binding Site in CCN1 (CYR61) Critical for Pro-angiogenic Activities in Vascular Endothelial Cells.* Journal of Biological Chemistry, 2004. **279**(42): p. 44166-44176.

204. Arnaout, M.A., S.L. Goodman, and J.-P. Xiong, *Coming to grips with integrin binding to ligands.* Current Opinion in Cell Biology, 2002. **14**(5): p. 641-652.

205. Xiong, J.-P., et al., *Crystal Structure of the Extracellular Segment of Integrin alpha Vbeta 3 in Complex with an Arg-Gly-Asp Ligand.* Science, 2002. **296**(5565): p. 151-155.

206. McLane, M.A., et al., *Importance of the structure of the RGD-containing loop in the disintegrins echistatin and eristostatin for recognition of [alpha]IIb[beta]3 and [alpha]v[beta]3 integrins.* FEBS Letters, 1996. **391**(1-2): p. 139-143.

207. Yamada, T. and A. Kidera, *Tailoring echistatin to possess higher affinity for integrin [alpha]IIb[beta]3.* FEBS Letters, 1996. **387**(1): p. 11-15.

208. Koivunen, E., D.A. Gay, and E. Ruoslahti, *Selection of peptides binding to the alpha 5 beta 1 integrin from phage display library.* Journal of Biological Chemistry, 1993. **268**(27): p. 20205-20210.

209. Akagawa, M. and K. Suyama, *Mechanism of formation of elastin crosslinks.* Connect Tissue Res, 2000. **41**(2): p. 131-41.

210. Rosenbloom, J., W.R. Abrams, and R. Mecham, *Extracellular matrix 4: the elastic fiber.* FASEB J, 1993. **7**(13): p. 1208-18.

211. Rucker, R.B. and M.A. Dubick, *Elastin metabolism and chemistry: potential roles in lung development and structure.* Environ Health Perspect, 1984. **55**: p. 179-91.

212. Roach, M.R. and A.C. Burton, *The reason for the shape of the distensibility curves of arteries.* Can J Biochem Physiol, 1957. **35**(8): p. 681-90.

213. Li, D.Y., et al., *Novel arterial pathology in mice and humans hemizygous for elastin.* J Clin Invest, 1998. **102**(10): p. 1783-7.

214. Wagenseil, J.E., et al., *Effects of elastin haploinsufficiency on the mechanical behavior of mouse arteries.* Am J Physiol Heart Circ Physiol, 2005. **289**(3): p. H1209-17.

215. Cappello, J., et al., *Genetic engineering of structural protein polymers.* Biotechnology Progress, 1990. **6**(3): p. 198-202.

216. Bellingham, C.M., et al., *Self-aggregation characteristics of recombinantly expressed human elastin polypeptides.* Biochim Biophys Acta, 2001. **1550**(1): p. 6-19.

217. Urry, D.W., et al., *Hydrophobicity Scale for Proteins Based on Inverse Temperature Transitions.* Biopolymers, 1992. **32**(9): p. 1243-1250.

218. Wright, E.R. and V.P. Conticello, *Self-assembly of block copolymers derived from elastin-mimetic polypeptide sequences.* Advanced Drug Delivery Reviews, 2002. **54**(8): p. 1057-1073.

219. Wright, E.R., et al., *Thermoplastic elastomer hydrogels via self-assembly of an elastin-mimetic triblock polypeptide.* Advanced Functional Materials, 2002. **12**(2): p. 149-154.

220. Nettles, D.L., et al., *In situ crosslinking elastin-like polypeptide gels for application to articular cartilage repair in a goat osteochondral defect model.* Tissue Eng Part A, 2008. **14**(7): p. 1133-40.

221. Woodhouse, K.A., et al., *Investigation of recombinant human elastin polypeptides as non-thrombogenic coatings.* Biomaterials, 2004. **25**(19): p. 4543-53.

222. Lee, J., C.W. Macosko, and D.W. Urry, *Mechanical properties of cross-linked synthetic elastomeric polypentapeptides.* Macromolecules, 2001. **34**(17): p. 5968-5974.

223. Kagan, H.M., L. Tseng, and D.E. Simpson, *Control of elastin metabolism by elastin ligands. Reciprocal effects on lysyl oxidase activity.* J Biol Chem, 1981. **256**(11): p. 5417-21.

224. Kagan, H.M., et al., *Repeat polypeptide models of elastin as substrates for lysyl oxidase.* J Biol Chem, 1980. **255**(8): p. 3656-9.

225. Trabbic-Carlson, K., L.A. Setton, and A. Chilkoti, *Swelling and mechanical behaviors of chemically cross-linked hydrogels of elastin-like polypeptides.* Biomacromolecules, 2003. **4**(3): p. 572-80.

226. Girotti, A., et al., *Design and bioproduction of a recombinant multi(bio)functional elastin-like protein polymer containing cell adhesion sequences for tissue engineering purposes.* Journal of Materials Science: Materials in Medicine, 2004. **15**(4): p. 479-484.

227. Martínez-Osorio, H., et al., *Genetically Engineered Elastin-Like Polymer as a Substratum to Culture Cells from the Ocular Surface.* Current Eye Research, 2009. **34**(1): p. 48 - 56.

228. Liu, J.C. and D.A. Tirrell, *Cell Response to RGD Density in Cross-Linked Artificial Extracellular Matrix Protein Films.* Biomacromolecules, 2008. **9**(11): p. 2984-2988.

229. Nagapudi, K., et al., *Photomediated Solid-State Cross-Linking of an Elastin−Mimetic Recombinant Protein Polymer.* Macromolecules, 2002. **35**(5): p. 1730-1737.

230. Kaufmann, D., et al., *Chemical conjugation of linear and cyclic RGD moieties to a recombinant elastin-mimetic polypeptide--a versatile approach towards bioactive protein hydrogels.* Macromol Biosci, 2008. **8**(6): p. 577-88.

231. Teeuwen RL, v.B.S., van Dulmen TH, Schoffelen S, Meeuwissen SA, Zuilhof H, de Wolf FA, van Hest JC., *"Clickable" elastins: elastin-like polypeptides functionalized with azide or alkyne groups.* Chem Commun (Camb). 2009. **27**: p. 4022-4024.

232. Hoban LD, P.M., Quance J, Hayward I, McKee A, Gowda DC, Urry DW, Williams T., *Use of polypentapeptides of elastin to prevent postoperative adhesions: efficacy in a contaminated peritoneal model.* J Surg Res., 1994. **56**(2): p. 179-183.

233. Massodi, I., et al., *Inhibition of ovarian cancer cell proliferation by a cell cycle inhibitory peptide fused to a thermally responsive polypeptide carrier.* International Journal of Cancer, 2010. **126**(2): p. 533-544.

234. Meyer, D.E., et al., *Targeting a Genetically Engineered Elastin-like Polypeptide to Solid Tumors by Local Hyperthermia.* Cancer Research, 2001. **61**(4): p. 1548-1554.

235. Heilshorn, S.C., et al., *Endothelial cell adhesion to the fibronectin CS5 domain in artificial extracellular matrix proteins.* Biomaterials, 2003. **24**(23): p. 4245-4252.

236. Heilshorn, S.C., J.C. Liu, and D.A. Tirrell, *Cell-binding domain context affects cell behavior on engineered proteins.* Biomacromolecules, 2005. **6**(1): p. 318-323.

237. Liu, J.C., S.C. Heilshorn, and D.A. Tirrell, *Comparative cell response to artificial extracellular matrix proteins containing the RGD and CS5 cell-binding domains.* Biomacromolecules, 2004. **5**(2): p. 497-504.

238. Panitch, A., et al., *Design and biosynthesis of elastin-like artificial extracellular matrix proteins containing periodically spaced fibronectin CS5 domains.* Macromolecules, 1999. **32**(5): p. 1701-1703.

239. Betre, H., et al., *Chondrocytic differentiation of human adipose-derived adult stem cells in elastin-like polypeptide.* Biomaterials, 2006. **27**(1): p. 91-99.

240. Straley, K.S. and S.C. Heilshorn, *Design and adsorption of modular engineered proteins to prepare customized, neuron-compatible coatings.* Frontiers in Neuroengineering, 2009. **2**.

241. Lim, D.W., et al., *In Situ Cross-Linking of Elastin-like Polypeptide Block Copolymers for Tissue Repair.* Biomacromolecules, 2007. **9**(1): p. 222-230.

242. Mohammed, J.S. and W.L. Murphy, *Bioinspired Design of Dynamic Materials.* Advanced Materials, 2009. **21**(23): p. 2361-2374.

243. Kobatake, E., et al., *Design and gene engineering synthesis of an extremely thermostable protein with biological activity.* Biomacromolecules, 2000. **1**(3): p. 382-6.

244. Richman, G.P., D.A. Tirrell, and A.R. Asthagiri, *Quantitatively distinct requirements for signaling-competent cell spreading on engineered versus natural adhesion ligands.* J Control Release, 2005. **101**(1-3): p. 3-12.

245. De Arcangelis, A. and E. Georges-Labouesse, *Integrin and ECM functions: roles in vertebrate development.* 2000. **16**(9): p. 389-395.

246. Lutolf, M.P. and J.A. Hubbell, *Synthetic biomaterials as instructive extracellular microenvironments for morphogenesis in tissue engineering.* Nat Biotech, 2005. **23**(1): p. 47-55.

247. Chang, D.K. and D.W. Urry, *Molecular-Dynamics Calculations on Relaxed and Extended States of the Polypentapeptide of Elastin.* Chemical Physics Letters, 1988. **147**(4): p. 395-400.

248. Urry, D.W., *Physical chemistry of biological free energy transduction as demonstrated by elastic protein-based polymers.* Journal of Physical Chemistry B, 1997. **101**(51): p. 11007-11028.

249. Li, C., A. Hill, and M. Imran, *In vitro and in vivo studies of ePTFE vascular grafts treated with P15 peptide.* J Biomater Sci Polym Ed, 2005. **16**(7): p. 875-91.

250. Meinhart, J.G., et al., *Enhanced endothelial cell retention on shear-stressed synthetic vascular grafts precoated with RGD-cross-linked fibrin.* Tissue Engineering, 2005. **11**(5-6): p. 887-895.

251. von der Mark, K., et al., *Nanoscale engineering of biomimetic surfaces: cues from the extracellular matrix.* Cell and Tissue Research, 2010. **339**(1): p. 131-153.

252. Brooks, P., R. Clark, and D. Cheresh, *Requirement of vascular integrin alpha v beta 3 for angiogenesis.* Science, 1994. **264**(5158): p. 569-571.

253. Aota, S., M. Nomizu, and K.M. Yamada, *The short amino acid sequence Pro-His-Ser-Arg-Asn in human fibronectin enhances cell-adhesive function.* Journal of Biological Chemistry, 1994. **269**(40): p. 24756-24761.

254. Bowditch, R.D., et al., *Identification of a novel integrin binding site in fibronectin. Differential utilization by beta 3 integrins.* Journal of Biological Chemistry, 1994. **269**(14): p. 10856-10863.

255. van der Flier, A. and A. Sonnenberg, *Function and interactions of integrins.* Cell and Tissue Research, 2001. **305**(3): p. 285-298.

256. Mohri, H., *Interaction of Fibronectin With Integrin Receptors: Evidence by Use of Synthetic Peptides.* Peptides, 1997. **18**(6): p. 899-907.

257. Naik, M.U. and U.P. Naik, *Junctional adhesion molecule-A-induced endothelial cell migration on vitronectin is integrin {alpha}v{beta}3 specific.* J Cell Sci, 2006. **119**(3): p. 490-499.

258. Underwood, P. and F. Bennett, *A comparison of the biological activities of the cell-adhesive proteins vitronectin and fibronectin.* J Cell Sci, 1989. **93**(4): p. 641-649.

259. Massia, S.P. and J.A. Hubbell, *An RGD spacing of 440 nm is sufficient for integrin alpha V beta 3-mediated fibroblast spreading and 140 nm for focal contact and stress fiber formation.* The Journal of Cell Biology, 1991. **114**(5): p. 1089-1100.

260. Patel, S., et al., *Regulation of endothelial cell function by GRGDSP peptide grafted on interpenetrating polymers.* Journal of Biomedical Materials Research Part A, 2007. **83A**(2): p. 423-433.

261. Kiosses, W.B., et al., *Rac recruits high-affinity integrin [alpha]v[beta]3 to lamellipodia in endothelial cell migration.* Nat Cell Biol, 2001. **3**(3): p. 316-320.

262. Maheshwari, G., et al., *Cell adhesion and motility depend on nanoscale RGD clustering.* J Cell Sci, 2000. **113**(10): p. 1677-1686.

263. Byzova, T.V., et al., *Activation of Integrin alphaVbeta3 Regulates Cell Adhesion and Migration to Bone Sialoprotein.* Experimental Cell Research, 2000. **254**: p. 299-308.

264. Gao, B., T.M. Saba, and M.-F. Tsan, *Role of alpha vbeta 3-integrin in TNF-alpha - induced endothelial cell migration.* Am J Physiol Cell Physiol, 2002. **283**(4): p. C1196-1205.

265. Giancotti, F.G. and E. Ruoslahti, *Integrin Signaling.* Science, 1999. **285**(5430): p. 1028-1033.

266. Sastry, S.K. and K. Burridge, *Focal Adhesions: A Nexus for Intracellular Signaling and Cytoskeletal Dynamics.* Experimental Cell Research, 2000. **261**(1): p. 25-36.

267. Yamada, K.M. and B. Geiger, *Molecular interactions in cell adhesion complexes.* Current Opinion in Cell Biology, 1997. **9**: p. 76-85.

268. Palecek, S.P., et al., *Integrin-ligand binding properties govern cell migration speed through cell-substratum adhesiveness.* Nature, 1997. **385**(6616): p. 537-540.

269. Shiu, Y.-T., et al., *Rho Mediates the Shear-Enhancement of Endothelial Cell Migration and Traction Force Generation.* 2004. **86**(4): p. 2558-2565.

270. DiMilla, P., et al., *Maximal migration of human smooth muscle cells on fibronectin and type IV collagen occurs at an intermediate attachment strength.* The Journal of Cell Biology, 1993. **122**(3): p. 729-737.

271. DiMilla, P.A., K. Barbee, and D.A. Lauffenburger, *Mathematical model for the effects of adhesion and mechanics on cell migration speed.* 1991. **60**(1): p. 15-37.

272. Wacker, B.K., et al., *Endothelial Cell Migration on RGD-Peptide-Containing PEG Hydrogels in the Presence of Sphingosine 1-Phosphate.* 2008. **94**(1): p. 273-285.

273. Ridley, A.J., et al., *Cell Migration: Integrating Signals from Front to Back.* Science, 2003. **302**(5651): p. 1704-1709.

274. Zhan, X., et al., *Murine cortactin is phosphorylated in response to fibroblast growth factor-1 on tyrosine residues late in the G1 phase of the BALB/c 3T3 cell cycle.* Journal of Biological Chemistry, 1993. **268**(32): p. 24427-24431.

275. Yao, C.-H., et al., *Preparation of networks of gelatin and genipin as degradable biomaterials.* Materials Chemistry and Physics, 2004. **83**(2-3): p. 204-208.

276. Sung HW, H.D., Chang WH, Huang LL, Tsai CC, Liang IL., *Gelatin-derived bioadhesives for closing skin wounds: an in vivo study.* J Biomater Sci Polym Ed., 1999. **10**(7): p. 751-771.

277. Chang, W.H., et al., *A genipin-crosslinked gelatin membrane as wound-dressing material: in vitro and in vivo studies.* Journal of Biomaterials Science, Polymer Edition, 2003. **14**: p. 481-495.

278. Lau, T.T., C. Wang, and D.-A. Wang, *Cell delivery with genipin crosslinked gelatin microspheres in hydrogel/microcarrier composite.* Composites Science and Technology. **In Press, Corrected Proof**.

279. Sung, H.-W., et al., *Crosslinking of biological tissues using genipin and/or carbodiimide.* Journal of Biomedical Materials Research, 2003. **64A**(3): p. 427-438.

280. Touyama R, I.K., Takeda Y, Yatsuzuka M, Ikumoto T, Moritome N, Shingu T, Yokoi T, Intuye H, *Studies on the Blue Pigments Produced from Genipin and Methylamine. II. ON the Formation Mechanisms of Brownish-Red Intermediates Leading to the Blue Pigment Formation.* Chem. Pharm. Bull., 1994. **42**: p. 1571-1578.

281. Garcia, A.J., M.D. Vega, and D. Boettiger, *Modulation of Cell Proliferation and Differentiation through Substrate-dependent Changes in Fibronectin Conformation.* Mol. Biol. Cell, 1999. **10**(3): p. 785-798.

282. Vogel, V., et al., *Structural insights into the mechanical regulation of molecular recognition sites.* Trends in Biotechnology, 2001. **19**(10): p. 416-423.

283. Xu, L.-C. and C.A. Siedlecki, *Effects of surface wettability and contact time on protein adhesion to biomaterial surfaces.* Biomaterials, 2007. **28**(22): p. 3273-3283.

284. Keselowsky, B.G., D.M. Collard, and A.J. García, *Surface chemistry modulates fibronectin conformation and directs integrin binding and specificity to control cell adhesion.* Journal of Biomedical Materials Research Part A, 2003. **66A**(2): p. 247-259.

285. Keselowsky, B.G., D.M. Collard, and A.J.A.J. García, *Surface chemistry modulates focal adhesion composition and signaling through changes in integrin binding.* Biomaterials, 2004. **25**(28): p. 5947-5954.

286. Michael, K.E., et al., *Adsorption-Induced Conformational Changes in Fibronectin Due to Interactions with Well-Defined Surface Chemistries.* Langmuir, 2003. **19**(19): p. 8033-8040.

287. Lee, M.H., et al., *Effect of biomaterial surface properties on fibronectin-[alpha]5[beta]1 integrin interaction and cellular attachment.* Biomaterials, 2006. **27**(9): p. 1907-1916.

288. Neff, J.A., K.D. Caldwell, and P.A. Tresco, *A novel method for surface modification to promote cell attachment to hydrophobic substrates.* Journal of Biomedical Materials Research, 1998. **40**(4): p. 511-519.

289. Neff, J.A., P.A. Tresco, and K.D. Caldwell, *Surface modification for controlled studies of cell-ligand interactions.* Biomaterials, 1999. **20**(23-24): p. 2377-2393.

290. Ghosh, S.S., et al., *Use of maleimide-thiol coupling chemistry for efficient syntheses of oligonucleotide-enzyme conjugate hybridization probes.* Bioconjugate Chemistry, 1990. **1**(1): p. 71-76.

291. King, H.D., G.M. Dubowchik, and M.A. Walker, *Facile synthesis of maleimide bifunctional linkers.* Tetrahedron Letters, 2002. **43**(11): p. 1987-1990.

292. Dubowchik, G.M. and M.A. Walker, *Receptor-mediated and enzyme-dependent targeting of cytotoxic anticancer drugs.* Pharmacology & Therapeutics, 1999. **83**(2): p. 67-123.

293. Lattuada, L. and M. Gabellini, *Straightforward Synthesis of a Novel Maleimide-DTPA Bifunctional Chelating Agent.* Synthetic Communications: An International Journal for Rapid Communication of Synthetic Organic Chemistry, 2005. **35**(18): p. 2409 - 2413.

294. Ji, S., et al., *Maleimide Functionalized Poly(<I>ϵ</I>-caprolactone)-<I>block</I>-poly(ethylene glycol) (PCL-PEG-MAL): Synthesis, Nanoparticle Formation, and Thiol Conjugation.* Macromolecular Chemistry and Physics, 2009. **210**(10): p. 823-831.

295. Hermanson, G.T., *Bioconjuate Techniques*. 2nd Edition ed. 2008: Elsevier Inc. 81-94.

296. Lateef, S.S., et al., *GRGDSP peptide-bound silicone membranes withstand mechanical flexing in vitro and display enhanced fibroblast adhesion.* Biomaterials, 2002. **23**(15): p. 3159-3168.

297. Villanueva, I., C.A. Weigel, and S.J. Bryant, *Cell-matrix interactions and dynamic mechanical loading influence chondrocyte gene expression and bioactivity in PEG-RGD hydrogels.* Acta Biomaterialia, 2009. **5**(8): p. 2832-2846.

298. Salinas, C.N. and K.S. Anseth, *The enhancement of chondrogenic differentiation of human mesenchymal stem cells by enzymatically regulated RGD functionalities.* Biomaterials, 2008. **29**(15): p. 2370-2377.

299. Stile, R.A. and K.E. Healy, *Thermo-Responsive Peptide-Modified Hydrogels for Tissue Regeneration.* Biomacromolecules, 2001. **2**(1): p. 185-194.

300. Tugulu, S., et al., *RGD--Functionalized polymer brushes as substrates for the integrin specific adhesion of human umbilical vein endothelial cells.* Biomaterials, 2007. **28**(16): p. 2536-2546.

301. Jacob, J.T., et al., *Corneal epithelial cell growth over tethered-protein/peptide surface-modified hydrogels.* Journal of Biomedical Materials Research, 2005. **72B**(1): p. 198-205.

302. Schofer, M., et al., *Effect of direct RGD incorporation in PLLA nanofibers on growth and osteogenic differentiation of human mesenchymal stem cells.* Journal of Materials Science: Materials in Medicine, 2009. **20**(7): p. 1535-1540.

303. Cook, A.D., et al., *Characterization and development of RGD-peptide-modified poly(lactic acid-<I>co</I>-lysine) as an interactive, resorbable biomaterial.* Journal of Biomedical Materials Research, 1997. **35**(4): p. 513-523.

304. He, X., J. Ma, and E. Jabbari, *Effect of Grafting RGD and BMP-2 Protein-Derived Peptides to a Hydrogel Substrate on Osteogenic Differentiation of Marrow Stromal Cells.* Langmuir, 2008. **24**(21): p. 12508-12516.

305. Jo, S., P.S. Engel, and A.G. Mikos, *Synthesis of poly(ethylene glycol)-tethered poly(propylene fumarate) and its modification with GRGD peptide.* Polymer, 2000. **41**(21): p. 7595-7604.

306. Shin, H., S. Jo, and A.G. Mikos, *Modulation of marrow stromal osteoblast adhesion on biomimetic oligo[poly(ethylene glycol) fumarate] hydrogels modified with Arg-Gly-Asp peptides and a poly(ethylene glycol) spacer.* Journal of Biomedical Materials Research, 2002. **61**(2): p. 169-179.

307. Lin H B, G.-E.C.A.S.S.W.M.D.F. and S.L. Cooper, *Endothelial cell adhesion on polyurethanes containing covalently attached RGD-peptides.* 1992. **13**(13): p. 905.

308. Lin Y S, W.S.S.C.T.W.W.Y.H.C.S.H.H.J.J.C.N.K.H.K.H. and S.H. Chu, *Growth of endothelial cells on different concentrations of Gly-Arg-Gly-Asp photochemically grafted in polyethylene glycol modified polyurethane.* 2001. **25**(8): p. 617.

309. Wang D A, J.J.S.Y.H.S.J.C.F.L.X. and J.H. Elisseeff, *In situ immobilization of proteins and RGD peptide on polyurethane surfaces via poly(ethylene oxide) coupling polymers for human endothelial cell growth.* 2002. **3**(6): p. 1286.

310. Burgess, B.T., J.L. Myles, and R.B. Dickinson, *Quantitative Analysis of Adhesion-Mediated Cell Migration in Three-Dimensional Gels of RGD-Grafted Collagen.* Annals of Biomedical Engineering, 2000. **28**(1): p. 110-118.

311. Monteiro, G.A., et al., *Positively and Negatively Modulating Cell Adhesion to Type I Collagen Via Peptide Grafting.* Tissue Engineering Part A. **0**(0).

312. Grzesiak, J.J., et al., *Enhancement of cell interactions with collagen/glycosaminoglycan matrices by RGD derivatization.* Biomaterials, 1997. **18**(24): p. 1625-1632.

313. Kim, J., et al., *Characterization of low-molecular-weight hyaluronic acid-based hydrogel and differential stem cell responses in the hydrogel microenvironments.* Journal of Biomedical Materials Research Part A, 2009. **88A**(4): p. 967-975.

314. Cui, F., et al., *Hyaluronic acid hydrogel immobilized with RGD peptides for brain tissue engineering.* Journal of Materials Science: Materials in Medicine, 2006. **17**(12): p. 1393-1401.

315. Rowley, J.A., G. Madlambayan, and D.J. Mooney, *Alginate hydrogels as synthetic extracellular matrix materials.* Biomaterials, 1999. **20**(1): p. 45-53.

316. Yu, J., et al., *The use of human mesenchymal stem cells encapsulated in RGD modified alginate microspheres in the repair of myocardial infarction in the rat.* Biomaterials. **In Press, Corrected Proof**.

317. Ferreira, L.S., et al., *Bioactive hydrogel scaffolds for controllable vascular differentiation of human embryonic stem cells.* Biomaterials, 2007. **28**(17): p. 2706-2717.

318. Massia, S.P. and J. Stark, *Immobilized RGD peptides on surface-grafted dextran promote biospecific cell attachment.* Journal of Biomedical Materials Research, 2001. **56**(3): p. 390-399.

319. Nakamura, M., et al., *Construction of multi-functional extracellular matrix proteins that promote tube formation of endothelial cells.* Biomaterials, 2008. **29**(20): p. 2977-2986.

320. Meinel, L., et al., *The inflammatory responses to silk films in vitro and in vivo.* Biomaterials, 2005. **26**(2): p. 147-155.

321. Caplan, A.I., *Adult mesenchymal stem cells for tissue engineering versus regenerative medicine.* Journal of Cellular Physiology, 2007. **213**(2): p. 341-347.

322. Daamen, W.F., et al., *Elastin as a biomaterial for tissue engineering.* Biomaterials, 2007. **28**(30): p. 4378-4398.

323. Sallach, R.E., et al., *Long-term biostability of self-assembling protein polymers in the absence of covalent crosslinking.* Biomaterials, 2010. **31**(4): p. 779-791.

324. Pittenger, M.F., et al., *Multilineage Potential of Adult Human Mesenchymal Stem Cells.* Science, 1999. **284**(5411): p. 143-147.

325. Reyes, M., et al., *Origin of endothelial progenitors in human postnatal bone marrow.* The Journal of Clinical Investigation, 2002. **109**(3): p. 337-346.

326. Jiang, Y., et al., *Pluripotency of mesenchymal stem cells derived from adult marrow.* Nature, 2002. **418**(6893): p. 41-49.

327. Nagaya, N., et al., *Transplantation of Mesenchymal Stem Cells Improves Cardiac Function in a Rat Model of Dilated Cardiomyopathy.* Circulation, 2005. **112**(8): p. 1128-1135.

328. Shabbir, A., et al., *Muscular Dystrophy Therapy by Nonautologous Mesenchymal Stem Cells: Muscle Regeneration Without Immunosuppression and Inflammation.* Transplantation, 2009. **87**(9): p. 1275-1282 10.1097/TP.0b013e3181a1719b.

329. Miyahara, Y., et al., *Monolayered mesenchymal stem cells repair scarred myocardium after myocardial infarction.* Nat Med, 2006. **12**(4): p. 459-465.

330. Brooke, G., et al., *Therapeutic applications of mesenchymal stromal cells.* Seminars in Cell & Developmental Biology, 2007. **18**(6): p. 846-858.

331. Segers, V.F.M., et al., *Mesenchymal stem cell adhesion to cardiac microvascular endothelium: activators and mechanisms.* Am J Physiol Heart Circ Physiol, 2006. **290**(4): p. H1370-1377.

332. Rho GJ, K.B., Balasubramanian SS., *Porcine mesenchymal stem cells--current technological status and future perspective.* Frontiers in Bioscience, 2009. **14**: p. 3942-3961.

333. Caves JM, K.V., Martinez AW, Kim J, Ripberger CM, Haller CA, Chaikof EL, *The use of microfiber composites of elastin-like protein matrix reinforced with synthetic collagen in the design of vascular grafts.* Biomaterials, 2010.

334. Caves, J.M., et al., *Fibrillogenesis in continuously spun synthetic collagen fiber.* Journal of Biomedical Materials Research Part B: Applied Biomaterials, 2010. **93B**(1): p. 24-38.

335. Nerurkar, N.L., et al., *Nanofibrous biologic laminates replicate the form and function of the annulus fibrosus.* Nat Mater, 2009. **8**(12): p. 986-992.

336. Sakhalkar, H.S., et al., *Leukocyte-inspired biodegradable particles that selectively and avidly adhere to inflamed endothelium in vitro and in vivo.* Proceedings of the National Academy of Sciences of the United States of America, 2003. **100**(26): p. 15895-15900.

337. Nemir, S. and J. West, *Synthetic Materials in the Study of Cell Response to Substrate Rigidity.* Annals of Biomedical Engineering, 2010. **38**(1): p. 2-20.

338. Ingber, D.E., *Tensegrity II. How structural networks influence cellular information processing networks.* J Cell Sci, 2003. **116**(8): p. 1397-1408.

339. Ingber, D.E. and J. Folkman, *Mechanochemical switching between growth and differentiation during fibroblast growth factor-stimulated angiogenesis in vitro: role of extracellular matrix.* The Journal of Cell Biology, 1989. **109**(1): p. 317-330.

340. Reinhart-King, C.A., M. Dembo, and D.A. Hammer, *Cell-Cell Mechanical Communication through Compliant Substrates.* 2008. **95**(12): p. 6044-6051.

341. Koo, L.Y., et al., *Co-regulation of cell adhesion by nanoscale RGD organization and mechanical stimulus.* J Cell Sci, 2002. **115**(7): p. 1423-1433.

342. Lo, C.-M., et al., *Cell Movement Is Guided by the Rigidity of the Substrate.* 2000. **79**(1): p. 144-152.

343. Pelham, R.J. and Y.-l. Wang, *Cell locomotion and focal adhesions are regulated by substrate flexibility.* Proceedings of the National Academy of Sciences of the United States of America, 1997. **94**(25): p. 13661-13665.

344. Engler, A.J., et al., *Matrix Elasticity Directs Stem Cell Lineage Specification.* 2006. **126**(4): p. 677-689.

345. Rowlands, A.S., P.A. George, and J.J. Cooper-White, *Directing osteogenic and myogenic differentiation of MSCs: interplay of stiffness and adhesive ligand presentation.* Am J Physiol Cell Physiol, 2008. **295**(4): p. C1037-1044.

346. Leipzig, N.D. and M.S. Shoichet, *The effect of substrate stiffness on adult neural stem cell behavior.* Biomaterials, 2009. **30**(36): p. 6867-6878.

347. Bryant, S.J., et al., *Crosslinking Density Influences Chondrocyte Metabolism in Dynamically Loaded Photocrosslinked Poly(ethylene glycol) Hydrogels.* Annals of Biomedical Engineering, 2004. **32**(3): p. 407-417.

348. Wang, H.-B., M. Dembo, and Y.-L. Wang, *Substrate flexibility regulates growth and apoptosis of normal but not transformed cells.* Am J Physiol Cell Physiol, 2000. **279**(5): p. C1345-1350.

349. Solon, J., et al., *Fibroblast Adaptation and Stiffness Matching to Soft Elastic Substrates.* 2007. **93**(12): p. 4453-4461.

350. Yeung, T., et al., *Effects of substrate stiffness on cell morphology, cytoskeletal structure, and adhesion.* Cell Motility and the Cytoskeleton, 2005. **60**(1): p. 24-34.

351. Paszek, M.J., et al., *Tensional homeostasis and the malignant phenotype.* 2005. **8**(3): p. 241-254.

352. Montesano, R., L. Orci, and P. Vassalli, *In vitro rapid organization of endothelial cells into capillary-like networks is promoted by collagen matrices.* The Journal of Cell Biology, 1983. **97**(5): p. 1648-1652.

353. Donald, E.I., et al., *Cell shape, cytoskeletal mechanics, and cell cycle control in angiogenesis.* Journal of biomechanics, 1995. **28**(12): p. 1471-1484.

354. Califano, J. and C. Reinhart-King, *A Balance of Substrate Mechanics and Matrix Chemistry Regulates Endothelial Cell Network Assembly.* Cellular and Molecular Bioengineering, 2008. **1**(2): p. 122-132.

355. Deroanne, C.F., C.M. Lapiere, and B.V. Nusgens, *In vitro tubulogenesis of endothelial cells by relaxation of the coupling extracellular matrix-cytoskeleton.* Cardiovascular Research, 2001. **49**: p. 647-658.

356. L'Heureux, N., et al., *Human tissue-engineered blood vessels for adult arterial revascularization.* Nat Med, 2006. **12**(3): p. 361-365.

357. Urry, D.W., et al., *Biocompatibility of the Bioelastic Materials, Poly(GVGVP) and Its γ-Irradiation Cross-Linked Matrix: Summary of Generic Biological Test Results.* Journal of Bioactive and Compatible Polymers, pp. 263-282 vol. 6:, 1991.

358. Rincón, A.C., et al., *Biocompatibility of elastin-like polymer poly(VPAVG) microparticles: in vitro and in vivo studies.* Journal of Biomedical Materials Research Part A, 2006. **78A**(2): p. 343-351.

359. Wei SM, K.E., Fachet J, Fülöp T Jr, Robert L, Jacob MP., *Epitope specificity of monoclonal and polyclonal antibodies to human elastin.* Int Arch Allergy Immunol. , 1998. **115**(1): p. 33-41.

360. Okano, T., et al., *A novel recovery system for cultured cells using plasma-treated polystyrene dishes grafted with poly(N-isopropylacrylamide).* Journal of Biomedical Materials Research, 1993. **27**(10): p. 1243-1251.

361. Okano, T., et al., *Mechanism of cell detachment from temperature-modulated, hydrophilic-hydrophobic polymer surfaces.* Biomaterials, 1995. **16**(4): p. 297-303.

362. Kubo, H., et al., *Creation of myocardial tubes using cardiomyocyte sheets and an in vitro cell sheet-wrapping device.* Biomaterials, 2007. **28**(24): p. 3508-3516.